

Fermionic superoperators for zero-temperature, non-linear transport: real-time perturbation theory and renormalization group for Anderson quantum dots

R. B. Saptsov^(1,2) and M. R. Wegewijs^(1,2,3)

(1) Peter Grünberg Institut, Forschungszentrum Jülich, 52428 Jülich, Germany

(2) JARA- Fundamentals of Future Information Technology

(3) Institute for Theory of Statistical Physics, RWTH Aachen, 52056 Aachen, Germany

(Dated: July 16, 2012)

We study the quantum transport through a strongly interacting Anderson quantum dot at finite bias voltage and magnetic field at *zero-temperature* using the real-time renormalization group (RT-RG) in the framework of a kinetic (generalized master) equation for the reduced density operator. To this end we further develop the general finite temperature real-time transport formalism by introducing *field superoperators* that obey fermionic statistics. This direct second quantization in Liouville-Fock space strongly simplifies the construction of operators and superoperators which transform irreducibly under the Anderson-model symmetry transformations. The fermionic field superoperators naturally arise from the univalence (fermion-parity) superselection rule for the total system of quantum dot plus reservoirs. Expressed in these field superoperators, the *causal structure* of the perturbation theory for the effective time-evolution superoperator-kernel becomes explicit. Using the constraints of the causal structure, we construct a parametrization of the *exact* effective time-evolution kernel for which we analytically find the eigenvectors and eigenvalues in terms of a minimal set of only 30 independent coefficients. The causal structure also implies the existence of a *fermion-parity protected eigenvector* of the exact Liouvillian, explaining a recently reported result on adiabatic driving [Phys. Rev. B 85, 075301 (2012)] and generalizing it to arbitrary order in the tunnel coupling Γ . Furthermore, in the wide-band limit the causal representation exponentially reduces the number of diagrams for the time-evolution kernel. The remaining diagrams can be identified simply by their topology and are manifestly independent of the energy cut-off term-by-term. By an exact reformulation of this series we integrate out all *infinite-temperature effects*, obtaining an expansion targeting only the non-trivial, finite-temperature corrections, and the exactly conserved transport current follows directly from the time-evolution kernel. From this series the previously formulated, RT-RG equations are obtained naturally. We perform a complete 1- plus 2- loop RG analysis at finite voltage and magnetic field, while systematically accounting for the dependence of all renormalized quantities on both the quantum dot *and* reservoir frequencies. Using the second quantization in Liouville-space and symmetry restrictions we obtain analytical RT-RG equations with an efficient numerical solution and we extensively study the model parameter space, excluding the Kondo regime where the 1 plus 2-loop approach is obviously invalid. The incorporated renormalization effects result in an enhancement of the inelastic cotunneling peak, even at a voltage \sim magnetic field \sim tunnel coupling Γ . Moreover, we find a *tunnel-induced* non-linearity of the stability diagrams (Coulomb diamonds) at finite voltage, both in the SET and ICT regime.

PACS numbers: 73.63.Kv, 05.10.Cc, 03.65.Yz, 05.60.Gg

I. INTRODUCTION

Non-linear transport spectroscopy of nanoscale systems is a key technique in modern day physics. Although well-understood in linear transport (equilibrium)^{1,2}, see³ for a review, the theoretical description of the non-equilibrium transport regime, especially at low temperature, remains challenging and the recent progress in this direction has led to an improved understanding of quantum transport through strongly interacting systems. For a recent comparative review see⁴. Recent years have seen the appearance of many fully numerical approaches, such as the scattering-state time-dependent numerical renormalization group (TD-NRG)⁵ relying on the discretization parameter approximation⁶, time-dependent density matrix RG (TD-DMRG)⁷⁻⁹, iterative path integrals (IPSI)¹⁰, numerically-exact influence functional path integrals (INFPI)^{11,12}, quantum Monte Carlo (QMC) in combination with Nakajima-Zwanzig projec-

tion technique¹³ or with imaginary-time formalism¹⁴ and diagrammatic Monte Carlo (diagMC)¹⁵. Partially analytical approaches involve the non-crossing approximation (NCA)^{16,17}, equations of motion for Green functions¹⁸, Bethe-Ansatz^{19,20} and the flow-equation approach²¹. Fully analytical approaches include Keldysh perturbation theory to high orders in U ^{22,23} or dual-fermion superperturbation theory²⁴. Finally, perturbative renormalization group studies have mostly started from the Kondo-model mapping of the Anderson model, either working with Keldysh-Green functions²⁵ or the reduced density operator approach^{26,27}.

The density operator approach has a long history in various fields in physics and chemistry. In the context of nanoscale transport, it is a natural starting point for the description of systems with large interaction energies in the high temperature - weak coupling limit, $U \gg T \gg \Gamma$. It can be systematically extended to include high-order tunneling processes using the real-time diagrammatic²⁸

or Nakajima-Zwanzig approach²⁹ technique, in particular when combined with Liouville space techniques³⁰. However, at low temperature this approach becomes problematic due to effect of high-energy contributions which renormalize the effective low-energy physics. In this paper we show how this approach can be extended to this regime. In particular, we show that much of the insightful structure of generalized master / kinetic equation approach at high temperature is preserved in this regime. We formulate a real-time renormalization group approach that naturally connects to the generalized quantum master or kinetic equation approach.

For this purpose we study the simplest possible, benchmark model of an interacting quantum dot coupled to metal electrodes, the Anderson model. We explicitly set up a general approach to deal with the non-linear transport at very low temperature making use of real-time perturbation theory and a renormalization group formulated based on this. We proceed analytically as far as possible, making this a technically challenging task. In fact, the problem is not really manageable without a new physical approach for dealing with superoperators. The development of this *Liouville-Fock space approach* is a central topic of this paper. Our approach differs by both construction and the scope of the application from the previous formulations^{31–34}. The most close to the our approach is one introduced by Prosen³¹, which was used to calculate steady states of quadratic effective Liouvillians. Here we extend it to the reservoirs with continuous fields as well and further develop it to simplify the microscopic *derivation* of effective Liouvillians for non-quadratic problems. The approach introduced by Schmutz³² and used by other authors^{33,34} differs from our approach in principal details which are essential for our application.

A large part of the paper is devoted to this new approach since it allows for general physical insights into the problem and is crucial for overcoming of technical difficulties in setting up RT-RG. We will illustrate its potential in application to RT-RG calculation of the non-linear transport at zero temperature. As result this paper by necessity extensive. Further motivation for this is that several general physical insights into the the real-time approach haven not been pointed out, although this approach has been developed for some time and have found widespread use, see²⁶ for a review. To include these it is required that the approach is set up from scratch, paying special attention to: (i) causal structure and the related Keldysh rotation (ii) Liouville space formulation, in particular a 2nd quantization for *superoperators* (iii) spin and charge rotation symmetry (iv) the infinite temperature limit as a reference point for both the 2nd quantization technique that we develop, as well as the perturbation theory. Only by fully exploiting these the simplest application of RT-RG to the Anderson model becomes practically possible. Clearly, these developments are best presented coherently in the context of the application to the RT-RG for which it is absolutely crucial.

To indicate the impact of these developments for the Anderson model study, we note that the simplest approximation which includes the exact result for the $U = 0$ limit requires an infinite series of diagrams in the standard RT-PT. Using the RT-RG this result is recovered only when performing a 1- and 2-loop analysis for the effective Liouvillian *and* including 1-loop vertex corrections. We emphasize that when applied to the interacting case, this incorporates renormalization effects from strong tunneling, while neglecting spin-fluctuation processes relevant only in the Kondo regime, which enter only in a 3-loop RG analysis (the latter has been addressed previously based on a Kondo-model mapping²⁷). Naively formulating these equations leads to hundreds of non-linear coupled integro-differential RG equations for frequency-dependent coupling functions. The central result of this paper is the derivation of 30 coupled differential coupling functions systematically incorporating the leading frequency dependence which includes the $U = 0$ limit exactly. On the way we derived several exact results of general importance. This makes an efficient numerical implementation possible and allows experimentally relevant stability diagrams to be calculated from wide ranges of parameters in the non-linear zero-temperature regime (excluding the narrow Kondo regime).

Many of the results can be extended to generic models involving local interactions (multi-orbital Anderson type models) with bilinear tunnel coupling to reservoirs. See Ref. 35 for a recent study of non-local interactions using the RT-RG.

The paper is organized in two main parts as follows. In the first part, starting in Sec. (II), we formulate the model and directly change to a Liouville space description and develop the kinetic equation approach for the stationary QD density operator. We formulate the perturbation series for the effective Liouvillian $L(z)$ appearing in this equation using a new *causal representation* of field *superoperators* G with fermionic statistics. We emphasize that this formulation of the perturbation theory – although equivalent to previous formulations^{29,30,36} – leads to many simplifications beyond the application of interest here, and therefore warrants a proper, extensive discussion. Several of these results have already found application³⁷, and even provide insights into and generalization of recent interesting predictions³⁸. Moreover, a renormalized perturbation theory, which takes the *infinite temperature limit* as a formal reference point, suggests itself. It also connects in a natural way to the renormalization group approach while preserving much of its general perturbative structure. We show how the calculation of the current requires little additional calculation and prove that in our non-linear approach the linear current vanishes at zero bias, which is not obvious from the general structure of the theory.

In the second main part of the paper, starting in Sec. (III), the explicit 1- and 2-loop RT-RG equations are derived accounting for the energy dependence of both the Liouvillian and vertices due to the finite non-equilibrium

transport voltage. The non-interacting *current* is shown to arise naturally as an exact result already in 1-loop RT-RG, implying that all 2-loop corrections *to this observable* arise from the strong local Coulomb interaction. We find, however, that for $U = 0$ non-zero 2-loop terms exist which are relevant when one is interested in, e.g., the density matrix (and not just the current). The non-trivial frequency dependence of 2-loop equations is systematically accounted for in powers of the renormalized dimensionless coupling superoperators \tilde{G} , resulting in an effective RG equation *for the effective Liouvillian only*, which accounts for vertex renormalization corrections.

This simplification enables the detailed numerical study in Sec. (IV) of the zero-temperature non-linear transport in all regimes excluding the Kondo regime of low applied voltage and magnetic field. The importance of accounting for both 1- and 2-loop corrections as well as the Matsubara axes is demonstrated numerically. Finally, in Sec. (IV) we show that the *tunnel-induced* renormalization effects incorporated in our 1 plus 2 loop approach enhance the inelastic cotunneling resonance at finite magnetic field and voltage and generate non-linearities of the SET stability diagrams (Coulomb diamonds).

II. MODEL AND REAL-TIME TRANSPORT THEORY

A. Anderson model

In this section we introduce the model and our compact notation which is crucial to the Liouville space formulation of the theory. The simplest model Hamiltonian of a QD which takes into account Coulomb interaction effects involves just a single orbital

$$H = \epsilon n + BS_z + Un_\uparrow n_\downarrow \quad (1)$$

Here ϵ denotes the energy of the orbital with occupation operators $n = \sum_\sigma n_\sigma$, $n_\sigma = d_\sigma^\dagger d_\sigma$. The index $\sigma = \pm$ corresponds to spin \uparrow, \downarrow and $S_z = \frac{1}{2} \sum_\sigma \sigma n_\sigma$ is the z component of the spin vector operator $\mathbf{S} = \sum_{\sigma\sigma'} \frac{1}{2} \sigma_{\sigma\sigma'} d_\sigma^\dagger d_{\sigma'}$ along the external magnetic field $\mathbf{B} = B\mathbf{e}_z$ (in units where $g\mu_B = 1$) and $\boldsymbol{\sigma}$ is the vector of Pauli matrices. The dot is attached to electrodes which are treated as free electron reservoirs:

$$H^R = \sum_{\sigma,r,k} \epsilon_{r,k} a_{\sigma,r,k}^\dagger a_{\sigma,r,k} \quad (2)$$

where the reservoir index $r = \pm$ corresponds to L, R , k is the orbital index and σ the spin index, quantized along the z -axis. The reservoir electron number and spin can be decomposed into $n^R = \sum_r n^r$ and $\mathbf{s}^R = \sum_r \mathbf{s}^r$ where

$$n^r = \sum_{\sigma,k} a_{\sigma,r,k}^\dagger a_{\sigma,r,k} \quad (3)$$

$$\mathbf{s}^r = \sum_{\sigma,k} \frac{1}{2} \boldsymbol{\sigma}_{\sigma\sigma'} a_{\sigma,r,k}^\dagger a_{\sigma',r,k} \quad (4)$$

In the continuum limit the reservoirs are described by the density of states $\nu_r(\omega) = \sum_k \delta(\omega - \epsilon_{r,k} + \mu_r)$ and we go to the energy representation of the fermionic operators,

$$a_{\sigma,r}(\omega) = \frac{1}{\sqrt{\nu_r(\omega)}} \sum_k a_{\sigma,r,k} \delta(\omega - \epsilon_{r,k} + \mu_r), \quad (5)$$

with the anti-commutation relations:

$$[a_{\sigma,r}(\omega), a_{\sigma',r'}^\dagger(\omega')]_+ = \delta_{\sigma,\sigma'} \delta_{r,r'} \delta(\omega - \omega') \quad (6)$$

$$[a_{\sigma,r}(\omega), a_{\sigma',r'}(\omega')]_+ = 0. \quad (7)$$

where we denote (anti)commutators by $[A, B]_\pm = AB \pm BA$. Thus we have for the reservoir Hamiltonian:

$$H^R = \sum_{\sigma,r} \int d\omega (\omega + \mu_r) a_{\sigma,r}^\dagger(\omega) a_{\sigma,r}(\omega) \quad (8)$$

In contrast to $\epsilon_{r,k}$ the energy ω is the electron energy relative to μ_r , i.e., the reference energy depends which reservoir is considered.

The junctions connecting the dot and reservoirs are modeled by the tunneling Hamiltonian

$$V = \sum_r V^r \quad (9)$$

$$V^r = \sum_\sigma \int d\omega \sqrt{\nu_r(\omega)} (t_r(\omega) a_{\sigma,r}^\dagger(\omega) d_\sigma + h.c.) \quad (10)$$

The Hamiltonian of the total system is denoted by

$$H^{\text{tot}} = H + H^R + V \quad (11)$$

We assume $t_r(\omega)$ to be real and introduce the spectral density

$$\Gamma_r(\omega) = 2\pi \nu_r(\omega) |t_r(\omega)|^2 \quad (12)$$

and rescaled field operators:

$$b_{\sigma,r}(\omega) = \sqrt{\frac{\Gamma_r(\omega)}{2\pi}} a_{\sigma,r}(\omega) \quad (13)$$

To make the notation more compact we introduce an additional particle-hole index⁶⁶

$$b_{\eta,\sigma,r}(\omega) = \begin{cases} b_{\sigma,r}^\dagger(\omega), & \eta = + \\ b_{\sigma,r}(\omega), & \eta = - \end{cases}, \quad (14)$$

$$d_{\eta,\sigma} = \begin{cases} d_\sigma^\dagger, & \eta = + \\ d_\sigma, & \eta = - \end{cases}. \quad (15)$$

Throughout the paper we will denote the inverse value of a two-valued index with a bar. A prominent example, is given by

$$\bar{\eta} = -\eta \quad (16)$$

We combine all indices into a multiindex variable written as a number:

$$1 = \eta, \sigma, r, \omega; \quad \bar{1} = \bar{\eta}, \sigma, r, \omega. \quad (17)$$

where by way of exception the bar denotes inversion of the particle-hole index only. Then $b_1 = b_{\eta,\sigma,r}(\omega)$ and $b_{\bar{1}} = b_{-\eta,\sigma,r}(\omega)$ and the various independent anticommutation relations are compactly summarized by

$$[d_1, d_2]_+ = \delta_{1\bar{2}} \quad (18)$$

$$[b_1, b_2]_+ = \frac{\Gamma_1}{2\pi} \delta_{1\bar{2}} \quad (19)$$

where $\Gamma_1 = \Gamma_r(\omega)$. The interaction then simply reads

$$V = b_{\bar{1}} d_1 \quad (20)$$

where we implicitly assume summation over all discrete parts of the multi-index 1 (i.e. η, σ, r) and integration over its continuous part (ω). We usually omit subscripts in the multiindex components η, σ, r, ω if we have the only multiindex. If we have more than one multiindex we distinguish their components by corresponding subscripts: $1 = \eta_1, \sigma_1, r_1, \omega_1$, $2 = \eta_2, \sigma_2, r_2, \omega_2$. Importantly, operators (and, below also superoperators) of the dot and the reservoirs can be treated *as if* they commute (rather than anticommute)⁶⁷.

The reservoirs are assumed to be at thermal equilibrium with temperature T , each described by its own grand-canonical density operator,

$$\rho^R = \prod_r \rho^r, \quad \rho^r = \frac{1}{z^r} e^{-\frac{1}{T}(H^r - \mu^r n^r)}, \quad (21)$$

where $z^r = \text{Tr} e^{-\frac{1}{T}(H^r - \mu^r n^r)}$. We assume that a symmetric bias is applied to the electrodes, i.e., $\mu_{L,R} = \pm V/2$. We note the key property

$$b_1 \rho^R = e^{\eta_1 \omega_1 / T} \rho^R b_{\bar{1}}. \quad (22)$$

In Eq. (12) the density of states varies on the energy scale of the bandwidth D which we assume to be much larger than any other energy scale in the problem. In this wide-band limit we can assume $\Gamma_r(\omega)$ to be energy independent and cut off all reservoir energy integrals (ω) at the scale D . The detailed energy dependence of $\Gamma_r(\omega)$ at high energies is not crucially important for the results²⁶. In the actual applications in Sec. (IV) we will assume for simplicity that the tunnel couplings are symmetric, i.e. $\Gamma_L = \Gamma_R = \Gamma$ and consider the low temperature limit i.e. $T \ll U, V, \Gamma_r$ by setting $T = 0$. The results of the present section and much of Sec. (III), however, do *not* depend on these assumptions unless explicitly indicated.

For a non-zero magnetic field B and finite Coulomb interaction U the total system possesses two locally and globally conserved quantities that will play an important role. Locally on the dot and the reservoirs the charge and spin component along the magnetic field on the dot are conserved,

$$[H, n]_- = 0 \quad [H, S_z]_- = 0 \quad (23)$$

$$[H^R, n^R]_- = 0 \quad [H^R, S_z^R]_- = 0 \quad (24)$$

These conservation laws extend to the total charge, $N^{\text{tot}} = n + n^R$, and spin, $S_z^{\text{tot}} = S_z + S_z^R$, since the interaction V commutes with these operators:

$$[H^{\text{tot}}, N^{\text{tot}}]_- = 0 \quad (25)$$

$$[H^{\text{tot}}, S_z^{\text{tot}}]_- = 0 \quad (26)$$

B. Density operator and diagram rules

The purpose of this section is twofold. Firstly, we briefly review the real-time approach to the calculation of the stationary reduced density operator, introducing the central quantities $\Sigma(z)$, the self-energy superoperator, and $L(z)$, the effective Liouvillian, and their perturbative expansions in vertex superoperators G . Secondly, we introduce a “causal” representation of the perturbation theory which allows for a new compact formulation and derivation of the diagrammatic rules for the self-energy Σ . Moreover, many general physical insights become explicitly clear in this representation. In particular, starting from this new formulation, the possibility of a two-stage real-time renormalization group (RT-RG) that will be set up in Sec. (II B 4) and Sec. (III) arises quite naturally.

1. Stationary density operator

In order to find the QD stationary state we need to consider the evolution of the total system density-operator. It evolves according to the Liouville- von Neumann equation:

$$\partial_t \rho^{\text{tot}}(t) = -i [H^{\text{tot}}, \rho^{\text{tot}}(t)]_- = -i L^{\text{tot}} \rho^{\text{tot}}(t) \quad (27)$$

with the superoperator Liouvillian $L^{\text{tot}} = [H^{\text{tot}}, \bullet]_-$. Superoperators are linear transformations of operators and throughout the paper we let \bullet indicate the operator on which a superoperator acts (if needed). Explicit matrix representations of superoperators are only required for the QD part and will be discussed later on in Sec. (II C)

The initial state of the total system at the initial time t_0 is assumed to be the direct product of the dot density matrix and the equilibrium density matrices (21) of the electrodes:

$$\rho^{\text{tot}}(t_0) = \rho(t_0) \rho^R \quad (28)$$

We will discuss some properties of $\rho(t_0)$ further below. The formal solution of Eq. (27) is:

$$\rho^{\text{tot}}(t) = e^{-i H^{\text{tot}}(t-t_0)} \rho^{\text{tot}}(t_0) e^{i H^{\text{tot}}(t-t_0)} \quad (29)$$

$$= e^{-i L^{\text{tot}}(t-t_0)} \rho^{\text{tot}}(t_0) \quad (30)$$

and the reduced density matrix of the dot is obtained by integrating out of reservoirs degrees of freedom:

$$\rho(t) = \text{Tr}_R \rho(t) = \text{Tr}_R \left(e^{-i L^{\text{tot}}(t-t_0)} \rho(t_0) \rho^R \right) \quad (31)$$

We now decompose $L^{\text{tot}} = L + L^R + L^V$, with $L = [H, \bullet]_-$, $L^R = [H^R, \bullet]_-$ and set up the perturbation series in the tunnel coupling $L^V = [V, \bullet]_- \sim \sqrt{\Gamma}$. It is then more convenient²⁶ to use the Laplace transform of the dot reduced density matrix for $\text{Im}z > 0$:

$$\rho(z) = \int_{t_0}^{\infty} dt e^{iz(t-t_0)} \rho(t) \quad (32)$$

$$= \text{Tr}_R \left(\frac{i}{z - L - L^R - L^V} \rho^{\text{tot}}(t_0) \right) \quad (33)$$

We will refer to z as the dot frequency. We expand the resolvent in L^V , resulting in a geometric series with terms of the form

$$\text{Tr}_R \left(\frac{1}{z - L - L^R} L^V \dots L^V \frac{1}{z - L - L^R} \rho^{\text{tot}}(t_0) \right) \quad (34)$$

The average over the reservoirs can now be calculated directly using a Wick theorem for field superoperators (see Eq. (60) and App. A). Collecting irreducible contractions into the self-energy superoperator $\Sigma(z)$ (see below, Sec. (IIB3)) the perturbation series can be resummed:

$$\rho(z) = \frac{i}{z - L(z)} \rho(t_0) \quad (35)$$

where we have introduced the effective Liouville operator

$$L(z) = L + \Sigma(z) \quad (36)$$

To keep the notation to a minimum we distinguish this quantity from the “bare” dot Liouvillian $L = [H, \bullet]$ by simply appending the dependence on the frequency z . $L(z)$ completely determines the time-evolution of the reduced density operator. A key idea exploited both in the perturbation theory and the renormalization group is that one is free to modify L and $\Sigma(z)$ as long as their sum remains equal to $L(z)$. The equation determining the stationary density matrix $\rho = \lim_{t \rightarrow \infty} \rho(t) = \lim_{z \rightarrow i0} (-iz) \rho(z)$ is now obtained by multiplying Eq. (35) by $-iz(z - L(z))$ and taking $z \rightarrow i0$:

$$L(i0)\rho = 0 \quad (37)$$

Before deriving the perturbation series for $\Sigma(z)$ in Sec. (IIB3), we first introduce a convenient representation of the field *superoperators*.

2. Causal representation of fermionic field superoperators

Below we integrate out explicitly the reservoir degrees of freedom while keeping track of those of the QD. To facilitate this the tunnel coupling superoperator $L^V = [V, \bullet]_-$ should be written as a convenient product of the dot and the reservoir superoperators: inserting Eq. (20) we have

$$L^V = p^{L^{N^{\text{tot}}}} p \mathcal{J}_1^p \mathcal{G}_1^p \quad (38)$$

when we define field superoperators as follows:

$$\mathcal{J}^p \bullet = \begin{cases} b_1 \bullet, & p = + \\ \bullet b_1, & p = - \end{cases} \quad (39)$$

$$\mathcal{G}^p \bullet = \begin{cases} d_1 \bullet, & p = + \\ \bullet d_1, & p = - \end{cases} \quad (40)$$

The superscript $p = \pm$ keeps track of whether a field operator acts from the left or right and is referred to as Keldysh index by analogy to the Green-function and functional integral techniques. In Eq. (38) we implicitly sum over p , in addition to the multiindex 1. A crucial difference to the formulation of Ref. 26 is that we introduced a harmless additional superoperator

$$p^{L^{N^{\text{tot}}}} \bullet = p^{L^{n^R}} p^{L^n} \bullet \quad (41)$$

into Eq. (38), where

$$L^{N^{\text{tot}}} = [N^{\text{tot}}, \bullet]_- = L^n + L^{n^R}, \quad (42)$$

$$L^n = [n, \bullet]_-, \quad (43)$$

$$L^{n^R} = [n^R, \bullet]_-, \quad (44)$$

are the superoperators associated with the total, QD and reservoir electron numbers respectively. Clearly for $p = +1$ this factor is trivially equal to 1. However, it may seem at first sight that for $p = -1$ this is not the case: when applied to a projector of states of the total system this superoperator counts the relative parity of the fermion numbers N and N' : $(-1)^{L^{N^{\text{tot}}}} |N\lambda\rangle\langle N'\lambda'| = \pm |N\lambda\rangle\langle N'\lambda'|$ for $N - N' = \text{even} / \text{odd}$, where λ, λ' denotes further quantum numbers. However, in all calculations we can assume that the total-system state operators on which it acts have even parity, since odd fermion-parity components of states can neither be measured by any physical operator nor be prepared using physical evolutions. This is referred to as the fermion-parity superselection rule^{39,40}.

Since the fermion parity plays an important role in what follows but is often not mentioned or used explicitly in density operator approaches it warrants some discussion, in particular since odd-fermion parity operators do appear in the renormalization group approach. Physical Hamiltonians and observables (and their corresponding superoperators) always contain only products of even numbers of fermionic operators. This implies that only the part of the density operator $\rho^{\text{tot}}(t)$ with even fermion parity can enter into the calculation of any physical observable $\langle A \rangle(t) = \text{Tr} A \rho^{\text{tot}}(t)$. This even part of $\rho^{\text{tot}}(t)$ is generated solely from the even parity part of $\rho^{\text{tot}}(t_0)$ at earlier times since by the same token the parity of the total fermion number is conserved during time evolution. Therefore only the even fermion-parity part of the initial state $\rho^{\text{tot}}(t_0)$ can contribute to an observable and one may set any odd-fermion part of any density matrix equal to zero. As a result, we can take in Eq. (38) $p^{L^{N^{\text{tot}}}} \bullet = 1\bullet$, even for $p = -1$. For the factorized initial state Eq. (28) that we assumed here, this implies that

$\rho(t_0)$ must be assumed to be of even fermion parity, since ρ^R also has even fermion parity ($L_{n^R}\rho^R = [n^R, \rho^R]_- = 0$, which follows from Eq. (21)).

The useful implications of this fermion-parity conservation become clear when performing a linear transformation of the field superoperators with respect to their Keldysh indices p . The naively chosen field superoperators (39) and (40) have the disadvantage that they commute or anticommute depending on the Keldysh index p :

$$\mathcal{G}_1^p \mathcal{G}_2^{p'} + pp' \mathcal{G}_1^p \mathcal{G}_2^{p'} = \delta_{pp'} \delta_{1\bar{2}} \quad (45)$$

$$\mathcal{J}_1^p \mathcal{J}_2^{p'} + pp' \mathcal{J}_1^p \mathcal{J}_2^{p'} = \delta_{pp'} \delta_{1\bar{2}} \quad (46)$$

This complicates many calculations as noted, e.g., in Ref. 41. However, the factorization of the total fermion parity into a dot and reservoir factor in (41) naturally suggests a transformation of the field operators. By absorbing the fermion parity superoperators of each subsystem into new field superoperators,

$$\mathcal{G}_1^p = p^{L^n} \mathcal{G}_1^p \quad (47)$$

$$\mathcal{J}_1^p = p^{L^{n^R}} \mathcal{J}_1^p \quad (48)$$

they obey definite anticommutation relations

$$[\mathcal{G}_1^p, \mathcal{G}_2^{p'}]_{++} = p \delta_{pp'} \delta_{1\bar{2}} \quad (49)$$

$$[\mathcal{J}_1^p, \mathcal{J}_2^{p'}]_{++} = \frac{\Gamma}{2\pi} p \delta_{pp'} \delta_{1\bar{2}} \quad (50)$$

This allows one to prove the Wick theorem directly for the operators \mathcal{J} using simple algebra³⁷, avoiding the need to carefully keep track of sign factors as done in Ref. 26. However, the non-vanishing anticommutators still depend on the Keldysh index p on the right hand side. Moreover, the fields have no simple Hermitian superconjugation relation (see App. B). This can be avoided by a rotation of the QD fields

$$G^q = \begin{cases} \tilde{G}_1 = \frac{1}{\sqrt{2}} \sum_p \mathcal{G}^p = \frac{1}{\sqrt{2}} \sum_p p^{L^n} \mathcal{G}_1^p & q = + \\ \bar{G}_1 = \frac{1}{\sqrt{2}} \sum_p p \mathcal{G}^p = \frac{1}{\sqrt{2}} \sum_p p^{L^n+1} \mathcal{G}_1^p & q = - \end{cases} \quad (51)$$

and a contravariant rotation (cf. Sec. (IIB3)) of the reservoir fields

$$J_1^q = \begin{cases} \tilde{J}_1 = \frac{1}{\sqrt{2}} \sum_p p \mathcal{J}^p = \frac{1}{\sqrt{2}} \sum_p p^{L^{n^R}+1} \mathcal{J}_1^p & q = + \\ \bar{J}_1 = \frac{1}{\sqrt{2}} \sum_p \mathcal{J}^p = \frac{1}{\sqrt{2}} \sum_p p^{L^{n^R}} \mathcal{J}_1^p & q = - \end{cases} \quad (52)$$

To facilitate later discussions, we introduce both an index $q = \pm$ as well as $\tilde{}$ and $\bar{}$ symbols to distinguish the new field components. Now the anticommutation relations are completely analogous to those of the usual fermionic

operators,

$$[G_1^q, G_1^{q'}]_+ = \delta_{q,\bar{q}'} \delta_{1,\bar{1}'} \quad \begin{cases} [\tilde{G}_1, \bar{G}_1]_+ = \delta_{1,\bar{1}'} \\ [\tilde{G}_1, \tilde{G}_1]_+ = 0 \\ [\bar{G}_1, \bar{G}_1]_+ = 0 \end{cases} \quad (53)$$

whereas in the reservoirs we incorporate the coupling into the normalization factor:

$$[J_1^q, J_1^{q'}]_+ = \frac{\Gamma_1}{2\pi} \delta_{q,\bar{q}'} \delta_{1,\bar{1}'} \quad \begin{cases} [\tilde{J}_1, \bar{J}_1]_+ = \frac{\Gamma_1}{2\pi} \delta_{1,\bar{1}'} \\ [\tilde{J}_1, \tilde{J}_1]_+ = 0 \\ [\bar{J}_1, \bar{J}_1]_+ = 0 \end{cases} \quad (54)$$

This second transformation is known as the Keldysh rotation⁴² and is, e.g., applied to fermionic fields represented by Grassman-numbers in functional integral theories⁴³ or in Green-function formalism⁴². Here we find that it also considerably simplifies the real-time transport theory in which not all degrees of freedom can be integrated out, in contrast to the cited approaches. We note that a transformation similar to Eqs.(47)-(48) which also results in the usual anti-commutation and conjugation relations for the fermionic superoperators superoperators was introduced in Ref. 32–34, however, without performing of the Keldysh-rotation (see also discussion in App.D). This transformation, however, is less convenient in general since it does not reveal a general structure of the fermionic superoperators which is important for the our applications and which we will relate to causality below.

We therefore will refer to (51)-(52) as the *causal representation* in Keldysh space and the index $q = \pm$ as the *causal index*. Again we denote its inverse by $\bar{q} = -q$.

For the *dot* field superoperators (G^q) this representation was already introduced in Ref. 26, but it was not exploited in the context of the perturbation theory, where it provides many useful additional simplifications that we now address. First of all, the property

$$\text{Tr}_D(\tilde{G}\bullet) = 0 \quad (55)$$

ensures the probability conservation on the dot during the time-evolution, see Eq. (69). It is extremely important for the formulation of the RT-RG in Sec. (III) and is preserved during renormalization. We note that probability conservation in the Liouville approach corresponds to the normalization conservation for the partition function in the path-integral approach⁴³. Eq. (55) follows directly from the definition of the causal representation: using $\text{Tr}_D L^n = 0$, and, using the cyclic property of the trace, $\text{Tr}_D \mathcal{G}_1^p \bullet = \text{Tr}_D d_1 \bullet$ is independent of $p = \pm$. Therefore

$$\text{Tr}_D(\tilde{G}\bullet) = \sum_p \text{Tr}_D p^{L^n+1} \mathcal{G}_1^p \bullet = \sum_p p \text{Tr}_D d_1 \bullet = 0. \quad (56)$$

Secondly, the fields \tilde{G}_1 and \tilde{G}_1^\dagger are related by Hermitian conjugation of superoperators:

$$\tilde{G}_1 = (\tilde{G}_1^\dagger)^\dagger. \quad (57)$$

For a superoperator S the Hermitian conjugate S^\dagger is defined by $\text{Tr}(A^\dagger SB) = \text{Tr}((S^\dagger A)^\dagger B)$ where A and B are arbitrary operators, see also Sec. (II C 1) and App. B. This indicates that the conjugate fields \tilde{G}_1 and \tilde{G}_1^\dagger are similar to usual creation and annihilation operators, respectively. In Sec. (II C) we exploit this “2nd quantization” in Liouville space to construct a convenient basis the QD Liouville space that includes the left and right zero super-eigenvectors of both vertices. This considerably simplifies the matrix representations of many superoperators required in perturbation theory and the RG. An immediate consequence of the probability conservation property (57) is that \tilde{G} has the unit operator $\mathbb{1}$ as a right zero super eigenvector:

$$\tilde{G}_1 \mathbb{1} = 0 \quad (58)$$

The above properties of these causal field superoperators acting on the QD Liouville space provide explicit insight into important physical issues that are otherwise not obvious in the general form of the perturbation theory, e.g., the wide-band limit, the infinite temperature limit, and the energy cut-off D dependence which we discuss in Sec. (II B 3). Introducing the corresponding causal representation for the *reservoir* field superoperators also yields several simplifications which we now discuss.

a. Wick theorem First, we note that due to the local interactions on the QD Eq. (53) cannot be used to formulate a Wick theorem for the vertices G . In contrast to this, for the reservoir field superoperators this is possible due to the relation

$$\bar{J}_1 \rho^R = \tanh(\eta_1 \omega_1 / 2T) \tilde{J}_1 \rho^R \quad (59)$$

This result follows from Eq. (22) by writing it in superoperator notation, $\mathcal{J}_1^+ \rho^R = e^{\eta_1 \omega_1 / T} \mathcal{J}_1^- \rho^R$, and then applying the transformations (48) and (52). With Eq. (59) we can algebraically prove the Wick theorem for the superoperators J_1^q in close analogy to the usual case of fermionic operators (see App. A): the average of a product equals the product of pair contractions summed over all contractions of pairs $\langle ik \rangle$,

$$\text{Tr}_R (J_1^{q_1} \dots J_m^{q_m} \rho^R) = \sum_{i < k} \prod_{\langle ik \rangle} (-1)^P \langle J_i^{q_i} J_k^{q_k} \rangle_R \quad (60)$$

with the usual fermionic sign $(-1)^P$ of the permutation P that disentangles the contractions.

b. Causal structure The number of possible pair-contractions appearing on the right hand side of Eq. (60) is strongly reduced. Applying $\text{Tr}_R \tilde{J}_1 \bullet$ to Eq. (59) written for the operator \bar{J}_2 we obtain a relation between two of the possible four pair contractions:

$$\langle \bar{J}_1 \bar{J}_2 \rangle_R = \tanh(\eta_2 \omega_2 / 2T) \langle \tilde{J}_1 \tilde{J}_2 \rangle_R \quad (61)$$

This is actually a statement of the equilibrium fluctuation-dissipation theorem for each reservoir separately, see, e.g., Ref. 44. In close analogy to Eq. (55) one proves

$$\text{Tr}_R (\tilde{J}_1 \bullet) = 0 \quad (62)$$

This implies in particular, $\langle \tilde{J}_1 \tilde{J}_2 \rangle_R = 0$ which is related to the well-known fact that of the four reservoir Green’s functions only three are independent⁴⁵. This is analogous to the absence of so called “quantum-quantum” contractions (or “classical-classical” term in the Keldysh action) in the Keldysh functional integral approach and has been referred to as the “causal” structure of Green functions in that approach⁴³. However, Eq. (62) entails an additional simplification: $\langle \tilde{J}_1 \bar{J}_2 \rangle_R = 0$. This is particular to our real-time superoperator approach, and is most explicitly related to causality. To see this, note that we keep track of the left and right action of operators using superoperator notation and that these superoperators inherit their ordering in the Laplace representation from their *forward* time-ordering in the time-evolution, cf. Eq. (34). We never have to introduce a fictitious backward time-propagation as in the Keldysh technique. Therefore no advanced reservoir Green functions can appear in our theory, which is expressed by $\langle \tilde{J}_1 \bar{J}_2 \rangle_R = 0$.

c. Energy and temperature dependence The only reservoir correlation functions that can appear in the Wick expansion (60) for the causal fields have a simpler energy (ω) and temperature (T) dependence than in the representations (39)-(40) and (47)-(48). This correlates with the physical information that these functions incorporate, the retarded function⁶⁸

$$\tilde{\gamma}_{1,2}(\eta_2 \omega_2) := \langle \bar{J}_1 \tilde{J}_2 \rangle_R = \frac{\Gamma_2}{2\pi} \delta_{1,\bar{2}}, \quad (63)$$

and Keldysh function

$$\tilde{\gamma}_{1,2}(\eta_2 \omega_2) := \langle \bar{J}_1 \bar{J}_2 \rangle_R = \frac{\Gamma_2}{2\pi} \tanh(\eta_2 \omega_2 / 2T) \delta_{1,\bar{2}}. \quad (64)$$

In the causal representation the superoperator ordering explicitly shows that the retarded contraction $\tilde{\gamma}$ contains no information about the distribution function of the reservoirs and is therefore temperature independent. Eq. (63) follows directly from the anticommutation relation (54) and the property (62), and is indeed independent of the reservoir density operator ρ^R . In contrast, for the Keldysh contraction, one first needs to use the property (59) specific to the equilibrium state of the non-interacting reservoirs, before Eq. (54) and Eq. (62) can be applied. The above shows that the representation (52) reflects most explicitly the causal structure of the perturbation theory, motivating its denotation. It thereby automatically achieves the decomposition of the reservoir Fermi distribution function into its symmetric (trivial) and antisymmetric (non-trivial) part with respect to the energy ω that was introduced in Ref. 26, where it is crucial in setting up the RT-RG. Below we show that in the

causal representation for the QD fields the perturbation theory also drastically simplifies and that in this new formulation the RT-RG appears quite naturally.

3. Perturbation series and diagram rules

a. Diagram rules When defining the causal representation (Eq. (51) and Eq. (52)) we performed opposite Keldysh rotations for the dot and the reservoirs. This is motivated by the form of the tunneling Liouvillian Eq. (38), which in the causal representation can be written compactly as

$$L^V = \bar{G}_1 \bar{J}_1 + \tilde{G}_1 \tilde{J}_1 = \sum_{q=\pm} G_1^q J_1^q \quad (65)$$

We can now integrate out the reservoir degrees of freedom in each term of the expansion (34) in the way discussed in Ref. 26 by commuting all reservoir operator to the right side using the relation

$$J_1^q L^R = (L^R - \eta_1(\omega_1 + \mu_1)) J_1^q \quad (66)$$

resulting for the order m contributions to $\Sigma(z)$ in

$$\begin{aligned} & \frac{1}{z-L} G_1^{q_1} \frac{1}{z-X_1-L} G_2^{q_2} \frac{1}{z-X_2-L} \dots \\ & \frac{1}{z-X_{m-1}} G_m^{q_m} \frac{1}{z-L} \rho(t_0) \text{Tr}_R (J_1^{q_1} J_2^{q_2} \dots J_m^{q_m} \rho^R) \end{aligned} \quad (67)$$

Here $X_i = \sum_{k \leq i} x_k$ where the summation runs over the reservoir frequencies $x_k = \eta_k(\omega_k + \mu_k)$ of the $G_k^{q_k}(J_k^{q_k})$ originally standing to the left to the resolvent i . Applying the Wick theorem (60) we can represent the terms diagrammatically by propagators connecting vertices that are contracted in pairs by lines with frequencies x_k . The irreducible parts of these diagrams, i.e., those parts which cannot be cut without hitting at least one reservoir contraction, are collected into the irreducible kernel or *self-energy superoperator* $\Sigma(z)$. In Fig. 1 we show the diagrams for $\Sigma(z)$ to 1- and 2-loop order. Leaving the sum over all possible configurations of pair contractions, all indices and all orders m implicit we can write:

$$\begin{aligned} \Sigma(z) &= (-1)^P \left(\prod \gamma \right)_{\text{irr}} \times \\ & G_1^- \frac{1}{z-X_1-L} G^{q_2} \dots G^{q_{m-1}} \frac{1}{z-X_{m-1}-L} G^{q_m} \end{aligned} \quad (68)$$

Here γ denotes that the function $\bar{\gamma}(\bar{\gamma})$, given by Eq. (64) (Eq. (63)), should be written for pair contraction connecting a \bar{G} vertex on the left with a \bar{G} (\tilde{G}) vertex on the right. By Eq. (65) it is the *earliest* vertex (rightmost) that decides the type of contraction, i.e., its indices appear as the argument of the contraction function. Here X_i is now the sum over the frequencies of all reservoir contractions which go over i -th resolvent (since contractions that start and end to the left and to the right cancel out).

Importantly, since on the left we always have \bar{G} (i.e. G^{q_1} with $q_1 = -$), the property (55) of the causal field of type \bar{G} is seen to guarantee the conservation of probability:

$$\text{Tr}_D \Sigma(z) = 0 \quad (69)$$

Another general property restricts the frequency dependence:⁶⁹

$$K \Sigma(z) K = -\Sigma(-z^*). \quad (70)$$

Here $K = K^{-1}$ is the anti-linear superoperator that effects the Hermitian conjugation of an *operator*, see App. G. This guarantees through Eq. (35)-(36) that the reduced density operator remains Hermitian during the time-evolution, i.e., $\rho(z) = \rho(-z^*)$. This property is guaranteed by the conjugation properties (120) and $KLK^{-1} = -L$. The above causal representation of the diagrammatic perturbation theory is very useful in general and is extended and applied extensively to time-dependent problems in Ref. 37. We now discuss the main advantages, which will be important for setting up the RG and the construction of a convenient supervector basis in Sec. (II C).

b. Wide-band limit First of all, the number of *contributing terms* is strongly reduced since the trivial ($\bar{\gamma}$) and non-trivial ($\tilde{\gamma}$) energy dependence of the contractions is automatically separated which in other representations would have to be done separately³⁰: Terms which do not contribute in the large bandwidth limit can be identified diagrammatically, using their diagram topology as illustrated in Fig. 1: all diagrams where one or more vertices are enclosed between contracted vertices \bar{G}_1 and \bar{G}_1 give contributions of order $\Gamma/D \ll 1$ or smaller and can be neglected. This can be proved by careful examination of the poles appearing when closing all integrals in the complex upper half plane, see Ref. 37, or argued in the time-representation.⁷⁰ As a result $\tilde{\gamma}$ contractions can only occur inside $\bar{\gamma}$ contractions in diagrams with more than 1 loop, see Fig. 1. This results in an exponential reduction in the number of contributing terms.

This feature also naturally suggests a starting point for a two stage RG approach. First, all terms which contain retarded contractions $\tilde{\gamma}$ can be integrated out explicitly by a one-step diagram resummation, leading to a renormalization of L discussed in Sec. (II B 4). The remaining diagrams will then contain only \bar{G} dot superoperators with non-trivial contractions $\bar{\gamma}$ which require a second, continuous RG. This approach will be worked out in detail in Sec. (III).

c. Infinite-temperature limit The choice of the supervector basis is simplified very much by noting that the superoperator structure of $\Sigma(z)$ is strongly restricted in the causal representation: in the wide-band limit (see above) there is only one diagram that starts with \bar{G} on the right and ends with \bar{G} on the left. We denote this special 1-loop diagram by $\tilde{\Sigma}$. Importantly, all other diagrams start and end with a \bar{G} vertex. The ω integral for

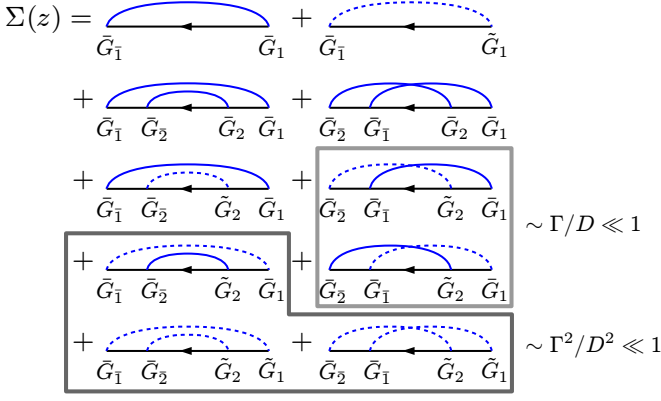


FIG. 1: 1- and 2-loop contributions to the self-energy kernel Σ . The full black line denotes the free dot propagation, the arrow indicates the ordering of superoperators (“late goes left”) in Laplace space that is “inherited” from the time-ordering. The curves denote the contraction of dot superoperators. Here the line connects the dot superoperators whose corresponding reservoir superoperator are contracted: $\langle GJ \dots GJ \rangle^R = \langle JJ \rangle^R G \dots G \rightarrow \bar{G} \dots \bar{G}$. This is in contrast to standard techniques where a contraction line connects contracted operators *themselves*. The full blue line denotes a Keldysh contraction $\tilde{\gamma}$ of two \bar{G} type vertices (cf. Eq. (64)) whereas the dashed blue contraction corresponds to the retarded contraction $\tilde{\gamma}$ of a \bar{G} with an earlier \bar{G} vertex to the right (cf. Eq. (63)). Diagrams with vanishing contractions, i.e., where \tilde{G} is contracted to the right (cf. Eq. (62)), are not drawn. Furthermore, the 2 loop diagrams in the light and dark gray boxes contain a $\tilde{\gamma}$ contraction enclosing $k = 1$ and respectively $k = 2$ other vertices and therefore scale with Γ^k/D^k and can be neglected in the wide band limit. In the causal representation only 5 diagrams remain, in contrast to formulations using “naive” super-operators³⁰ where 20 terms remain which partially cancel out.

the $\tilde{\Sigma}$ diagram can be performed by closing the integration contour in the upper/lower half-plane of the complex plane for $\eta = \mp$ and neglecting small corrections of order $\Gamma/D \ll 1$:

$$\tilde{\Sigma}(z) = \int d\omega \bar{G}_1 \frac{\tilde{\gamma}(\eta\omega)}{z - L - \eta\omega - \eta\mu_1} \bar{G}_{\bar{1}} = -i \frac{\Gamma_1}{2} \bar{G}_1 \bar{G}_{\bar{1}}. \quad (71)$$

where $\Gamma_1 = \Gamma_r$ for multi-index $1 = \eta, \sigma, r, \omega$. The self-energy $\tilde{\Sigma}$ has a clear physical meaning: it is the self-energy one obtains in the infinite temperature limit. This follows from its definition since all contractions $\tilde{\gamma} = 0$ for $T = \infty$, and $\tilde{\Sigma}$ is the only diagram in wide-band limit without this contraction function. As discussed in Sec. (IIB2) the retarded correlation function of the reservoirs $\tilde{\gamma}$ contains only spectral information (see the discussion of Eq. (63)) and is therefore independent of T . Therefore $\Sigma = \tilde{\Sigma}$ at $T = \infty$. Since at $T = \infty$ no energy scale matters any more, $\tilde{\Sigma}$ is independent of the QD frequency z or any QD energy scale in the problem as well as the cut-off D . The dependence on Γ remains, however: in the high-temperature limit all quantum dot

states are equally accessible by tunneling processes. This is described by the self-energy $\tilde{\Sigma}$.

The action of $\tilde{\Sigma}$ is very different from that of the Liouvillian L of the isolated QD: it is not super-Hermitian, as L is, but rather anti-Hermitian,

$$\tilde{\Sigma}^\dagger = -\tilde{\Sigma}, \quad (72)$$

which simply follows from the Hermitian conjugation property of the causal representation Eq. (57). For $T = \infty$ the effective Liouvillian thus reduces to $L(z) = L + \tilde{\Sigma}(z)$ with stationary state

$$\rho = \frac{1}{4} \mathbb{1}, \quad (73)$$

which is the maximal entropy state. This follows directly from the causal representation of $\tilde{\Sigma}$, Eq. (71), which shows that $\tilde{\Sigma}$ and \bar{G} share the same right eigenvectors, combined with the probability conservation Eq. (58). By the same argument it is clear that in this limit the current vanishes: anticipating the result Eq. (185) from Sec. (IIE), we find for the self-energy required for the current equals

$$\tilde{\Sigma}^r(z) = -i \frac{\Gamma_1}{2} \bar{G}_1 \bar{G}_{\bar{1}}|_{r_1=r} \quad (74)$$

where in the sum over 1 we exclude the reservoir index r . This also vanishes by Eq. (58) and therefore $\langle I^r \rangle = 0$.

d. Cut-off dependence and complete basis Another advantage of the causal representation is that the cut-off dependence of integrals in the *individual* diagrams that do contribute in the wide-band limit can be analyzed on the level of super-operators. These self-energy contributions seem to depend on the energy integral cut-off D . However, using the causal structure of the perturbation theory one can *explicitly* see that such dependence cancels out due to the superoperator structure of the vertices (i.e. the matrices multiplying the D -dependent contributions integrals vanish). The condition for this is that one keeps the complete basis of many body eigenstates of the dot Hamiltonian. To see this, however, one needs to consider the entire Liouville space, including all off-diagonal density operator elements and not restrict the analysis to only diagonal density matrix elements based on symmetry properties as is often done. The idea is best illustrated by considering the 1 loop contributions in Fig. 1. By Eq. (71) the 1-loop diagram with a $\tilde{\gamma}$ contraction is explicitly independent of D . For the $\tilde{\gamma}$ contraction of two \bar{G} type vertices

$$\int d\omega \bar{G}_1 \frac{\tilde{\gamma}(\eta\omega)}{z - L - \eta\omega - \eta\mu_1} \bar{G}_{\bar{1}}. \quad (75)$$

the D dependence enters through the most divergent part of the integral, obtained by neglecting L_D in the denominator. This part is thus proportional to the superoperator

$$\bar{G}_1 \bar{G}_{\bar{1}} = -\bar{G}_1 \bar{G}_1 = \bar{G}_2 \bar{G}_2 = 0, \quad (76)$$

which is identically zero due to anti-commutation relations (53) (we renamed the dummy summation indices $1 = \eta, \sigma, r, \omega$; in fact, only the summation over η_1 is relevant here). Importantly, this argument breaks down as soon as many-body states have been excluded from the Hilbert space basis, e.g., based on their large energy. For example, in the limit $U \rightarrow \infty$ one can exclude the doubly occupied QD state $|2\rangle$ and thereby eliminate Liouville-space elements with eigenvalues exceeding D . This simplifies the calculations, but for vertex operators projected onto this subspace the relation Eq. (76) does *not* hold anymore (since it is a non-linear relation). As a result the explicit D -dependence remains and does not cancel out from such expressions and the cut-off should be set to $D \sim U$ if one makes this approximation.

The above analysis can be extended to higher-order diagrams and one finds that also there the D dependence drops out. Here one uses that diagrams containing \tilde{G} vertices are always expressible in terms of the cut-off independent $\tilde{\Sigma}$ skeleton (see also Sec. (II B 4)). This analysis confirms observations made *after* explicit calculations of the kernel, e.g.⁴⁶ but on a very general level: the cut-off dependence can be completely assessed based on superoperator algebra, without the need for explicit calculation of the matrix-elements of Σ .

4. Finite temperature perturbation theory - elimination of infinite temperature contractions

As already mentioned at the end of Sec. (II B 3), the causal structure of the perturbation theory naturally suggests to proceed in two stages. We first eliminate all diagrams containing the retarded contraction $\tilde{\gamma}$, i.e. the skeleton diagram Eq. (71). Since this contraction always occurs isolated and inside other Keldysh contractions (c.f. Sec. (II B 3)), we can use (71) as a skeleton diagram and on each propagator line resum the series,

$$\frac{1}{z - \bar{L} - X} \sum_{n=0}^{\infty} \left(\tilde{\Sigma} \frac{1}{z - \bar{L} - X} \right)^n = \frac{1}{z - \bar{L} - X}, \quad (77)$$

thereby renormalizing the dot Liouvillian to

$$\bar{L} = L + \tilde{\Sigma}. \quad (78)$$

This is illustrated in Fig. 2. As discussed in Sec. (II B 3 c), $\tilde{\Sigma}$ equals the QD self-energy in the limit of infinite temperature in all reservoirs. As discussed in Sec. (II B 2) the retarded correlation function of the reservoirs contains only spectral information through the energies (see the discussion of Eq. (63)). The lack of energy dependence of $\tilde{\Sigma}$ reflects that in the high-temperature limit, all QD states are equally accessible via transitions induced by the electrodes. Physically, one expects that the Keldysh contractions $\tilde{\gamma}$, describing the non-trivial, temperature dependent part of the distribution function⁴⁷, should drop out in this limit.

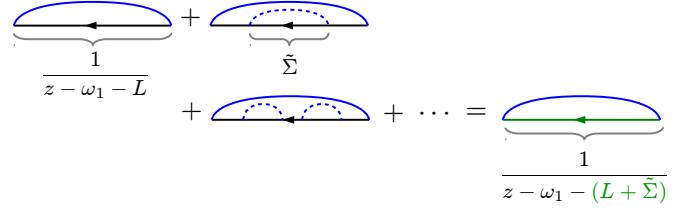


FIG. 2: Example resummation of diagrams with a single $\tilde{\gamma}$ loop (solid blue curve) and $n = 0, 1, 2, \dots$ skeleton diagrams $\tilde{\Sigma}$, resulting in 1 loop diagram with a renormalized propagator. Since in the wide-band limit $\tilde{\gamma}$ contractions (dashed blue curve) cannot contain other vertices this can be extended to any irreducible diagrams with any number of $\tilde{\gamma}$ loops.

In a second stage we calculate the finite temperature effects which are all incorporated through the self-energy $\tilde{\Sigma}(z)$. Its diagrammatic perturbation series has the same structure as for Σ , but is expressed entirely in terms of the contraction $\tilde{\gamma}$, the vertex \tilde{G} and the Liouvillian \bar{L} :

$$\tilde{\Sigma}(z) = \left(\prod_i \tilde{\gamma}_i \right)_{irr} \tilde{G}_1 \frac{1}{z - X_1 - \bar{L}} \tilde{G}_2 \dots \frac{1}{z - X_{n-1} - \bar{L}} \tilde{G}_n \quad (79)$$

Summing this renormalized perturbation theory, one obtains of course the same exact result Eq. (36) for the effective Liouvillian, which, however, is now decomposed in a new way:

$$L(z) = \bar{L} + \tilde{\Sigma}(z) \quad (80)$$

Since all contractions $\tilde{\gamma}$ have been eliminated simultaneously in the above two stage transformation of the perturbation series we previously referred to it as the discrete step of a renormalization group procedure²⁶. In the Anderson model in the wide-band limit only one skeleton diagram contributes to \bar{L} through $\tilde{\Sigma}$ and no renormalization of vertex \tilde{G} is required to eliminate $\tilde{\gamma}$.⁷¹ This discrete first step is a necessary preparation for the second step RG in which we will integrate out the $\tilde{\gamma}$ contractions as well in a continuous RG-flow. In contrast to the \tilde{G} , the vertices \tilde{G} do not share the left zero eigenvector $|Z_L\rangle$ with the effective Liouvillian, cf. Eq. (86) below. If they were still present during a process of continuous renormalization, this would lead to divergences whenever the zero eigenvalue of L would appear in the resolvent $(z - X - L)^{-1}$, see also Ref. 48. The vertices \tilde{G} *must* therefore be integrated out before any continuous RG can be formulated. This is a characteristic feature of an RG for dissipative systems that exhibit stationary states (zero eigenvectors). The causal structure of the renormalized perturbation theory (79) makes clear that this elimination has been achieved: the zero eigenvalue term of \bar{L} always drops out due to the presence of \tilde{G} 's adjacent to the propagator $(z - X - \bar{L})^{-1}$.

At this point we can already make an observation which is important for the construction of an explicit expansion for the effective Liouvillian $L(z)$ in Sec. (II C 5):

no continuous RG scheme, which reorganizes the perturbation series Eq. (79) involving only \bar{G} vertices, can ever generate terms of the form $\bar{G}\dots\bar{G}$, i.e., with a \bar{G} superoperator standing on the far right. In the notation of Sec. (II C 5) this implies that the coefficient of the term $|Z_R\rangle\langle Z_R|$ in the expansion Eq. (137) is not changed during a RG flow (or any non-perturbative approximation to the series (79)).

What was done so far can be understood as a formal expansion around the infinite-temperature limit as a reference point. We start from the exact (in the wide-band limit) solution for the infinite temperature and then reformulate perturbation theory for the finite temperature (including also the zero-temperature limit which we are going to consider) such that it explicitly contains the infinite-temperature limit. Note that this is *not* to be confused with the expansion in powers of T : we formally expand in the Keldysh distribution functions functions (contractions) $\bar{\gamma}$. Actually one meets this expansion already in most standard applications of the generalized master equation when calculating the kernel (“rates”) such that they correspond to Fermi’s Golden Rule. In this case one calculates only the corrections to $\tilde{\Sigma}$ to the first order in $\bar{\gamma}$. Here we reformulated the exact perturbation theory around this reference point in order to perturbatively calculate the important higher order corrections to that result. To this end we performed a second natural step by exactly incorporating the “trivial” infinite-temperature fluctuations into a redefinition of the Liouvillian. We will develop an RT-RG approach in order to incorporate “non-trivial” finite temperature fluctuations also non-perturbatively. This second step is the crucial starting point for it since this step prevents a serious technical problem related to the zero-eigenvalue from appearing, see Sec.III A and Sec.II C 5.

C. Basis of the Anderson-model in Liouville Fock-space

To obtain explicit RG equations that can be efficiently solved numerically we need to construct a basis that exploits the advantages of (i) selection rules for the self-energy superoperator induced by the global symmetries (ii) the causal structure of $\bar{\Sigma}(z)$ and (iii) fermion-parity superselection rule. Again, these can be useful in perturbation theory as well.

1. Liouville space bra-ket formalism

By Eq. (68) and (79) the QD self-energy Σ ($\bar{\Sigma}$) is a functional of the QD Liouvillian L (\bar{L}) and the vertex superoperators G^q (\bar{G}) which linearly act on the QD Hilbert space of many-body states. To explicitly calculate these it is convenient to introduce a “bra-ket” formalism analogous to that of standard quantum mechanics: we write a 16-component supervector (representing

an operator acting on the 4-dimensional Hilbert space) as a rounded superket $A = |A\rangle$ and introduce its dual supervector $\langle A| \bullet = \text{Tr}(A^\dagger \bullet)$ as a linear functional acting on operators. An operator A is orthogonal to B if $\langle A|B\rangle = \text{Tr}(A^\dagger B) = 0$ (see for example Ref. 49). The dual vector may be written as the Hermitian conjugate of a superket:

$$\langle A| = |A\rangle^\dagger, \quad |A\rangle = \langle A|^\dagger \quad (81)$$

where \dagger is not to be confused with the supervector corresponding to the Hermitian conjugate of the operator A , $A^\dagger = |A^\dagger\rangle$. An operator basis $|A_i\rangle$, $i = 1, \dots, 16$ of mutually orthonormal operators $\text{Tr}(A_i^\dagger A_j) = \delta_{i,j}$ is complete if any operator B can be expanded as $B = \sum_i (A_i|B) A_i$ with coefficients $(A_i|B) = \text{Tr}(A_i^\dagger B)$. Any superoperator S acting on such operators can then be expressed in general as a sum of 256 terms:

$$S = \sum_{i,j=1}^{16} (A_i|S|A_j) |A_i\rangle\langle A_j|. \quad (82)$$

2. Liouville Fock-space basis

To maximally reduce the number of terms in the expansions of superoperators (82) we now exploit the close analogy of Liouville field superoperators in the causal representation to the usual fermionic field operators. In this section we first construct a suitable orthonormal basis of operators (supervectors) in which any QD operator can be expanded. In Sec. (II C 3) we analyse their transformation properties under the symmetry transformations of the Anderson model. In this basis we can then easily construct superoperator expansions compatible with these symmetries in Sec. (II C 5).

We start from the key property (55) of the vertex operators in the causal representation. In bra-ket notation the trace operation

$$\text{Tr}_D \bullet = \text{Tr}_D \mathbb{1} \bullet = 2 \langle Z_L| \quad (83)$$

corresponds to the action of the dual on the normalized supervector

$$|Z_L\rangle = \frac{1}{2} \mathbb{1}. \quad (84)$$

Therefore, by Eq. (55), $\langle Z_L|$ is a left zero super-eigenvector of \bar{G} and by (57) it follows that $|Z_L\rangle$ must be a right super-eigenvector of \bar{G} :

$$\langle Z_L|\bar{G}_1 = 0 \quad \bar{G}_1|Z_L\rangle = 0 \quad (85)$$

We can formally consider the state annihilated by operators \bar{G} as a “super-vacuum”. (Note that the “super-vacuum” state is the most symmetric dot operator similar to standard field theories where the vacuum state usually is the most symmetric one). This vacuum supervector is proportional to the physical infinite temperature

density operator (cf. Eq. (73)) with maximal von Neumann entropy $S = -\rho \ln(\rho)$. It is then also natural to construct the corresponding right zero super-eigenvector of \tilde{G}_1 whose dual is the left zero super-eigenvector of \tilde{G}_1 :

$$\tilde{G}_1|Z_R\rangle = 0 \quad (Z_R|\tilde{G}_1 = 0 \quad (86)$$

Since \tilde{G}_1 is a non Hermitian superoperator these eigen-supervectors are not simply related by Hermitian conjugation in Liouville space, $|Z_R\rangle \neq (Z_L|^\dagger$ (cf. Eq. (81)).

The operator Z_R will be found to play a key role throughout this work. In App. E we discuss its many interesting properties, including its similarity to Grassmann numbers and its relation to the spin- and charge rotations of Sec. (II C 3). To construct $|Z_R\rangle$ we now exploit the close analogy to regular field operators: \tilde{G}_1 is a creation operator in *Liouville Fock-space*, since its Hermitian super-conjugate \tilde{G}_1^\dagger annihilates the super-vacuum state $|Z_L\rangle$ by Eq. (85). The state annihilated by \tilde{G}_1 is therefore simply the maximally occupied state in the QD Liouville Fock-space, starting from the vacuum:⁷²

$$|Z_R\rangle = \prod_{\sigma} \left(\prod_{\eta} \tilde{G}_{\eta\sigma} \right) |Z_L\rangle \quad (87)$$

As for the regular fermionic field operators, action of creation operators preserves the normalization: this follows directly using Eq. (81) and the anticommutation relations (53):

$$\begin{aligned} (Z_R|Z_R) &= (Z_L| \prod_{\sigma} \left(\prod_{\eta} \tilde{G}_{\eta\sigma} \tilde{G}_{\eta\sigma} \right) |Z_L) \\ &= (Z_L|Z_L) = 1 \end{aligned} \quad (88)$$

Note that by Eq. (53) reordering the \tilde{G} 's in the definition of Z_R only amounts to an unimportant redefinition of the overall sign. Using Eq. (51) we can write for the explicit action on any operator (denoted by \bullet) with even fermion-parity

$$\tilde{G}_{+\sigma} \tilde{G}_{-\sigma} \bullet = \frac{1}{2} ([n_{\sigma}, \bullet]_+ - 1 + d_{\sigma}^\dagger \bullet d_{\sigma} - d_{\sigma} \bullet d_{\sigma}^\dagger). \quad (89)$$

Inserting this into Eq. (87) we obtain

$$|Z_R\rangle = \frac{1}{2} \prod_{\sigma} (2n_{\sigma} - 1). \quad (90)$$

Since $(Z_L|$ is a left eigenvector of \tilde{G} (cf. Eq. (85)) we immediately see that the two zero eigen supervectors are orthonormal, $(Z_L|Z_R) = 0$.⁷³ Therefore, it is natural to include $|Z_R\rangle$ into the orthonormal Liouville space basis. By successively acting on the super-vacuum state $|Z_L\rangle$ we can generate more normalized, orthogonal operators. There are in total 8 bosonic operators:

$$|Z_L\rangle = \frac{1}{2} \mathbb{1}, \quad (91)$$

$$|\chi_{\sigma}\rangle = \tilde{G}_{+\sigma} \tilde{G}_{-\sigma} |Z_L\rangle, \quad (92)$$

$$|T_{\eta}\rangle = \eta \tilde{G}_{\eta\uparrow} \tilde{G}_{\eta\downarrow} |Z_L\rangle, \quad (93)$$

$$|S_{\sigma}\rangle = \tilde{G}_{+\sigma} \tilde{G}_{-\sigma} |Z_L\rangle, \quad (94)$$

$$|Z_R\rangle = \tilde{G}_{+\uparrow} \tilde{G}_{-\uparrow} \tilde{G}_{+\downarrow} \tilde{G}_{-\downarrow} |Z_L\rangle, \quad (95)$$

and there are 8 fermionic operators:

$$\begin{aligned} |\alpha_{+,\sigma}^+\rangle &= \tilde{G}_{+\sigma} |Z_L\rangle, \\ |\alpha_{-,\sigma}^+\rangle &= \sigma \tilde{G}_{-\sigma} |Z_L\rangle, \\ |\alpha_{+,\sigma}^-\rangle &= \tilde{G}_{+\sigma} \tilde{G}_{+\sigma} \tilde{G}_{-\sigma} |Z_L\rangle, \\ |\alpha_{-,\sigma}^-\rangle &= \sigma \tilde{G}_{-\sigma} \tilde{G}_{-\sigma} \tilde{G}_{+\sigma} |Z_L\rangle. \end{aligned} \quad (96)$$

The labeling of these basis super vectors is motivated by their explicit expressions in terms of the field operators $d_{\sigma}, d_{\sigma}^\dagger$ (see Eq. (103)-(113)) and their behavior under symmetry transformations which will be discussed in the next section. We see that the index ν of the operators $|\alpha_{\nu,\sigma}^\nu\rangle$ only has a meaning in Liouville space: it distinguishes $\nu = +$ states with one excess excitation relative to the super-vacuum $|Z_L\rangle$ (super-particles), from $\nu = -$ states with one deficit particle with respect to the maximally occupied super-state $|Z_R\rangle$ (super-holes). By construction these 16 operators form a complete orthonormal basis of the QD Liouville space. This basis includes only one operator which has non-zero trace, namely $|Z_L\rangle = \frac{1}{2} \mathbb{1}$. Since all other supervectors are orthogonal to $|Z_L\rangle$, their corresponding operators are traceless according to Eq. (83).

We emphasize that the choice of basis supervectors $|Z_L\rangle$ and $|Z_R\rangle$ relies on a general physical property of the problem, the probability conservation (cf. Eq. (69) and Eq. (85)). The choice of the signs of the remaining operators, however, is motivated by considering the symmetry transformations of the Anderson model. These will be discussed in the next section. We note that similar Fock-space and superoperators were introduced by Prosen³¹, see App.(C).

Before we proceed, we emphasize the necessity of working with a complete basis for the QD Liouville space, which includes operators that are *non-diagonal* in both spin and/or charge quantum numbers. In perturbation theory, one can disregard all matrix elements of the self-energy $\Sigma(z)$ involving the latter operators (cf. Sec. (II B 3)), due to the conservation laws (101). However, the inner part of a diagram contributing to $\Sigma(z)$ (i.e. a virtual intermediate state) the states are less restricted by the conservation laws, requiring the matrix elements of the vertices and the QD Liouvillian L between all of the above off-diagonal operators.⁷⁴ In the RT-RG that we set up below such matrix elements involving odd fermion parity operators cannot be avoided for $\Sigma(z)$ as well since one needs to describe the *renormalization of all virtual intermediate states*, both fermionic and as well as bosonic ones.

3. Irreducible transformation under symmetry operations

For the total system of QD and reservoirs both the charge and spin component along the magnetic field are conserved, cf. Eq. (25)-(26). The particle number conser-

vation on the dot is conveniently expressed using charge-polarization operator

$$T_z = \frac{1}{2}(n - 1) \quad (97)$$

which measures the difference of the occupation probabilities of the empty and double occupied QD states $|0\rangle$ and $|2\rangle$. It follows from Eq. (25) and (26) that the dot superoperators for charge polarization (cf. Eq. (43)) and spin,

$$L^{T_z} = [T_z, \bullet] = \frac{1}{2}L^n, \quad (98)$$

$$L^{S_z} = [S_z, \bullet], \quad (99)$$

respectively, commute with each other as well as with the Liouvillian L and the self-energy $\Sigma(z)$. Therefore the effective Liouvillian $L(z) = L + \Sigma(z)$ which determines the time-evolution of the reduced density operator conserves these super-observables (see App. F for a derivation):

$$[L(z), L^{T_z}]_- = 0, \quad (100)$$

$$[L(z), L^{S_z}]_- = 0. \quad (101)$$

Thus $L(z)$ can be simultaneously block diagonalized with the superoperators for charge- and spin polarization and they have common super-eigenstates. In the basis of Sec. (II C 3) the initial dot Hamiltonian operator Eq. (1) has the form:

$$H = (2\epsilon + \frac{U}{2})|Z_L\rangle + \frac{U}{2}|Z_R\rangle + 2\left(\epsilon + \frac{U}{2}\right)|T_z\rangle + B|S_z\rangle \quad (102)$$

In two cases the total system has a higher symmetry group: for $\epsilon = -U/2$ and $\mu_L = \mu_R$ it exhibits *full* charge-rotation symmetry and for $B = 0$ full spin-rotation symmetry. These full symmetry groups are obtained by adding S_x and S_y operators to S_z (c.f. Eq. (106)) to obtain the SU(2) spin-algebra and adding T_x and T_y to T_z (c.f. Eq. (110)) to obtain another SU(2) algebra generating “charge rotations” (see below). The construction of *superoperators* that transform in the simplest possible way under these symmetry operations is greatly simplified by first constructing basis operators that can be classified with respect to the corresponding irreducible representations. Importantly, the Liouville-Fock basis (91)-(96) that we constructed using the causal field superoperators is already very close to a symmetry-adapted basis and we now merely complete the classification. We first group these operators according to their even or odd fermion parity, and refer to these *bosonic* resp. *fermionic operators*. We subsequently classify them according to the transformation behavior under the two SU(2) rotation groups as an irreducible tensor (ITO). This allows us to identify which supervectors correspond to diagonal operators acting on the Hilbert space, either with respect to the QD charge and/or spin: in perturbation theory one only needs the self-energies connecting such diagonal components of the density matrix. In the RG we set up

below this is no longer true but it is important to single out this block of matrix elements of $\Sigma(z)$, $\bar{\Sigma}(z)$ and $L(z)$.

We have 8 bosonic operators with integer charge and spin ITO ranks:

- The zero-eigenvectors of the vertex superoperators are scalars (rank 0 spin- and charge-ITO) with respect to both spin and charge rotations since the zero-eigenvalue equations Eq. (85)-(86) are invariant under these transformations. They are therefore charge- and spin-diagonal operators. This is also clear from their explicit form in terms of the Casimir operators of the spin- ($S^2 = \sum_i S_i^2$) and charge- rotation ($T^2 = \sum_i T_i^2$) SU(2) Lie algebras:

$$|Z_L\rangle = \frac{1}{2}\mathbb{1} = \frac{4}{3}(T^2 + S^2) \quad (103)$$

$$|Z_R\rangle = 2n_\uparrow n_\downarrow - n + \frac{1}{2}\mathbb{1} = \frac{2}{3}(T^2 - S^2) \quad (104)$$

- The generators of rotations in spin space:

$$|S_0\rangle = \frac{1}{\sqrt{2}} \sum_\sigma \sigma |\chi_\sigma\rangle = \frac{1}{\sqrt{2}} \sum_\sigma \sigma n_\sigma$$

$$|S_\sigma\rangle = d_\sigma^\dagger d_\sigma, \quad \sigma = \uparrow, \downarrow \quad (105)$$

Operators: $-|S_+ \rangle, |S_0 \rangle, |S_- \rangle$ transform as the components of a rank 1 spin-ITO (vector), i.e., simpler than the more familiar Cartesian components of the spin-operator,

$$|S_{x,y}\rangle = \frac{1}{2(i)}(|S_+ \rangle \pm |S_- \rangle), \quad |S_z\rangle = \frac{1}{\sqrt{2}}|S_0\rangle \quad (106)$$

which satisfy $[|S_i \rangle, |S_j \rangle] = i\epsilon_{ijk}|S_k \rangle$. They transform as a rank 0 ITO (scalar) with respect to charge-rotations and are therefore charge-diagonal.

- The generators of rotations in charge space:

$$|T_0\rangle = \frac{1}{\sqrt{2}} \sum_\sigma |\chi_\sigma\rangle = \frac{1}{\sqrt{2}}(n - 1) \quad (107)$$

$$|T_+\rangle = d_\uparrow^\dagger d_\downarrow^\dagger; \quad (108)$$

$$|T_-\rangle = d_\downarrow d_\uparrow \quad (109)$$

Operators: $-|T_+ \rangle, |T_0 \rangle, |T_- \rangle$ transform as a rank one ITO (vector) under rotations in charge space, and as a rank 0 ITO (scalar) with respect to spin rotations. Therefore they are all spin-diagonal. These are more convenient than the Cartesian components

$$|T_{x,y}\rangle = \frac{1}{2(i)}(|T_+ \rangle \pm |T_- \rangle), \quad |T_z\rangle = \frac{1}{\sqrt{2}}|T_0\rangle \quad (110)$$

satisfying the SU(2) algebra $[|T_i \rangle, |T_j \rangle] = i\epsilon_{ijk}|T_k \rangle$. In contrast to the spin-operators, here the indices x, y, z are not related to the axes in the real space, but merely label the components of the SU(2) generators.

In the bosonic sector we can thus use either

$$|\chi_\sigma\rangle = n_\sigma - \frac{1}{2}\mathbb{1} = \frac{1}{\sqrt{2}}[|T_0\rangle + \sigma|S_0\rangle] \quad (111)$$

or $|S_0\rangle$ and $|T_0\rangle$ as basis vectors. Only the latter two are adapted to charge- and spin- rotation symmetry, but the former two allow for greater notational simplicity. Both will be used.

The other half of the QD Liouville space is spanned by 8 fermionic operators with half-integer charge and spin ITO rank:

- The fermionic operators, denoted by $\alpha_{\eta,\sigma}^\nu$, act in three subspaces of dimension two labeled by $\sigma = \pm$ (spin), $\eta = \pm$ (particle-hole) and, additionally, $\nu = \pm$. These basis operators are ITOs of rank $\frac{1}{2}$ with respect to both charge (η) and spin rotations (σ). For $\nu = +$ these are the rank $\frac{1}{2}$ spin-ITOs constructed from creation and annihilation operators:

$$|\alpha_{+,\sigma}^+\rangle = \frac{1}{\sqrt{2}}d_\sigma^\dagger, \quad |\alpha_{-,\sigma}^+\rangle = \frac{1}{\sqrt{2}}\sigma d_{\bar{\sigma}}, \quad (112)$$

$$|\alpha_{+,\sigma}^-\rangle = \sqrt{2}|Z_R\alpha_{+,\sigma}^+\rangle, \quad |\alpha_{-,\sigma}^-\rangle = \sqrt{2}|Z_R\alpha_{-,\sigma}^+\rangle. \quad (113)$$

All these operators are both charge- and spin off-diagonal. We give their above explicit form to emphasize that there is an additional set of fermionic operators in the charge off-diagonal subspace which is linearly independent of the standard field operators d_σ and d_σ^\dagger , see the discussion of the index ν in Eq. (96). Noting the property $(2Z_R)^2 = \mathbb{1}$ we find the following explicit relation between these two sets:

$$|\alpha_{\eta,\sigma}^\nu\rangle = 2Z_R|\alpha_{\bar{\eta},\sigma}^{\bar{\nu}}\rangle \quad (114)$$

where as usual $\bar{\nu} = -\nu$.

The above simple transformation behavior of the basis supervectors motivates all the relative signs we anticipated in writing Eq. (91)-(96). The basis is therefore completely fixed up to irrelevant phases by general physical properties (probability conservation, symmetries) together with the supervector normalization. Table I summarizes the transformation properties.

Finally, we note the transformation behavior under the action of the Hermitian conjugation K (see Eq. (70)). For all diagonal basis operators $D = Z_L, Z_R, \chi_\sigma, S_0, T_0$

$$K|D\rangle = |D\rangle \quad (115)$$

whereas for the off-diagonal operators

$$K|S_\pm\rangle = |S_\mp\rangle, \quad (116)$$

$$K|T_\pm\rangle = |T_\mp\rangle \quad (117)$$

$$K|\alpha_{\eta,\sigma}^\nu\rangle = -\nu\eta\sigma|\alpha_{\bar{\eta},\bar{\sigma}}^\nu\rangle \quad (118)$$

4. Expansion of the vertices

The calculation of bra-ket representation of the vertex operators in the basis Eq. (91)-(96) reduces entirely to

Operator	fermion -parity	S -ITO (rank,index)	T -ITO (rank, index)	
$ Z_i\rangle$	+	(0,0)	(0,0)	$i = L, R$
$ S_m\rangle$	+	(1, m)	(0,0)	$m = 0, \pm 1$
$ T_m\rangle$	+	(0,0)	(1, m)	$m = 0, \pm 1$
$ \alpha_{\eta,\sigma}^\nu\rangle$	-	($\frac{1}{2}, \frac{\sigma}{2}$)	($\frac{1}{2}, \frac{\eta}{2}$)	$\eta, \sigma = \pm 1$

TABLE I: Fermion-parity and irreducible transformation behavior of basis operators under spin and charge rotations. Schematically denoting these operators by $|s, m_s; t, m_t\rangle$, these transform as (i) spin-irreducible tensor operators (S -ITOs) with rank s and index m_s , $L^{S_z}|s, m_s; t, m_t\rangle = m_s|s, m_s; t, m_t\rangle$ and $L^{S_\pm}|s, m_s; t, m_t\rangle = \sqrt{s(s+1) - m_s(m_s \pm 1)}|s, m_s \pm 1; t, m_t\rangle$. and (ii) as charge-ITOs (T -ITOs) with rank t and m_t , $L^{T_z}|s, m_s; t, m_t\rangle = m_t|s, m_s; t, m_t\rangle$ and $L^{T_\pm}|s, m_s; t, m_t\rangle = \sqrt{t(t+1) - m_t(m_t \pm 1)}|s, m_s; t, m_t \pm 1\rangle$. All zero-index S -ITOs (T -ITOs) correspond to operators acting on Hilbert space that are diagonal in spin (charge).

the calculation of

$$\begin{aligned} \tilde{G}_{+\sigma} = & |\alpha_{+,\sigma}^+\rangle(Z_L + \sigma|Z_R\rangle)(\alpha_{-,\sigma}^-| \\ & + \sigma|T_+\rangle)(\alpha_{+,\sigma}^+| + |\alpha_{-,\sigma}^-|)(T_-| + |\alpha_{+,\sigma}^-|)(\chi_{\bar{\sigma}}| \\ & - \sigma|\chi_\sigma\rangle)(\alpha_{-,\sigma}^+| + \sigma|S_\sigma\rangle)(\alpha_{-,\sigma}^+| - |\alpha_{+,\sigma}^-|)(S_{\bar{\sigma}}| \end{aligned} \quad (119)$$

This is easily performed using the 2nd quantization technique that we introduced in Liouville-Fock space, i.e., using algebra rather than the explicit matrix representations of Sec. (II C 3). All other vertices follow from general relations. First, using the transformation under Hermitian-conjugation (see Eq. (70))

$$\tilde{G}_{\eta\sigma} = (-1)^{L^n+1} K \tilde{G}_{\bar{\eta}\sigma} K \quad (120)$$

the result for opposite charge index $\eta = -$ follows using the transformation properties Eq. (115)-(118):

$$\begin{aligned} \tilde{G}_{-\sigma} = & -\sigma|\alpha_{-,\sigma}^+\rangle(Z_L - |Z_R\rangle)(\alpha_{+,\sigma}^-| \\ & - \sigma|\alpha_{+,\sigma}^-|)(T_+| - |T_-|)(\alpha_{+,\sigma}^+| + \sigma|\alpha_{-,\sigma}^-|)(\chi_{\bar{\sigma}}| \\ & - |\chi_\sigma\rangle)(\alpha_{+,\sigma}^+| - |S_{\bar{\sigma}}\rangle)(\alpha_{+,\sigma}^+| + \sigma|\alpha_{-,\sigma}^-|)(S_{\bar{\sigma}}| \end{aligned} \quad (121)$$

The vertex superoperators $\tilde{G}_{\eta\sigma}$ can be obtained from $\tilde{G}_{\bar{\eta}\sigma}$ by Hermitian conjugation in the Liouville space using Eq. (57). In the Liouville bra-ket formalism this simply means that we can interchange bra and ket vectors in the expansions Eq. (119) and Eq. (121) to obtain $\tilde{G}_{\mp\sigma}$.

We point out that under the 2-loop RG-flow to be discussed in Sec. (III) the structure of the vertex operators is changed and the above relations cease to hold (\tilde{G} will be modified whereas \tilde{G} is not changed, implying that Eq. (57) breaks down). However, in Sec. (IV C) we show how a such vertex corrections can be incorporated effectively into the flow of the effective Liouvillian *only*, allowing us to work with the “bare” vertices with the nice properties discussed above. One property of the bare vertices that remains valid under the RG-flow is

$$(\alpha_{\eta\sigma}^+|\tilde{G}_1 \propto |Z_L| \text{ or } 0, \quad (122)$$

$$\tilde{G}|\alpha_{\eta\sigma}^-\rangle \propto |Z_R\rangle \text{ or } 0, \quad (123)$$

Eq. (122) follows since $|\alpha_{\eta\sigma}^+\rangle$ is obtained from the vacuum $|Z_L\rangle$ by the action of a single creation superoperator (cf. Eq. (96)). Using Eq. (57)

$$|\alpha_{\eta,\sigma}^+\rangle = \sigma^{(1-\eta)/2} (Z_L | \tilde{G}_{\bar{\eta},(\eta\sigma)} \rangle. \quad (124)$$

When inserted in the left hand side of Eq. (122) this \tilde{G} can be anticommutated past the \tilde{G} using Eq. (53) and the super vacuum property $(Z_L | \tilde{G} = 0$ (see Eq. (85)). Analogously Eq. (123) follows by noting that Eq. (96) for the $|\alpha_{\eta,\sigma}^-\rangle$ can be rewritten as a single destruction superoperator acting on the maximally occupied state in Liouville-Fock space:

$$|\alpha_{\eta,\sigma}^-\rangle = \bar{\sigma}^{(1-\eta)/2} \tilde{G}_{\eta,(\eta\sigma)} |Z_R\rangle. \quad (125)$$

Commuting the \tilde{G} to the left and using $\tilde{G}|Z_R\rangle = 0$ (see Eq. (86)) on the right of each term we obtain Eq. (123).

5. Expansion of the effective Liouvillian

a. Causal structure By the general properties (85) and (86) the vertices must have an expansion of the form (confirmed by the explicit results Eq. (119)-(121)):

$$\tilde{G} = ..|Z_R\rangle(\bullet| + ..|\bullet\rangle(Z_L| + \dots \quad (126)$$

$$\tilde{G} = ..|\bullet\rangle(Z_R| + ..|Z_L\rangle(\bullet| + \dots \quad (127)$$

where the remaining terms involve neither Z_L or Z_R . Therefore the terms in the expansion of the effective Liouvillian involving these vectors are strongly restricted. Combined with the general causal structure of the perturbative series, i.e., the way \tilde{G} and \tilde{G} can appear, this imposes further -constraints (cf. Sec. (II B 3)):

- Terms of the form $|Z_L\rangle(\bullet|$ are prohibited by probability conservation, since otherwise the trace condition (69) would be violated:

$$(Z_L | \bar{L} = (Z_L | L(z) = (Z_L | \Sigma(z) \quad (128)$$

$$= (Z_L | \tilde{\Sigma} = (Z_L | \bar{\Sigma}(z) = 0 \quad (129)$$

This is guaranteed by the causal structure which requires that the leftmost vertex is always of the type \tilde{G} , with expansion Eq. (126).

- Terms of form $|\bullet\rangle(Z_R|$ can only appear due to the diagrams collected in $\tilde{\Sigma} = -i\frac{1}{2}\Gamma_1 \tilde{G}_1 \tilde{G}_{\bar{1}}$. Expanding Eq. (71) in the basis (91)-(96) one finds that only the term $|Z_R\rangle(Z_R|$ with coefficient $-i4\Gamma$ can appear, see also Eq. (135). Importantly, this implies that $|Z_R\rangle$ is a right eigenvector of both \bar{L} as well as the *exact* effective Liouvillian $L(z)$ and the kernel $\Sigma(z)$, see discussion of Eq. (137):

$$\bar{L}|Z_R\rangle = L(z)|Z_R\rangle = \Sigma(z)|Z_R\rangle \quad (130)$$

$$= \tilde{\Sigma}|Z_R\rangle = -i4\Gamma|Z_R\rangle \quad (131)$$

In contrast,

$$\bar{\Sigma}(z)|Z_R\rangle = 0 \quad (132)$$

Note that this eigenvector and eigenvalue are independent of the QD frequency z .

- The term $|Z_R\rangle(Z_L|$ is not forbidden by general considerations. However, such terms always drop out in the calculations of the transport current that interest us here (see Sec. (II E)). This happens because in all required expressions the renormalized Liouvillian \bar{L} , parametrized as (137), is evaluated between two \tilde{G} vertices c.f. Eq. (79). Therefore, by Eq. (126) the term $|Z_R\rangle(Z_L|$ with coefficient ζ always drops out. We emphasize, however, that ζ does enter into the stationary state (cf. Eq. (152)) and other physical quantities, such as the average dot energy, and may therefore be important for, e.g., thermal transport problems.
- Terms of the form $|\alpha_{\eta,\sigma}^+\rangle(\bullet|$ and $|\bullet\rangle(\alpha_{\eta,\sigma}^-|$ can appear *only* in the bare Liouvillian $L = [H, \bullet]$ or the infinite-temperature kernel $\tilde{\Sigma} = -i\frac{1}{2}\Gamma_1 \tilde{G}_1 \tilde{G}_{\bar{1}}$, but *not* in the non-trivial kernel $\bar{\Sigma}(z)$:

$$(\alpha_{\eta,\sigma}^+ | \bar{\Sigma}(z) = 0 \quad (133)$$

$$\bar{\Sigma}(z) | \alpha_{\eta,\sigma}^- \rangle = 0 \quad (134)$$

Both relations follow from the fact that $\bar{\Sigma}(z)$ contains *only* vertices of the type \tilde{G} in expansion Eq. (79). Eq. (133) follows from Eq. (122) applied to Eq. (79) and using $(Z_L | \bar{L} = 0$ and $(Z_L | \tilde{G} = 0$, the vacuum property (see Eq. (85)). Analogously Eq. (134) follows from Eq. (123) using our general result $\bar{L}|Z_R\rangle = -i4\Gamma|Z_R\rangle$ (see above) and then $\tilde{G}|Z_R\rangle = 0$ (see Eq. (86)). Eq. (133)-(134) allow us to make general predictions about the excitation spectrum of the *exact* dot Liouvillian, $L(z)$, see Sec. (II D 3) and (III B 4).

b. Spin and charge rotation symmetry We now first expand the infinite-temperature self-energy $\tilde{\Sigma}$ and the renormalized Liouvillian \bar{L} in the basis (91)-(96). Substituting the above bra-ket expansions of the superoperators \tilde{G}_1 and $\tilde{G}_{\bar{1}}$ into Eq. (71) we get:

$$\begin{aligned} \tilde{\Sigma} = & -i\Gamma \left[4|Z_R\rangle(Z_R| + 2 \sum_{\sigma=\pm} |\chi_\sigma\rangle(\chi_\sigma| \right. \\ & + 2 \sum_{\sigma=\pm} |T_\sigma\rangle(T_\sigma| + 2 \sum_{\sigma=\pm} |S_\sigma\rangle(S_\sigma| \\ & \left. + \sum_{\sigma=\pm} \sum_{\eta=\pm} \sum_{\nu=\pm} (2-\nu) |\alpha_{\eta,\sigma}^\nu\rangle(\alpha_{\eta,\sigma}^\nu| \right] \end{aligned} \quad (135)$$

Clearly, $\tilde{\Sigma}$ is explicitly anti-Hermitian in the superoperator sense (cf. Eq. (72)). Combining this with the bare dot Liouvillian, obtained by expanding the commutator

$L = [H, \bullet]$ of (102) we obtain

$$\begin{aligned} \bar{L}_\Lambda|_{\Lambda=\infty} &:= \bar{L} = L + \tilde{\Sigma} = -i4\Gamma|Z_R\rangle\langle Z_R| - 2i\Gamma\chi_0 \\ &+ \sum_\sigma \left[(\sigma B - 2i\Gamma)|S_\sigma\rangle\langle S_\sigma| + (\sigma(U + 2\epsilon) - 2i\Gamma)|T_\sigma\rangle\langle T_\sigma| \right. \\ &+ \sum_{\eta,\nu} \left(\eta \left(\epsilon + \frac{U}{2} \right) + \sigma \frac{B}{2} - i(2 - \nu)\Gamma \right) |\alpha_{\eta,\sigma}^\nu\rangle\langle \alpha_{\eta,\sigma}^\nu| \\ &\left. + \frac{U}{2} \sum_{\eta,\nu} |\alpha_{\eta,\sigma}^\nu\rangle\langle \alpha_{\eta,\sigma}^\nu| \right], \end{aligned} \quad (136)$$

where for reference we introduced the notation $\bar{L}_\Lambda|_{\Lambda=\infty} := \bar{L}$ of Sec. (III). All non-zero eigenvalues of \bar{L} have negative imaginary parts, thereby automatically regularizing all resolvents that can appear $\bar{G}(z - \bar{L} - X)^{-1}\bar{G}$ in the perturbation theory for $\tilde{\Sigma}(z)$ for $z \rightarrow i0$. This can be seen explicitly since all terms are already in diagonal superoperator form, with the exception of the odd-fermion terms (the last two lines in Eq. (136)) whose eigenvalues are given below (set $\Delta F_{\eta,\sigma}^-,+ = 0$ in Eq. (164)). Note that the right zero eigenvector of $\bar{L}_{\Lambda=\infty}$ is $\frac{1}{2}|Z_L\rangle$ – it is the only basis vector missing in Eq. (136) – in agreement with the result (73) in Sec. (IIB 4). We further note that the infinite temperature kernel $\tilde{\Sigma}$ (135) contributes terms to Eq. (136) that are diagonal in the index ν , whereas contributions off-diagonal in ν are produced in Eq. (136) by the Coulomb interaction included in the bare dot Liouvillian L . We will show in Sec. (IIIB 4) that the continuous RT-RG to be set up in the next section produces only ν -off-diagonal contributions in the effective Liouvillian $L(z)$ with important consequences.

We can now write down the exact *form* of the QD effective Liouvillian $L(z)$ taking into account all general restrictions that we have derived above. In the most general case that we consider only restricted spin- and charge rotation symmetry about the z -axis: this implies that the effective Liouvillian must be a sum of superoperators that (i) transform as an irreducible tensor of any rank but with index zero with respect to both the charge- and spin-rotation group (i.e. by pairing only bras and kets of basis supervectors with the same charge and spin indices) (ii) preserve the fermion-parity (i.e. by avoiding combinations of fermion and boson kets and bras). Using Table I which lists these transformation properties of the basis supervectors (91)-(96), we can readily construct the most general form of superoperators of this kind that are furthermore compatible with the causal structure of the perturbative series (68). In Table II we have classified all these superoperators according to their irreducible transformation properties under the *full* symmetry group of both spin and charge rotations. This makes it easy to impose further restrictions on the expansion coefficients in cases of higher symmetry ($B = 0$ and / or $\epsilon = -U/2, \mu_L = \mu_R$), see Sec. (IID 4). The most general form of the *exact* QD effective Liouvillian

Superoperator	S -ITSO (rank, index)	T -ITSO (rank, index)
$ Z_R\rangle\langle Z_R , Z_R\rangle\langle Z_L $	(0,0)	(0,0)
$\sum_{m=0,\pm 1} S_m\rangle\langle S_m $	(0,0)	(0,0)
$\sum_{m=0,\pm 1} T_m\rangle\langle T_m $	(0,0)	(0,0)
$ S_0\rangle\langle Z_L , Z_R\rangle\langle S_0 $	(1,0)	(0,0)
$\sum_{m=\pm 1} m S_m\rangle\langle S_m $	(1,0)	(0,0)
$ T_0\rangle\langle Z_L , Z_R\rangle\langle T_0 $	(0,0)	(1,0)
$\sum_{m=\pm 1} m T_m\rangle\langle T_m $	(0,0)	(1,0)
$ S_0\rangle\langle T_0 , T_0\rangle\langle S_0 $	(1,0)	(1,0)
$\sum_{\sigma,\eta=\pm} \sigma^{\tau_\sigma} \eta^{\tau_\eta} \alpha_{\eta,\sigma}^{\nu'}\rangle\langle \alpha_{\eta,\sigma}^{\nu'} $	$(\tau_\sigma, 0)$ $\tau_\sigma = 0, 1$	$(\tau_\eta, 0)$ $\tau_\eta = 0, 1$
$\sum_{m=0,\pm 1} (3m^2 - 2) S_m\rangle\langle S_m $	(2,0)	(0,0)
$\sum_{m=0,\pm 1} (3m^2 - 2) T_m\rangle\langle T_m $	(0,0)	(2,0)

TABLE II: Irreducible tensor *superoperators* (ITSOs) of different rank but with (i) *zero index* with respect to both spin and charge rotations and (ii) satisfying the causal structure constraints (cf. Sec. (IIC 5 a)). The general effective Anderson Liouvillian (137) is a linear combination of all of these, where the coefficient of $|Z_R\rangle\langle Z_R|$ is always fixed to $-4i\Gamma$ in the wide-band limit, see Sec. (IIC 5 a). In the special limits of higher symmetry only (0,0) S -ITSO resp. T -ITSOs can appear in this expansion, see Sec. (IID 4). The ITSOs are constructed by standard angular momentum coupling. For this one takes the supervectors in Table I, denoted schematically by $|s, m_s; t, m_t\rangle$ where s, t and m_s, m_t are the rank and index with respect to spin and charge rotations in Liouville space. Then one constructs conjugate bra supervectors which transform with the *same* rank and index: these are $(-1)^{s-m_s+t-m_t} |s, -m_s; t, -m_t|$. Coupling these kets and bras with Clebsch-Gordan coefficients gives the *superoperators* transforming with definite rank and index with respect to spin and charge rotations.

$L(z) = L + \Sigma(z) = \bar{L} + \bar{\Sigma}(z)$ then reads:

$$\begin{aligned} iL(z) = & \quad (137) \\ & 4\Gamma|Z_R\rangle\langle Z_R| + \zeta|Z_R\rangle\langle Z_L| + |Z_R\rangle\langle \vec{\phi}| + |\vec{\psi}\rangle\langle Z_L| \\ & + \xi + \sum_\sigma \left[M_\sigma |T_\sigma\rangle\langle T_\sigma| + E_\sigma |S_\sigma\rangle\langle S_\sigma| + \sum_\eta F_{\eta,\sigma} \right] \end{aligned}$$

where here $\Gamma = \frac{1}{2} \sum_r \Gamma_r$ and $F_{\eta,\sigma}$ are superoperators acting in the 2-dimensional ν space spanned by $|\alpha_{\eta,\sigma}^\nu\rangle$.

This is a central result of the paper and before discussing it the coefficients in detail we point out its importance. By exploiting only general properties we have reduced the number of terms from 256 (cf. Eq. (82)) down to only just 30. The key simplification comes from using the causal field superoperators to construct the Liouville Fock-space. Moreover, the general Liouvillian can be easily diagonalized as we show in the next section. Furthermore, because of its general nature, the parametrization

(137) is useful in other applications than those considered here and may be extended to more complex Anderson-type models. For example, we note that $|Z_R\rangle$ is always a right eigen-supervector of the effective Liouvillian decaying with rate $2m\Gamma$ where m is the number of electrodes attached to the dot (for our case $m = 2$). This mode was recently also found in a study³⁸ investigating the time-relaxation of the density matrix of the Anderson-model. It was observed that this mode, appearing in 1-loop perturbation theory, is not affected by 2-loop corrections. Our work generalizes this result: the eigenvalue of the right eigen-supervector $|Z_R\rangle$ is not affected by *any* higher-order corrections. We also see how this relies on assuming the wide-band limit. Both insights directly rely on the causal representation of the field superoperators. The time-dependence will be discussed further elsewhere⁵⁰.

We now discuss how the expansion coefficients for $L(z)$ are incorporated in Eq. (137):

- The choice of the first coefficients of the terms involving the vertex zero super-eigenvectors $|Z_L\rangle$ and $|Z_R\rangle$ is based on the general properties of the perturbative series (cf. Sec. (II B 3)).
- A supervector in the two dimensional χ -subspace spanned $|\chi_\sigma\rangle$

$$|\vec{\psi}\rangle = \sum_{\sigma} \psi_{\sigma} |\chi_{\sigma}\rangle \quad (138)$$

- An independent vector in the corresponding dual space

$$\langle \vec{\phi} | = \sum_{\sigma} \phi_{\sigma} \langle \chi_{\sigma} | \quad (139)$$

- A superoperator acting on the χ -subspace

$$\xi = \sum_{\sigma, \sigma'} \xi_{\sigma, \sigma'} |\chi_{\sigma}\rangle \langle \chi_{\sigma'}| = \sum_{i=0,1,2,3} \xi_i \chi_i \quad (140)$$

Here, in the second line, the matrix $\xi_{\sigma, \sigma'}$ was decomposed in the standard basis $(\tau_i)_{\sigma, \sigma'}$ of the unit ($i = 0$) and three Pauli matrices ($i = 1, 2, 3$), giving another χ -subspace basis of superoperators:

$$\chi_i = \sum_{\sigma, \sigma'} (\tau_i)_{\sigma, \sigma'} |\chi_{\sigma}\rangle \langle \chi_{\sigma'}| \quad (141)$$

- Four superoperators acting on the 2 dimensional $\alpha_{\eta, \sigma}$ -subspaces spanned by $|\alpha_{\eta, \sigma}^{\pm}\rangle$

$$F_{\eta, \sigma} = \sum_{\nu, \nu'} F_{\eta, \sigma}^{\nu, \nu'} |\alpha_{\eta, \sigma}^{\nu}\rangle \langle \alpha_{\eta, \sigma}^{\nu'}| \quad (142)$$

$$= \sum_{i=0,1,2,3} F_{\eta, \sigma}^i \alpha_{\eta, \sigma}^i \quad (143)$$

with unit and Pauli-vector superoperators

$$\alpha_{\eta, \sigma}^i = \sum_{\nu, \nu'} (\tau_i)_{\nu, \nu'} |\alpha_{\eta, \sigma}^{\nu}\rangle \langle \alpha_{\eta, \sigma}^{\nu'}| \quad (144)$$

for each fixed $\sigma = \pm$ and $\eta = \pm$.

It is convenient to use both the four-vector as well as the 2×2 matrix representations for the superoperators ξ and $F_{\eta, \sigma}$

All the above expansion coefficients depend on the QD dot frequency z (not written) and satisfy the following conjugation relations, deriving from the Hermiticity condition (70): $K(iL(z))K = iL(-z^*)$. For the charge- and spin-diagonal operators these are

$$\begin{aligned} \vec{\phi}(z) &= \vec{\phi}^*(-z^*), & \vec{\psi}(z) &= \vec{\psi}^*(-z^*), \\ \xi(z) &= \xi^*(-z^*), \end{aligned} \quad (145)$$

implying that these are real only for zero frequency $z = i0$. For the charge- or spin- non-diagonal operators we have

$$F_{\eta, \sigma}^{\nu, \nu'}(z) = \nu \nu' F_{\eta, \sigma}^{\nu, \nu'}(-z^*), \quad \nu, \nu' = \pm \quad (146)$$

$$M_{\sigma}(z) = M_{\sigma}^*(-z^*), \quad (147)$$

$$E_{\sigma}(z) = E_{\sigma}^*(-z^*). \quad (148)$$

Therefore at finite dot frequency z all parameters are in general complex and all 2×2 coefficient matrices are non-Hermitian.

Note that in Eq. (137) we have parametrized $iL(z)$, rather than $L(z)$, i.e., including the imaginary factor i . This anticipates the application to the RT-RG where a renormalized version of the Liouvillian \bar{L} appears in the final RG equations only the combination $i\bar{L}$ (cf. Sec. (III C 1) and (III D 1)). Finally, we emphasize that the simplifications that led up to the parametrization Eq. (137) remain valid for the RT-RG: Eq. (69), as well as Eq. (85) and Eq. (86) do not change under the continuous renormalization as will be shown in Sec. (III).

D. Effective Liouvillian

1. Spectral decomposition of $L(z)$ and \bar{L}

Above we have reduced $L(z)$ to block diagonal form as far as possible by using symmetry and general properties. In the Sec. (III) we will see that $L(z)$ is closely related to a *renormalized* version of the QD Liouvillian \bar{L} that we will denote by \bar{L}_{Λ} . To make this clear we have to anticipate a result: \bar{L}_{Λ} interpolates between \bar{L} and $L(z)$ as the flow parameter Λ varies from ∞ to 0: $L(z) = \bar{L} + \int_{\infty}^0 d\Lambda \frac{d\bar{L}_{\Lambda}}{d\Lambda}$. This is done by redistributing diagrams of $\bar{\Sigma}$ in Eq. (80) and including a fraction of them into a redefinition of the Liouvillian \bar{L} . By construction $\bar{\Sigma}(z)$ is thus decomposed into “pieces” $\frac{d\bar{L}_{\Lambda}}{d\Lambda}$ with the same matrix structure that are accumulated during the flow. At the end of the flow \bar{L}_{Λ} equals $L(z)$. Therefore \bar{L}_{Λ} has an expansion of the same form Eq. (137) as $L(z)$. For notational simplicity we denote the expansion coefficients of \bar{L}_{Λ} by the same variables as for $L(z)$. In cases where this leads to confusion the coefficients of \bar{L}_{Λ} are distinguished from those of $L(z)$ by indicating their Λ dependence, e.g. $F_{\eta, \sigma, \Lambda}^{\nu, \nu'}$ vs.

$F_{\eta\sigma}^{\nu,\nu'}$, which can, however, often be omitted. All results obtained in this section thus apply to both the exact $L(z)$ as well as the renormalized \bar{L}_Λ . The explicit form of \bar{L}_Λ needs to be inserted in to perturbative expressions in expansions involving resolvent superoperators to evaluate RG-equations.

We therefore need to completely diagonalize \bar{L}_Λ such that it can be expanded into its eigen projectors $P^k = |\bar{\lambda}^k\rangle\langle\lambda^k| = (P^k)^2$:

$$\bar{L}_\Lambda = \sum_k \lambda^k P^k. \quad (149)$$

where the sum runs over the labels i of the eigenvalues. Here $|\bar{\lambda}^i\rangle$ and $|\lambda^i\rangle$ are the left and right eigen supervec-tors of \bar{L}_Λ for the same eigenvalue λ^k : $\bar{L}_\Lambda P^k = P^k \bar{L}_\Lambda = \lambda^k P^k$. Using this complete and orthogonal set of projectors one can then evaluate resolvent superoperators in Eq. (79) explicitly:

$$\dots \bar{G} \frac{1}{z - X - \bar{L}_\Lambda} \bar{G} \dots = \dots \sum_i \frac{1}{z - X - \lambda^i} \bar{G} P^i \bar{G} \dots \quad (150)$$

The diagonalization of Eq. (137) is also useful for higher-orders of (renormalized) perturbation theory Eq. (68) and (79): when expanding the QD L and \bar{L}_Λ in the form (137) it is directly adapted to all symmetries of the problem and one can efficiently construct explicit matrix representation of the self-energies $\Sigma(z)$ and $\bar{\Sigma}(z)$, respectively.

Applying the above spectral decomposition to the continuous RG of Sec. (III) involves two assumptions that should be pointed out here. First, we always assume that the zero eigen value of \bar{L}_Λ is non-degenerate, corresponding to the unique stationary state for the density operator. This is always found to be the case for the numerically calculated RG flows discussed in Sec. (III). However, in principle it may also happen that two (or more) *non-zero* eigenvalues of \bar{L}_Λ become degenerate during this flow. If this is the case, and additionally the supermatrix the \bar{L}_Λ has nonzero elements on its diagonal in the normal Jordan form in the degenerate subspace, then no complete eigenprojector basis exists. For the Anderson model this presents no crucial complication: the eigen basis can in principle be circumvented for the calculation of the 2 dimensional superoperators. However, numerically we never meet such a problem in the application of the RT-RG theory presented below.

2. Eigenvalues, super-eigenvectors and the stationary state

We now diagonalize $L(z)$ or \bar{L}_Λ , parametrized as in Eq. (137), explicitly in each of its block-diagonals. We start with the block spanned by the charge and spin diagonal bosonic operators $|Z_L\rangle, |Z_R\rangle, |S_0\rangle, |T_0\rangle$ which contains the stationary state:

- Eigenvalue $\lambda^{Z_L} = 0$:

$$P^{Z_L} = 2|\rho\rangle\langle Z_L| \quad (151)$$

with the stationary density operator

$$\rho = -\frac{1}{2\xi}|\vec{\psi}\rangle + \frac{1}{2}|Z_L\rangle - \frac{\zeta - (\vec{\phi}|\xi^{-1}|\vec{\psi})}{8\Gamma}|Z_R\rangle \quad (152)$$

We note that the coefficient ζ appears only in the stationary state and the next projector P^{Z_R} but not in any other eigen projector or eigenvalue.

- Eigenvalue $\lambda^{Z_R} = -i4\Gamma$.

$$P^{Z_R} = (\vec{\phi}|\frac{1}{4\Gamma(4\Gamma - \xi)}|\vec{\psi}\rangle|Z_R\rangle\langle Z_L| + |Z_R\rangle\langle Z_R| + \frac{\zeta}{4\Gamma}|Z_R\rangle\langle Z_L| + |Z_R\rangle(\vec{\phi}|\frac{1}{4\Gamma - \xi} \quad (153)$$

- Eigenvalue λ^{χ^\pm} with projectors:

$$P^{3,4} = P^{\chi,\pm} + \frac{(\vec{\phi}|P^{\chi,\pm}|\vec{\psi})}{(\lambda^{\chi,\pm} - 4\Gamma)\lambda^{\chi,\pm}}|Z_R\rangle\langle Z_L| + \frac{1}{\lambda^{\chi,\pm} - 4\Gamma}|Z_R\rangle(\vec{\phi}|P^{\chi,\pm} + \frac{1}{\lambda^{\chi,\pm}}P^{\chi,\pm}|\vec{\psi})\langle Z_L| \quad (154)$$

Here the eigenvalues λ^{χ^\pm} are determined by first diagonalizing ξ in the χ -subspace, i.e., finding

$$\xi P^{\chi,\sigma} = P^{\chi,\sigma} \xi = \lambda^{\chi,\sigma} P^{\chi,\sigma}. \quad (155)$$

Since $\xi_{\sigma,\sigma'}$ is a 2×2 non-Hermitian matrix, this can be expressed in the complex vector $\xi = (\xi_1, \xi_2, \xi_3)$ and complex coefficient ξ_0 (cf. Eq. (140)):

$$\lambda^{\chi,\sigma} = -i \left(\xi_0 + \sigma \sqrt{\xi^2} \right) \quad (156)$$

$$P^{\chi,\sigma} = \frac{1}{2}\chi_0 + \sigma \frac{\chi \cdot \xi}{2\sqrt{\xi^2}} \quad (157)$$

The remaining block-diagonals of \bar{L} acting on bosonic subspaces are 1-dimensional: for $\sigma = \pm$

$$\lambda^{T_\sigma} = -iM_\sigma, \quad P^{T_\sigma} = |T_\sigma\rangle\langle T_\sigma|, \quad (158)$$

$$\lambda^{S_\sigma} = -iE_\sigma, \quad P^{S_\sigma} = |S_\sigma\rangle\langle S_\sigma|. \quad (159)$$

Here the square root of the complex argument is defined such that the branch cut lies in the lower-half complex plane since effective Liouvillian must be regular in the upper half-plane according to Eq. (32),(35).

Finally, in the four two-dimensional fermionic subspaces, labeled by $\alpha_{\eta,\sigma}$, for fixed η and σ , the eigen values and projectors can be calculated as for the bosonic χ -block:

$$\lambda^{\alpha_{\eta,\sigma},\pm} = -i \left(F_{\eta\sigma}^0 \pm \sqrt{\mathbf{F}_{\eta\sigma}^2} \right) \quad (160)$$

$$P^{\alpha_{\eta,\sigma},\pm} = \frac{1}{2}\alpha_{\eta\sigma}^0 \pm \frac{\mathbf{F}_{\eta\sigma} \cdot \boldsymbol{\alpha}_{\eta\sigma}}{2\sqrt{\mathbf{F}_{\eta\sigma}^2}} \quad (161)$$

where the coefficients $F_{\eta\sigma}^0$ and $\mathbf{F}_{\eta\sigma} = (F_{\eta\sigma}^1, F_{\eta\sigma}^2, F_{\eta\sigma}^3)$ are again complex (c.f. Eq. (143)).

We note that in principle is possible that $\xi^2 = 0$ while $\xi \neq \vec{0}$. In this case the supermatrix representation of χ has non-zero diagonal element in its normal Jordan form. In this case χ has no eigenbasis and Eq. (156) does not apply. Still, the required matrix valued functions of χ can be calculated using the Hamilton-Cayley theorem. The same remarks apply to Eq. (160). However in practical applications we never meet such a situation. We also note that during the RG flows discussed in Sec. (III) we never run into points where $\lambda^{\chi,\pm} = -i4\Gamma$ and one therefore need not worry about vanishing of the denominators in Eq. (154) or the existence of the inverse of $(4\Gamma - \xi)$ in Eq. (153).

An important simplification applies to the first four bosonic projectors $P^{Z_L}, P^{Z_R}, P^{3,4}$ that involve the vectors $|Z_L\rangle$ and $|Z_R\rangle$, analogous to the corresponding terms in expansion (137) of the effective Liouvillian (cf. Sec. (II C 5 a)). When inserting projectors into Eq. (150) between two vertices \bar{G}

- the projectors P^{Z_L}, P^{Z_R} give no contributions
- the projectors $P^{3,4}$ only contribute through the first term $P^{\chi,\pm}$ in Eq. (154).

As a result in all applications below we can replace Eq. (149) with the simpler expansion

$$\bar{L}_\Lambda \xrightarrow{\bar{G} \dots \bar{G}} \lambda^\chi P^\chi + \sum_\sigma \left[\lambda^{S_\sigma} P^{S_\sigma} + \lambda^{T_\sigma} P^{T_\sigma} + \sum_\eta \lambda^{\alpha_{\eta,\sigma}} P^{\alpha_{\eta,\sigma}} \right]. \quad (162)$$

Here we leave implicit the sum over the two eigenvalues $\lambda^{\chi,\pm}$ and $\lambda^{\alpha_{\eta,\sigma},\pm}$ in the χ and $\alpha_{\eta,\sigma}$ -subspace, respectively. A crucial stability requirement for the RG in Sec. (III) is thereby explicitly satisfied: the zero eigenprojector (151), corresponding to the physical stationary state, never appear in the resolvents.

3. Fermionic excitations - spectral decomposition of $\bar{\Sigma}$

The expansion (137) can of course also be applied to $\bar{\Sigma}(z) = L(z) - \bar{L}$ as well. This however, involves additional simplifications causing certain terms appearing in the expansion of $L(z)$ (and \bar{L}_Λ) to be absent. First, due to Eq. (132) the term $|Z_R\rangle\langle Z_R|$ is missing. Secondly, due Eq. (133)-(134) deriving from the causal structure (cf. Sec. (II C 5 a)) most of the coefficients of the fermionic sector of $\bar{\Sigma}$, denoted by $-i\Delta F_{\eta\sigma}^{\nu,\nu'}$, vanish: $\Delta F_{\eta\sigma}^{\nu,\nu'} = \delta_{\nu,-\delta_{\nu'}} + \Delta F_{\eta\sigma}^{-,\nu'}$. We can express the coefficients matrices $F_{\eta\sigma}^{\nu,\nu'}$ of $L(z) = \bar{L} + \bar{\Sigma}(z)$ using Eq. (136), in terms of $\Delta F_{\eta\sigma}^{-,+}$:

$$\begin{aligned} & -i \begin{pmatrix} F_{\eta\sigma}^{+,+} & F_{\eta\sigma}^{+,-} \\ F_{\eta\sigma}^{-,+} & F_{\eta\sigma}^{-,-} \end{pmatrix} = \\ & = \begin{pmatrix} \eta \left(\epsilon + \frac{U}{2} \right) + \sigma \frac{B}{2} - i\Gamma & \frac{U}{2} \\ \frac{U}{2} - i\Delta F_{\eta\sigma}^{-,+} & \eta \left(\epsilon + \frac{U}{2} \right) + \sigma \frac{B}{2} - i3\Gamma \end{pmatrix} \end{aligned} \quad (163)$$

Converting to spherical coefficients $F_{\eta\sigma}^0$ and $\mathbf{F}_{\eta\sigma}$ and using Eq. (160) we find

$$\begin{aligned} \lambda^{\alpha_{\eta,\sigma},\pm} &= \eta \left(\epsilon + \frac{U}{2} \right) + \sigma \frac{B}{2} - 2i\Gamma \\ &\pm \eta \sqrt{\frac{U^2}{4} - \Gamma^2 - i \frac{U \Delta F_{\eta,\sigma}^{-,+}}{2}} \end{aligned} \quad (164)$$

$$P^{\alpha_{\eta,\sigma},\pm} = \frac{\alpha_{\eta,\sigma}^0}{2} \pm \eta \frac{\frac{U}{2} \alpha_{\eta,\sigma}^1 + i\Gamma \alpha_{\eta,\sigma}^3 - i\Delta F_{\eta,\sigma}^{-,+} \alpha_{\eta,\sigma}^-}{2 \sqrt{\frac{U^2}{4} - \Gamma^2 - i \frac{U \Delta F_{\eta,\sigma}^{-,+}}{2}}}. \quad (165)$$

We thus find that the functional form of the fermionic eigenvalues is severely limited by the from the casual structure of $\bar{\Sigma}$: all the frequency dependent renormalization effects enter into the projectors and eigenvalues solely through the four complex numbers $\Delta F_{\eta,\sigma}^{-,+}$ in the four $\alpha_{\eta\sigma}$ blocks ($\eta, \sigma = \pm$).

For an isolated QD decoupled from the reservoirs, $\Gamma = 0$, we have $\bar{\Sigma} = 0 = \bar{\Sigma}(z) = 0$ and thus $\Delta F_{\eta,\sigma}^{-,+} = 0$:

$$\lambda^{\alpha_{\eta,\sigma},+} = \eta(\epsilon + U) + \sigma B/2 \quad (166)$$

$$\lambda^{\alpha_{\eta,\sigma},-} = \eta\epsilon + \sigma B/2 \quad (167)$$

This is the spectrum of *many-body* energy excitations when adding a single electron, starting from either an empty QD ($\lambda^{\alpha_{\eta,\sigma},+}$), or a singly occupied QD with spin $\bar{\sigma}$ ($\lambda^{\alpha_{\eta,\sigma},-}$). This is confirmed by the eigenprojectors of $\Gamma \rightarrow 0$ for finite U

$$P^{\alpha_{\eta,\sigma},\pm} = \frac{1}{2} (\alpha_{\eta,\sigma}^0 \pm \alpha_{\eta,\sigma}^1) = \begin{cases} |\sigma, 0\rangle\langle\sigma, 0| & + \\ |2, \bar{\sigma}\rangle\langle 2, \bar{\sigma}| & - \end{cases} \quad (168)$$

where $|\sigma, 0\rangle = |\sigma\rangle\langle 0| = (1/2 - Z_R)d_\sigma^\dagger$ and $|2, \bar{\sigma}\rangle = |2\rangle\langle \bar{\sigma}| = \sigma(1/2 + Z_R)d_\sigma^\dagger$. These are the virtual intermediate states and energies that enter through L into the perturbation expansion (68) for $\Sigma(z)$.

For any finite coupling Γ but infinite temperature, $\bar{\Sigma} = 0$ and therefore again $\Delta F_{\eta,\sigma}^{-,+} = 0$. Now, however, $\bar{\Sigma} \propto \Gamma \neq 0$ and the eigenvalues obtained from Eq. (164) depend qualitatively on the interaction strength U . For $U < 2\Gamma$ the coupling to the reservoirs Γ adds different imaginary parts to the degenerate real eigenvalues $\eta(\epsilon + U/2) + \sigma B/2$ whereas for $U > 2\Gamma$ it adds a uniform imaginary part $-i\Gamma$ to these eigenvalues while differently shifting their real parts. This dependence on U is plotted in Fig. 3 and shows a bifurcation at $U = 2\Gamma$. These are the energies and projectors that enter through \bar{L} into the renormalized perturbation theory (79).

Finally, for both finite coupling Γ and finite temperature T , the complex coefficients $\Delta F_{\eta,\sigma}^{-,+}$ are non-trivial functions that need to be calculated, e.g., either perturbatively or using the RG, see Sec. (III B 4). However, even in this case Eq. (164) provides an exact relation: the *average* of the complex particle and hole excitation

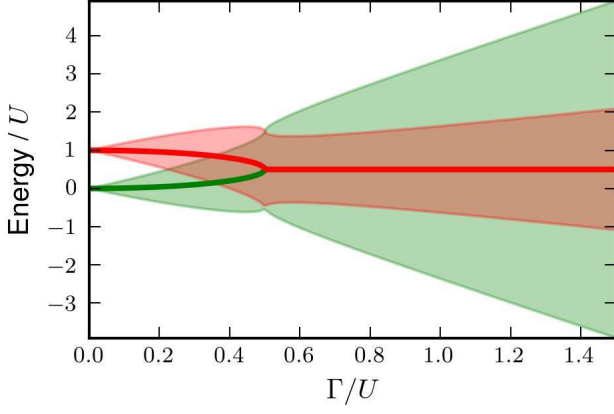


FIG. 3: Fermionic excitation energies and widths of the infinite temperature Liouvillian \bar{L} plotted as function of the tunnel coupling strength Γ/U for $\epsilon = B = 0$. The energy and width are given by the real and imaginary parts of the fermionic eigenvalues $\lambda^{\alpha_{\eta,\sigma},\nu}$. (Eq. (164) with $\Delta F_{\eta,\sigma}^{\pm} = 0$). The real parts for $\nu = +$ (red) and $\nu = -1$ (green), respectively, are given by the full lines and the imaginary parts are indicated by the shaded width of the level with the corresponding color. For $U > 2\Gamma$ the excitations have different energies - split by U - but with the same width 2Γ whereas for $2\Gamma > U$ they have the same energies but different widths: for $\Gamma \gg U$ $-\text{Im}\lambda^{\alpha_{\eta,\sigma},\pm} \approx \Gamma$ (red) 3Γ (green).

eigenvalues in each $\alpha_{\eta,\sigma}$ -block is independent of $\Delta F_{\eta,\sigma}^{\pm}$ and thereby, also independent of the frequency z :

$$\frac{1}{2} \sum_{\pm} \lambda^{\alpha_{\eta,\sigma},\pm} = \eta \left(\epsilon + \frac{U}{2} \right) + \sigma \frac{B}{2} - 2i\Gamma \quad (169)$$

Physically speaking, *both* the renormalized energies of single particle fermionic excitation energies (real part) as well as their decay rates / broadenings (imaginary parts) lie symmetric with respect to the above average values. E.g. if the particle excitation broadens, the hole excitation sharpens up and *vice-versa*.

Finally, we can infer an important physical stability constraint on the functions $\Delta F_{\eta,\sigma}^{\pm}$: they must be such that imaginary part of the square root is less than 2Γ for all Λ . Otherwise, inverse Laplace-transforming $L(z)$ to time-space would yield terms that diverge for $t \rightarrow \infty$, which is unphysical. This restricts the maximal excitation widths in the fermionic block: the negative imaginary part of eigenvalue λ^{α} cannot exceed the value 4Γ .

4. High-symmetry stationary states

As a cross check on the results of Sec. (IID 2), we now analyse the stationary density operator in the two special parameter regimes where the model has a higher symmetry than in general. In both cases the superoperator ξ has no off-diagonal terms in the basis of $|S_0\rangle$ and $|T_0\rangle$,

$$\xi = \xi_{TT}|T_0\rangle\langle T_0| + \xi_{SS}|S_0\rangle\langle S_0|, \quad (170)$$

because there are no scalars under spin or charge-rotations which contain such terms as components, see Table II. If either symmetry is broken, charge or/and spin rotations allow for mixing terms $|T_0\rangle\langle S_0|$ and $|S_0\rangle\langle T_0|$ in Eq. (137). For this reason we work in the general case with the $|\chi_{\sigma}\rangle$ basis (111).

a. Full spin-rotation symmetry, $B = 0$. At zero magnetic field all terms in the Liouvillian must be zero rank ITSO (scalar) with respect to spin-rotations, i.e., the terms $|S_0\rangle\langle S_0|$ and $|S_{\pm}\rangle\langle S_{\pm}|$ must have the same coefficients, $E_+ = E_- = \xi_{SS}$ and the coefficients of the rank 1 and 2 spin-ITSOs must vanish, i.e., in the χ -subspace $|\phi\rangle = \phi_T|T_0\rangle$ and $|\psi\rangle = \psi_T|T_0\rangle$ with real ϕ_T, ψ at $z = i0$ (cf Eq. (145))

$$\begin{aligned} i\bar{L}_{\Lambda} = & \dots + \phi_T|Z_R\rangle\langle T_0| + \psi_T|T_0\rangle\langle Z_L| \quad (171) \\ & + M_+|T_+\rangle\langle T_+| + M_-|T_-\rangle\langle T_-| + \xi_{TT}|T_0\rangle\langle T_0| \\ & + \xi_{SS}\left(|S_+\rangle\langle S_+| + |S_-\rangle\langle S_-| + |S_0\rangle\langle S_0|\right) + \dots \end{aligned}$$

See Table II where the ITSOs are listed. The expression for the stationary state ρ obtained using Eq. (152) is then independent of ξ_{SS} it is therefore explicitly invariant under spin-rotations, as required:

$$\rho = -\frac{1}{2}\psi_T|T_0\rangle + \frac{1}{2}|Z_L\rangle - \frac{\zeta - \phi_T\psi_T/\xi_{TT}}{8\Gamma}|Z_R\rangle \quad (172)$$

b. Full charge-rotation symmetry, $\epsilon = -U/2$ and $\mu_L = \mu_R$. At the particle-hole symmetric point, as similar reduction must take place: here $M_+ = M_- = \xi_{TT}$, $|\phi\rangle = \phi_S|S_0\rangle$ and $|\psi\rangle = \psi_S|S_0\rangle$:

$$\begin{aligned} i\bar{L}_{\Lambda} = & \dots + \phi_S|Z_R\rangle\langle S_0| + \psi_S|S_0\rangle\langle Z_L| \quad (173) \\ & + \xi_{TT}\left(|T_+\rangle\langle T_+| + |T_-\rangle\langle T_-| + |T_0\rangle\langle T_0|\right) \\ & + E_+|S_+\rangle\langle S_+| + E_-|S_-\rangle\langle S_-| + \xi_{SS}|S_0\rangle\langle S_0| \end{aligned}$$

and the stationary state is explicitly invariant under charge-rotations:

$$\rho = -\frac{1}{2}\psi_S|S_0\rangle + \frac{1}{2}|Z_L\rangle - \frac{\zeta - \phi_S\psi_S/\xi_{SS}}{8\Gamma}|Z_R\rangle \quad (174)$$

E. Current superoperator and its irreducible self-energy

Our main objective is to calculate the stationary current which flows through the QD. Having set up the perturbation theory formalism for the density operator, the expression for the average current can now be compactly derived. Moreover, we give a general proof that in general at zero bias the current vanishes, as it should, independent of the way the self-energy is calculated.

The current flowing out of reservoir $r = L, R$ is obtained from the Heisenberg operator of the time-derivative

$$I^r = -\frac{d}{dt}n^r = -i[H^{\text{tot}}, n^r] \quad (175)$$

$$= -i[V^r, n^r] \quad (176)$$

Note that there is no summation over the electrode index r , c.f. Eq. (10). The expectation value of the current operator can be expressed in superoperators using the cyclic invariance of the total system trace:

$$\begin{aligned}\langle I^r \rangle(t) &= \text{Tr}_D \text{Tr}_R (I^r \rho(t)) \\ &= -i \text{Tr}_D \text{Tr}_R \left(L^{I^r} e^{-iL^{\text{tot}}(t-t_0)} \rho(t_0) \rho^R \right)\end{aligned}\quad (177)$$

We note that observable averages involve anticommutators of the corresponding operator (see e.g., Ref. 41):

$$L^{I^r} = \frac{i}{2} [I^r, \bullet]_+ + . \quad (178)$$

This is in contrast to time-evolution superoperators which involve commutators of the Hamiltonian operator. This difference is exploited below. If one uses Eq. (175) in Eq. (177) the evaluation of the reservoir trace is unnecessarily complicated, since Eq. (175) involves two operators acting on the reservoir (V^r and n^r). Here we proceed differently: we first use that the tunneling through junction r conserves the particle number of the dot and the reservoir r : $[n^r + n, V^r] = 0$ and eliminate one electrode operator:

$$I^r = i[V^r, n] = -i[n, V^r] \quad (179)$$

Then, using the identity: $[[A, B]_-, \bullet]_+ = [A, [B, \bullet]_-]_+ - [B, [A, \bullet]_+]_-$ the current superoperator anti-commutator can be decomposed as

$$L^{I^r} = \frac{1}{2} (L^{n^+} L^{V,r} - L^{V,r} L^{n^+}) \quad (180)$$

Here we introduced the *anticommutator* superoperator for the particle number (cf Eq. (43)),

$$L^{n^+} = [n, \bullet]_+ \quad (181)$$

and decomposed the tunneling interactions into the junction contributions, $L^V = \sum_r L^{V,r}$. Importantly, the last term of Eq. (180) is irrelevant when inserted into Eq. (177) since $\text{Tr}_D \text{Tr}_R L^{V,r} \bullet = 0$ due to the commutator form of $L^{V,r}$. We obtain

$$\langle I^r \rangle(t) = -i \frac{1}{2} \text{Tr}_D L^{n^+} \left(\text{Tr}_R L^{V,r} \rho(t) \right) \quad (182)$$

Integrating out of the reservoirs and collecting terms into irreducible blocks (cf. Sec. (II B 3)) one now obtains

$$\begin{aligned}\langle I^r \rangle(z) &= \frac{1}{2} \text{Tr}_D L^{n^+} \Sigma^r(z) \frac{1}{z - L(z)} \rho(t_0) \\ &= -\frac{1}{2} i \text{Tr}_D L^{n^+} \Sigma^r(z) \rho(z)\end{aligned}\quad (183)$$

where Σ^r is just that part of the irreducible self-energy Σ where the latest (leftmost) vertex is associated with reservoir r . We can thus decompose

$$\Sigma(z) = \sum_r \Sigma^r(z). \quad (184)$$

For the stationary current $\langle I^r \rangle = \lim_{t \rightarrow \infty} \langle I^r \rangle(t) = \lim_{z \rightarrow i0} -iz \langle I^r \rangle(z)$ we then obtain the central result of this subsection

$$\langle I^r \rangle = -i \frac{1}{2} \text{Tr}_D L^{n^+} \Sigma^r(i0) \rho \quad (185)$$

where ρ is the stationary density operator (cf. Eq. (152)).

The first advantage of the Eq. (185) is that it allows one to explicitly see that the current is always zero at zero bias. For any number of electrodes, at zero voltage bias all electrochemical potentials are equal, $\mu_r = 0$, implying that all partial self-energies Σ^r are proportional to the total self-energy is proportional to this value:

$$\Sigma^r \propto \frac{\Gamma_r}{\sum_r \Gamma_r} \Sigma(i0) \quad (186)$$

We note that this proof depends on the assumption of reservoir frequency independent spectral densities, $\Gamma_r(\omega) = \Gamma_r$, which we make throughout this paper. We may furthermore add L to $\Sigma(i0)$ in Eq. (185) and express the current in the effective Liouvillian $L(z) = L + \Sigma(z)$ since by local charge conservation, Eq. (23), $\text{Tr}_D L^{n^+} L \bullet = \text{Tr}_D n[H, \bullet] = \text{Tr}_D [n, H] \bullet = 0$ when acting on any dot operator. We see that there is no stationary current at zero applied bias,

$$\langle I^r \rangle \propto -i \text{Tr}_D L^{n^+} L(i0) \rho = 0 \quad (187)$$

since the stationary state ρ is the zero super-eigenvector of $L(i0)$ (cf. Eq. (37)). Importantly the above proof holds no matter what approximations one makes for the calculation of the self-energy Σ as long as all reservoirs are treated in the same way. This applies to perturbation theory up to any finite order, as well as to the RT-RG approach that we set up in Sec. (III).

A second advantage of Eq. (185) is that we can easily directly relate the current to only a few supermatrix elements of the effective Liouvillian $L(z)$ at zero frequency $z = i0$ in the basis introduced in Eq. (137). The dot trace combined with the action of L^{n^+} can be expressed in the dual supervectors of (103) and (107)

$$\frac{1}{2} \text{Tr}_D (L^{n^+} \bullet) = \text{Tr}_D (n \bullet) = \left(\sqrt{2} \langle T_0 | + \sqrt{2} \langle Z_L | \right) \bullet \quad (188)$$

Eq. (85) implies probability conservation (69), but also more strongly that $\langle Z_L | \Sigma^r(i0) = 2 \text{Tr}_D \Sigma^r(i0) = 0$. From this we obtain

$$\langle I^r \rangle = -\sqrt{2} i \langle T_0 | \Sigma^r | \rho \rangle \quad (189)$$

Clearly, the partial self-energy Σ^r has the same general form as Eq. (137) and we distinguish its parameters with an additional reservoir superscript r

$$\begin{aligned}i \Sigma^r &= \\ &2 \Gamma_r |Z_R\rangle \langle Z_R| + \zeta^r |Z_R\rangle \langle Z_L| + |Z_R\rangle \langle \vec{\phi}^r| + |\vec{\psi}^r\rangle \langle Z_L| \\ &+ \xi^r + \sum_{\sigma} \left[M_{\sigma}^r |T_{\sigma}\rangle \langle T_{\sigma}| + E_{\sigma}^r |S_{\sigma}\rangle \langle S_{\sigma}| + \sum_{\eta} F_{\eta, \sigma}^r \right]\end{aligned}\quad (190)$$

Inserting this form and the explicit expression for the stationary state Eq. (152) into Eq. (189) we obtain the final explicit expression for the average stationary current in terms of the self-energy expansion coefficients:

$$\langle I^r \rangle = \frac{1}{\sqrt{2}} \left[(T_0 | \vec{\psi}^r \rangle - (T_0 | \xi^r \xi^{-1} | \vec{\psi} \rangle) \right] \quad (191)$$

We emphasize that this equation is exact, given that the coefficients ψ_σ^r and ξ^r of the partial self-energies Σ^r are known, from which $\psi_\sigma = \sum_r \psi_\sigma^r$ and $\xi = \sum_r \xi^r$ also follow. We can thus calculate the current very easily if we perform all calculations for fixed reservoir index r at the latest (leftmost) vertex and sum over r to obtain Eq. (184). Finally, we note that using Eq. (191), one can check explicitly that when imposing particle-hole symmetry on the expansion coefficients the current vanishes in agreement with the result obtained above (which makes explicit use of $\mu_L = \mu_R$): expanding Σ^r as Eq. (173), one finds that $|\psi^r\rangle$ and ξ^r have no components involving $|T_0\rangle$.

III. REAL-TIME RENORMALIZATION GROUP

In this section we set up the renormalization group calculation of the effective Liouvillian $L(z)$. It is based on the real-time perturbative expansion (RT-RG) for the “finite-temperature” self-energy $\bar{\Sigma}$ in the causal representation introduced in the previous section, cf. Sec. (II B 4). The procedure is to calculate $L(z)$ by introducing an RG flow of the “infinite-temperature” Liouvillian \bar{L} and the vertex \bar{G} as function of a decreasing energy scale cutoff Λ , with the initial condition that $\bar{L} = \bar{\Sigma} + L$ (thereby including the vertex of the type \tilde{G}) and \bar{G} the vertex of perturbation theory. There are a number of motivations for performing such an RG treatment of the perturbative series for $\bar{\Sigma}$.

- First of all, treating $\bar{\Sigma}$ perturbatively in \bar{G} , while infinite orders of \bar{G} have already been resummed into $\bar{\Sigma}$, would amount to an inconsistent treatment. We note that even in the non-interacting case $U = 0$ we already need to do a renormalized perturbation theory (79) up to 2-loop terms to recover the exact result all quantities (i.e., not just the current). For strong interaction U such corrections become of increasing importance since the broadening in $\bar{\Sigma}$ of the various excitations of the QD is uniformly $\sim \Gamma$ i.e. it is energy independent. At finite and especially at low T the strong interaction U leads to non-trivial modifications of these widths due to quantum fluctuations, resulting in different lifetime broadening for single- (SET) and two-electron excitations (COT), with a non-trivial voltage dependence. Moreover, the bare perturbation theory breaks down at these resonances and $T = 0$ and in the renormalized perturbation theory (79), the low energy cut-off T is replaced by the imaginary parts $\sim \Gamma$ in \bar{L} .

- Secondly, the resonance due to the Kondo effect causes even the renormalized perturbation theory to break down and 3-loop corrections result in the enhancement of Kondo exchange processes. These have been studied using the RT-RG extensively but only after a Schrieffer-Wolff transformation from the Anderson model (effective Kondo-model)²⁷. In the regimes of large applied bias voltage and magnetic field such 3-loop corrections can be neglected due to the dephasing of the Kondo correlations. This is the regime of interest in this work and we expect that the 1- and 2-loop RG approach to give a good first approximation here that deserves to be studied.
- In order to go beyond the study²⁷ by studying Kondo effect in the Anderson model at least a 3-loop treatment is necessary. The renormalization of the 1- and 2-loop terms that we study here will then couple to the 3-loop terms and still play a important role. Therefore, our study of the 2-loop RG provides an important starting point for such a much more involved study that in particular will address the low bias and low magnetic field regime.

A. Flow of Keldysh contractions - continuous RG

In general, RG approaches to transport aim to eliminate the *effect* of reservoirs states, starting at high energies, by incorporating it into a redefinition of the system parameters. Typically one eliminates *the states themselves*. Here, in contrast, we successively suppress the *occupations of the states* using an RG procedure while keeping the states. Before we specify the details and advantages of this cut-off scheme, we first outline the main idea of the functional renormalization group approach when applied to the real-time perturbation series (79). By our causal reformulation of the perturbation theory (cf. Sec. (II B 2)) it is clear that all the information about the occupations of the reservoir states is contained in the Keldysh components of its correlation functions, i.e., in the $\bar{\gamma}$ contraction. Therefore we introduce a cut-off dependent contraction function $\bar{\gamma}_\Lambda$ which monotonously flows from the initial, full contraction function $\bar{\gamma}_\Lambda|_{\Lambda=\infty} = \bar{\gamma}$ given by Eq. (64) to the trivial final function $\bar{\gamma}_\Lambda|_{\Lambda=0} = 0$ where all occupations are suppressed. During this flow we demand that the effective Liouvillian remains invariant: for every value of the cut-off parameter Λ ,

$$L(z) = \bar{L} + \bar{\Sigma}(\{\bar{\gamma}, \bar{L}, \bar{G}\}) \quad (192)$$

$$= \bar{L}_\Lambda + \bar{\Sigma}(\{\bar{\gamma}_\Lambda, \bar{L}_\Lambda, \bar{G}_\Lambda\}) \quad (193)$$

$$= \bar{L}_\Lambda|_{\Lambda=0}. \quad (194)$$

Thus $L(z)$ has the same functional dependence on the contractions γ_Λ , the Liouvillian \bar{L}_Λ , and vertices \bar{G}_Λ . The latter two now acquire a Λ dependence to maintain invariance. The same diagram rules are thus valid for any

value of Λ . As a result, at the end of the flow where $\bar{\gamma}_\Lambda|_{\Lambda=0} = 0$, the effective Liouvillian is given simply by $\bar{L}_\Lambda|_{\Lambda=0}$. The information about the reservoir degrees of freedom, previously incorporated into the self energy $\bar{\Sigma}$, has now been incorporated fully into the dot Liouvillian, cf. Eq. (194).

The RG flow is generated by making an infinitesimal change $d\Lambda$ of the cut-off, resulting in a infinitesimal change $d\bar{\gamma}_\Lambda \approx (d\bar{\gamma}_\Lambda/d\Lambda)d\Lambda$ of the Keldysh contraction function. In the perturbation series at scale Λ one splits up the contraction function as $\bar{\gamma}_\Lambda = \bar{\gamma}_{\Lambda-d\Lambda} + d\bar{\gamma}_\Lambda$ and collects all terms in a perturbation series of the same form but containing only $\bar{\gamma}_{\Lambda-d\Lambda}$ contractions. In this process the terms containing one infinitesimal contraction $d\bar{\gamma}_\Lambda$ can be identified with renormalizations $d\bar{L}$ of the Liouvillian, $d\bar{G}$ of the vertices and newly generated higher-order vertices with more than one leg. The process is illustrated in Fig. 4. The Liouvillian $\bar{L}_{\Lambda-d\Lambda} = \bar{L}_\Lambda - d\bar{L}_\Lambda$, and vertices $\bar{G}_{\Lambda-d\Lambda} = \bar{G}_\Lambda - d\bar{G}_\Lambda$ of the new perturbation series are then all defined for the new, lower cut-off scale $\Lambda - d\Lambda$. We obtain differential equations for these quantities describing their renormalization as one continuously reduces the cut-off Λ . These are the real-time renormalization group (RT-RG) equations.

A key requirement in setting up this continuous RG is that for any Λ the zero-eigen vector of \bar{L}^Λ does not appear in the resolvents $(z + X - \bar{L}^\Lambda)^{-1}$, to avoid divergences as function of the frequencies. The RG thus has to be formulated such that the property Eq. (85) of the vertices in the causal representation is preserved. This can be shown to be the case, see Eq. (214) below.

The final key point is the choice of a cut-off dependent distribution function in the contraction $\bar{\gamma}$. The numerical integration of the RG equations is more stable when we introduce a contraction function with a cut-off on the *imaginary frequency axis*:

$$\bar{\gamma}_{12,\Lambda}(\eta\omega) = \delta_{12} \frac{\Gamma}{\pi} T \sum_{l=0}^{\infty} \frac{\Theta_T(\Lambda - |\omega^l|)}{\eta\omega - \bar{\mu}_r - i\omega^l} \quad (195)$$

through the function

$$\Theta_T(\omega) = \begin{cases} \Theta(\omega), & |\omega| > \pi T \\ \frac{1}{2} + \frac{\omega}{2\pi T}, & |\omega| < \pi T \end{cases}, \quad (196)$$

where $\Theta(\omega)$ is the theta-function and

$$\omega^l = (2l+1)\pi T \quad (197)$$

is the l -th Matsubara frequency ($l = 0, 1, 2, \dots$). In the limit $\Lambda \rightarrow +\infty$ we recover the partial fraction expansion of the meromorphic function $(\Gamma/2\pi) \tanh(\omega/2T)$ as required. Imposing this cut-off in Matsubara space leads to a suppression of the tails of $\bar{\gamma}^\Lambda(\eta\omega)$ on the real frequency axis as $\Lambda \rightarrow 0$, rather than sharp truncation above frequency Λ . This implements the suppression of contributions from states above energy scale Λ . From hereon we will consider the zero-temperature limit $T \rightarrow 0$ for which

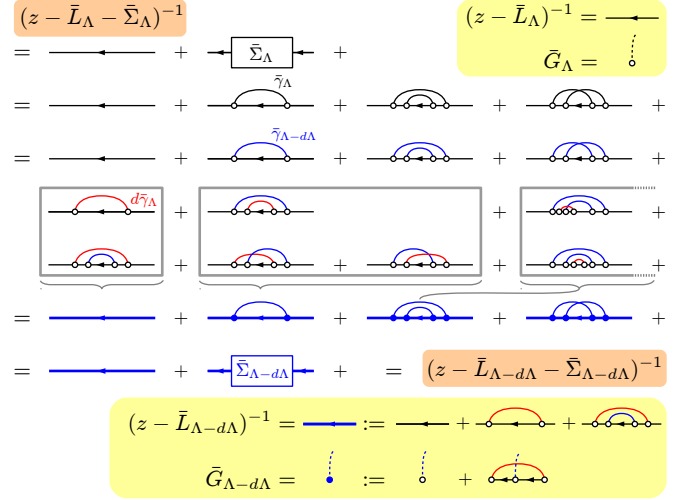


FIG. 4: Renormalization group transformation with an infinitesimal change $d\Lambda > 0$ of the flow parameter, $\Lambda \rightarrow \Lambda - d\Lambda$. The physical restriction is that the effective Liouvillian, $L(z) = \bar{L}_\Lambda + \bar{\Sigma}_\Lambda$, or equivalently, the density operator propagator $(z - L(z))^{-1}$ remains unchanged. In lines 1-2 we start from the perturbation theory at scale Λ and split up the contraction function γ_Λ (black curved lines) into the contraction function with reduced flow parameter ($\gamma_{\Lambda-d\Lambda}$, blue curved line), which should appear in the renormalized perturbation series and the change the contraction function ($-d\gamma_\Lambda$, red curve line). Next, in lines 3-5 the latter terms of linear order in $d\gamma_\Lambda$ are collected into 1- and 2-loop renormalizations $d\bar{L}_\Lambda$ of the Liouvillian in the resolvents and 1-loop renormalization $d\bar{G}_\Lambda$ of the vertices. Finally, the perturbation series is rewritten in terms of new Liouvillian $\bar{L}_{\Lambda-d\Lambda}$ and vertices $\bar{G}_{\Lambda-d\Lambda}$ defined on the new scale $\Lambda - d\Lambda$ (indicated by blue). This transformation is exact if one also accounts for the generation of higher order vertices²⁶, which we, however, neglect here (they are not drawn). We do account for the renormalization of the original vertices, i.e., of *single-charge fluctuations*.

the contraction function (195) reduces to the simple form:

$$\bar{\gamma}_{12,\Lambda}(\eta\omega) = \delta_{12} \frac{\Gamma}{\pi} \int_{-\Lambda}^{\Lambda} d\omega' \frac{1}{\eta\omega - \bar{\mu}_r - i\omega'} \quad (198)$$

See Ref. 26 for a detailed discussion.⁷⁵

B. RG in frequency space

1. Non-equilibrium Matsubara representation and frequency dependence

To formulate the RG equations we need a more compact notation for the various frequencies. Since the contraction functions $\bar{\gamma}^\Lambda$ depend on $\eta\omega = x - \eta\mu$ we re-express the reservoir energies in the resolvents in $\bar{\Sigma}$, Eq. (79), in explicit calculations as

$$E - X_i = E - x_{1\dots n} = E_{1\dots n} - \bar{\omega}_{1\dots n} \quad (199)$$

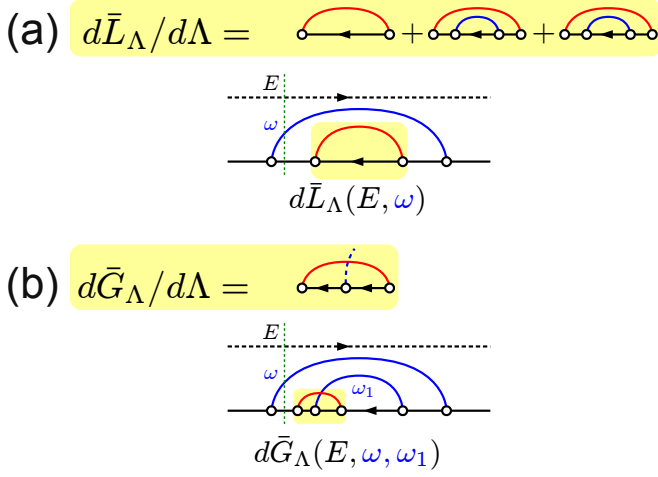


FIG. 5: RG-equations and frequency dependence generated by the renormalization transformation of the diagrammatic perturbation theory in Fig. 4, (using the same red and blue color). (a) Liouvillian renormalization by 1- and 2-loop corrections. The example diagram illustrates that the correction depends on the external frequency E of the diagram (Laplace variable) and on the sum of the reservoir frequencies ω running over the $d\bar{L}/d\Lambda$ -block (marked yellow). These frequencies are read off at the vertical cut (green dashed line) to the left of this block. (b) Vertex renormalization by 1-loop corrections. The example diagram illustrates that the vertex correction depends additionally on frequency ω_1 of the vertex leg.

Here $1, \dots, n$ are the multiindices of the contractions going over diagram segment i . The frequencies are now taken relative to the electrochemical potentials and we write their sums as repeated multiindices: for $k = \eta_k \sigma_k r_k \omega_k$,

$$x_k = \bar{\omega}_k + \bar{\mu}_{r_k}, \quad x_{1\dots n} = x_1 + \dots + x_n, \quad (200)$$

$$\bar{\omega}_k = \eta_k \omega_k, \quad \bar{\omega}_{1\dots n} = \bar{\omega}_1 + \dots + \bar{\omega}_n, \quad (201)$$

$$\bar{\mu}_r = \eta_k \mu_{r_k}, \quad \bar{\mu}_{1\dots n} = \bar{\mu}_1 + \dots + \bar{\mu}_n. \quad (202)$$

Similarly, we express the dot energies relative to these chemical potentials as

$$E_{1\dots n} = E - \sum_{i=1\dots n} \bar{\mu}_i. \quad (203)$$

A key advantage of the cut-off parametrization (195) is that it allows us to analytically perform all the integrations over the reservoir frequencies $\bar{\omega}$ in Eq. (79) by closing each integration contour in the complex lower half-plane and using the residual theorem. As a result, we can replace all integrations over real frequencies in the resolvents by summations over Matsubara frequencies lying in the lower half-plane and Eq. (199) becomes

$$E_{1\dots n} + i\omega_{1\dots n}. \quad (204)$$

For finite T the sum of ω_k runs over the positive discrete frequency values $(2l_k + 1)\pi T$, $l_k = 0, 1, 2, \dots$ which turns into an integral over positive ω_k for $T = 0$. As always, we do not explicitly indicate this integral.⁷⁶

2. RG equations

During the RG flow the Liouvillian develops a non-trivial dependence on both the real energy E of the QD and on the sum of the imaginary frequencies of the reservoirs, $i\omega$, of all contractions that pass over the propagator in a diagram. This is illustrated in Fig. 5(a). We separately keep track of these frequency dependencies by writing

$$\bar{L}_\Lambda(E, \omega) := \bar{L}_\Lambda(E + i\omega), \quad (205)$$

$$\Pi_\Lambda(E, \omega) := \frac{1}{E + i\omega - \bar{L}_\Lambda(E, \omega)}. \quad (206)$$

The renormalization of the vertex \bar{G}_1 introduces similar dependencies and an additional dependence on the reservoir frequency ω_1 of the vertex “leg”, i.e., the contraction connecting it to another vertex, see Fig. 5(b):

$$\bar{G}_{1,\Lambda}(E, \omega, \omega_1) := \bar{G}_{1,\Lambda}(E + i\omega, i\omega_1) \quad (207)$$

The formally exact, infinite hierarchy RT-RG equations were derived in general form in Ref. 26. Here we restrict ourselves to the 1- and 2-loop order approximation for the Liouvillian and the limit of $T \rightarrow 0$:

$$\begin{aligned} \frac{d\bar{L}(E, \omega)}{d\Lambda} &= i\frac{\Gamma}{\pi} \bar{G}_1(E, \omega, \Lambda) \Pi(E_1, \omega + \Lambda) \bar{G}_1(E_1, \omega + \Lambda, -\Lambda) + \frac{\Gamma^2}{\pi^2} \times \\ &\bar{G}_1(E, \omega, \Lambda) \Pi(E_1, \omega + \Lambda) \bar{G}_2(E_1, \omega + \Lambda, \omega_2) \Pi(E_{12}, \omega + \Lambda + \omega_2) \bar{G}_2(E_{12}, \omega + \Lambda + \omega_2, -\omega_2) \Pi(E_1, \omega + \Lambda) \bar{G}_1(E_1, \omega + \Lambda, -\Lambda) \end{aligned} \quad (208)$$

This approximation requires that one also accounts for the renormalization of vertices to 1-loop order:

$$\frac{d\bar{G}_1(E, \omega, \omega_1)}{d\Lambda} = -i\frac{\Gamma}{\pi} \bar{G}_2(E, \omega, \Lambda) \Pi(E_2, \omega + \Lambda) \bar{G}_1(E_2, \omega + \Lambda, \omega_1) \Pi(E_{12}, \omega + \omega_1 + \Lambda) \bar{G}_2(E_{12}, \omega + \omega_1 + \Lambda, -\Lambda). \quad (209)$$

Both here and below we leave the Λ dependence of the

renormalized \bar{L} and \bar{G} and the summation / integration

over all internal indices implicit.⁷⁷

By construction the self-energy $\bar{\Sigma}(z)$ is obtained by directly integrating Eq. (208):

$$\bar{\Sigma}(E + i\omega) = L(E + i\omega) - \bar{L} = \int_{\infty}^0 d\Lambda \frac{d\bar{L}_{\Lambda}}{d\Lambda}(E, \omega) \quad (210)$$

For the transport current we need reservoir-resolved parts $\bar{\Sigma}^r(z)$ of this self-energy (cf. Eq. (184)), which is obtained in the same way:

$$\bar{\Sigma}^r(E + i\omega) = L^r(E + i\omega) - \bar{L}^r = \int_{\infty}^0 d\Lambda \frac{d\bar{L}_{\Lambda}^r}{d\Lambda}(E, \omega) \quad (211)$$

where $\bar{L}_{\Lambda}^r|_{\Lambda=\infty} = \bar{L}^r := \tilde{\Sigma}^r$ is given by Eq. (71). The RG-equations determining \bar{L}_{Λ}^r and its associated vertex G^r have the same structure as the RG equations from Eq. (208)-(209) and are simply obtained from the latter²⁶ by providing the left most vertex on the right hand sides of Eq. (208) and (209) and the left hand side of Eq. (209) by a superscript r . We emphasize that $\sum_r \bar{L}^r = \tilde{\Sigma} = \bar{L} - L$ and $\sum_r \bar{L}_{\Lambda}^r|_{\Lambda=0} = \Sigma(z) = L(z) - L$.⁷⁸

The frequency dependence in the RG-equations Eq. (208)-(209) in the 1 and 2-loop approximation needs to be carefully discussed. Before we turn to this in Sec. (III C)-(III D), we discuss important general properties of the RG-equations in Sec. (III B 3) and their implications for the fermionic eigenvalues in Sec. (III B 4). Using these results, we can decouple some of the RG equations (see Sec. (III C)) and show that in the 1-loop approximation we already obtain the exact solution for the current in the limit $U = 0$, even though in this limit 2-loop corrections are *non-zero* (see Sec. (III C 3)).

3. Exact eigenvectors

Since according to Eq. (210) the self-energy $\bar{\Sigma}(z)$ is obtained by integration over Λ , the RG equations (208)-(209) must preserve the exact properties derived in Sec. (II C 5 a) from the causal structure of the perturbation theory, Eq. (79). Indeed, an exact left and right eigen supervector of the *renormalized* \bar{L} is given by

$$(Z_L|\bar{L}(E, \omega) = 0, \quad (212)$$

$$\bar{L}(E, \omega)|Z_R) = -i4\Gamma|Z_R), \quad (213)$$

respectively. Since we have the initial condition at $\Lambda = \infty$ ($Z_L|\bar{L} = 0$ and $\bar{L}|Z_R) = -i4\Gamma|Z_R)$, we only need to show that $(Z_L|\frac{d}{d\Lambda}\bar{L} = \frac{d}{d\Lambda}\bar{L}|Z_R) = 0$ respectively, to prove Eq. (212)-(213). We note that since (210) is an exact relation, Eq. (212)-(213) must hold for the exact, infinite hierarchy of RT-RG equations (i.e., including all higher vertices generated during the RG-flow that we neglect here). In our 2-loop approximation this relation directly follows by letting Eq. (208) act on these vectors using

$$(Z_L|\bar{G}(E, \omega, \omega_1) = 0 \quad (214)$$

$$\bar{G}(E, \omega, \omega_1)|Z_R) = 0. \quad (215)$$

Eq. (214)-(215) follow by assuming that they hold for a given Λ , and by $(Z_L|\frac{d}{d\Lambda}\bar{G} = \frac{d}{d\Lambda}\bar{G}|Z_R) = 0$, obtained acting with Eq. (209) on these vectors. Since Eq. (214)-(215) hold initially for $\Lambda = \infty$ the result follows for any Λ , E , ω , and ω_1 .

Similarly, we now show that for any Λ , E , ω , and ω_1 :

$$\frac{d}{d\Lambda}\bar{L}(E, \omega)|\alpha_{\eta\sigma}^- = 0, \quad (216)$$

$$(\alpha_{\eta\sigma}^+|\frac{d}{d\Lambda}\bar{L}(E, \omega) = 0, \quad (217)$$

In our 2-loop approximation for $d\bar{L}/d\Lambda$ this follows from the property of the renormalized 1-leg vertices

$$\bar{G}(E, \omega, \omega_1)|\alpha_{\eta\sigma}^- \propto |Z_R) \text{ or } 0 \quad (218)$$

$$(\alpha_{\eta\sigma}^+|\bar{G}(E, \omega, \omega_1) \propto (Z_L| \text{ or } 0. \quad (219)$$

The proof of Eq. (123)-(122) can be extended to the *renormalized* vertices as follows. We start by observing that the right hand sides of the RG equations (208)-(209) have the same structure as $\bar{\Sigma}(z)$ (cf. Eq. (79)). Assuming that Eq. (218) holds for a given scale Λ , the RG equation (209) implies that it is preserved under the flow: $(\alpha_{\eta\sigma}^+|\frac{d}{d\Lambda}\bar{G} = \frac{d}{d\Lambda}\bar{G}|\alpha_{\eta\sigma}^-) = 0$. Here we used that by Eq. (212)-(213) both $|Z_R)$ and $(Z_L|$ are eigen super-vectors of the *renormalized* \bar{L} for all $\Lambda, E, \omega, \omega_1$. Since Eq. (218)-(219) hold initially for $\Lambda = \infty$, this then implies it holds for all Λ . From this Eq. (216)-(217) follow directly. The above proofs are readily extended to the infinite hierarchy of *exact* RT-RG equations for vertices with multiple legs, confirming that Eq. (212), (213), (217) and (216) hold exactly (and not just in our 2-loop approximation) as required by Eq. (210).

4. Fermionic excitations

a. Fermionic eigenvalues We can now pick up the discussion of Sec. (II D). Since the supermatrix structure of $d\bar{L}_{\Lambda}/d\Lambda$ in the fermionic sector is preserved under the RG flow and is the same as that of $\bar{\Sigma}(z)$, we can now directly relate the coefficient $\Delta F_{\eta\sigma}^{-+}$ introduced in Sec. (II D 3) using Eq. (210):

$$\Delta F_{\eta\sigma}^{-+}(E + i\omega) = \int_{\infty}^0 d\Lambda \frac{dF_{\eta\sigma, \Lambda}^{-+}}{d\Lambda}(E + i\omega) \quad (220)$$

This coefficient determines the fermionic excitations at arbitrary complex frequency as given by Eq. (164) for the *exact* $L(z)$ when the infinite hierarchy of RG-equations is used to compute the right hand side. We see that the Λ -dependent coefficient $F_{\eta\sigma, \Lambda}^{-+}$ of \bar{L}_{Λ} interpolates between the infinite temperature limit, where $\Delta F_{\eta\sigma}^{-+} = 0$, and the exact value $\Delta F_{\eta\sigma}^{-+}$ of $\Sigma(z)$ through Eq. (220) as was anticipated in Sec. (II D). All renormalization effects enter into the fermionic excitations through the renormalization of the four complex coefficient $F_{\eta\sigma}^{-+}$ of \bar{L}_{Λ} . During this flow, the qualitative features of these excitations, discussed in Fig. 3, may change. During the continuous RG,

the complex parameters $\Delta F_{\eta\sigma}^{-,+}$ will grow from zero and modify both real and imaginary parts in Eq. (164). This happens only for the interacting Anderson model, $U \neq 0$, since U multiplies these coefficients in Eq. (164). This flow may include bifurcations as function of the flow parameter Λ but for large enough $U \gg 2\Gamma$ the excitations energies (real parts) remain non-degenerate. However, the general result Eq. (169) shows that during this non-trivial flow the *average* of the complex eigenvalues stays fixed for all frequencies. We conclude generally that *the fermionic excitation energies and decay rates are renormalized symmetrically with respect to the average values $\epsilon + \frac{U}{2} + \sigma \frac{B}{2}$ and 2Γ , respectively, for any complex frequency $E + i\omega$ with $\omega > 0$.*

Finally, we note that the stability constraint discussed in Sec. (IID 3) imposes a constraint on the RG flow: since at *any* stage of the RG flow the effective Liouvillian $L(z)$ (193) can be calculated from the perturbative expansion (79), the imaginary parts of all non-zero eigenvalues of the renormalized \bar{L}_Λ must be negative to avoid unphysical divergence of the time-dependent density operator. Such behavior would not go unnoticed in the RG, as it would lead to an instability in the flow since zero denominators would appear in the resolvents in Eq. (229). This provides a simple criterion for the stability of the RG flow for the Anderson model that can be checked easily in numerical approximations. Although in previous applications of the RT-RG no instabilities have been reported and in the present study none were encountered either, the general conditions for stability are currently not known.

b. Fermionic supermatrix elements The properties Eq. (218)-(219) strongly restrict the fermionic matrix elements of resolvents Π that can appear in the RG equations. We will see that implies that quite generally the RG equations decouple into smaller sets of equations (see Sec. (III C)) and that important simplifications arise in the $U = 0$ limit (see Sec. (III C 3)). These simplifications arise since in general on the right hand side of RG equations such as Eq. (208) and (209) the resolvent Π always appear sandwiched between pairs of \bar{G} vertices (all are renormalized quantities but Λ is not written here).

- In matrix elements of terms with only one resolvent, $(X|\bar{G}\Pi\bar{G}|Y)$ there are no restrictions only if $X = Z_R, Y = Z_L$. Indeed, upon inserting the completeness relation $1 = \sum_{\eta,\sigma,\nu} |\alpha_{\eta\sigma}^\nu\rangle\langle\alpha_{\eta\sigma}^\nu| +$ (bosonic terms) left and right of Π , we see that according to Eq. (218)-(219) all intermediate fermionic supermatrix elements contribute. However, when the basis supervectors X, Y involve one zero eigen-supervector only certain matrix elements contribute: for $\nu = \pm$

$$(\alpha_{\eta\sigma}^\nu|\Pi^\alpha|\alpha_{\eta\sigma}^-), \quad X = Z_R, Y \neq Z_L \quad (221)$$

$$(\alpha_{\eta\sigma}^+|\Pi^\alpha|\alpha_{\eta\sigma}^-), \quad X \neq Z_R, Y = Z_L, \quad (222)$$

whereas, if there are no zero eigen-supervector

among X, Y only one factor is possible:

$$(\alpha_{\eta\sigma}^+|\Pi^\alpha|\alpha_{\eta\sigma}^-), \quad X \neq Z_R, Y \neq Z_L. \quad (223)$$

- In terms with $n \geq 3$ resolvents $(X|\bar{G}\Pi\bar{G}\dots\bar{G}\Pi\bar{G}|Y)$ Eq. (221) and (223) apply to the leftmost “boundary” resolvent. Otherwise the expression vanishes for any Λ since by Eq. (219) $(X|\bar{G}\Pi|\alpha^+)(\alpha^+|\bar{G}\Pi\bar{G}\dots \propto (X|\bar{G}\Pi|\alpha^+)(Z_L|\Pi\bar{G}\dots = 0$ where we used that $(Z_L|$ an exact eigenvector of \bar{L} and thereby of Π by Eq. (212) and a zero eigenvector of \bar{G} by Eq. (214).
- Similarly, in such terms Eq. (222) and (223) apply to the rightmost “boundary” resolvents since $\dots\bar{G}\Pi\bar{G}\Pi|\alpha^-)(\alpha^-|\bar{G}|Y) = 0$ by Eq. (218), (213), and (215).
- Finally, in such terms with $n \geq 3$ resolvents, the resolvents which are not at the boundary can *only* contribute with fermionic matrix element $(\alpha_{\eta\sigma}^+|\Pi^\alpha|\alpha_{\eta\sigma}^-)$, irrespective of X and Y : this factor *must always occur* at least $n - 2 \geq 1$ times.

C. 1 loop RG equations

1. Frequency dependence

Since our goal is to calculate the stationary state from the effective Liouvillian $L(z) = \bar{L}(E, \omega)|_{\Lambda=0}$ at $z = E + i\omega = i0$, we first consider the RG equation for this quantity in the 1-loop approximation and at frequency $E = 0$

$$\frac{d\bar{L}^0(0)}{d\Lambda} = i\frac{\Gamma}{\pi}\bar{G}_1^0\Pi^0(\bar{\mu}_1, \Lambda)\bar{G}_1^0. \quad (224)$$

Here the superscript 0 indicates that we also evaluate the Liouvillian at zero reservoir frequency, $\omega = 0$: $\bar{L}^0(E) := \bar{L}(E, 0)$ Similarly, in Eq. (224) we approximate the vertices by their initial values, as given by Eq. (119) and (121) or Eq. (51),

$$\bar{G}_1(0, 0, \Lambda) \approx \bar{G}_1(\bar{\mu}_1, \Lambda, -\Lambda) \approx \bar{G}_1^0 \quad (225)$$

neglecting their dependence on the dot frequency ($E_1 = \bar{\mu}_1$), the reservoir frequency ($\omega = \Lambda$) and the vertex-leg frequency ($\omega_1 = \pm\Lambda$). Such frequency dependencies arises only when accounting for the renormalization of the vertices: for small frequencies we can approximate in Eq. (209),

$$\frac{d\bar{G}}{d\Lambda} \sim \frac{\Gamma}{\Lambda^2}\bar{G}^3 \quad (226)$$

on the right hand side $\bar{G} \sim \bar{G}^0 \sim 1$, giving $\bar{G} = \bar{G}^0 + O(\Gamma/\Lambda)$. In 1-loop order for \bar{L} one must therefore consistently neglect the renormalization of \bar{G} , Eq. (225), with respect to the log-corrections to the Liouvillian that

arise from Eq. (224). This will be checked later on. The resolvent is likewise evaluated at $\omega = \Lambda$. Note that ω -dependence of the resolvent in first approximation,

$$\Pi^0(E, \omega) = \frac{1}{E + i\omega - \bar{L}^0(E)} \quad (227)$$

does not originate from the Liouvillian.

In contrast, Eq. (224) depends on QD frequency E in an important way: due to the finite bias voltage the renormalization of the zero E -frequency Liouvillian couples to the finite frequency Liouvillian $E \rightarrow E_1 = \bar{\mu}_1 = \eta_1 r_1 V/2$ appearing in the (206) on the right hand side. We therefore need to consider instead the RG equations at *finite* QD frequencies,

$$\frac{d\bar{L}^0(E)}{d\Lambda} = i \frac{\Gamma}{\pi} \bar{G}_1^0 \Pi^0(E_1, \Lambda) \bar{G}_1^0 \quad (228)$$

which lie on a discrete grid: $E = k_L \bar{\mu}_L + k_R \bar{\mu}_R = \eta(k_L - k_R)V/2$ where $k_r = 0, 1, 2, \dots$, $r = L, R$. In the numerical calculations we keep as many equations as required to make the solution converge with respect to the k_r . This coupling of the RG flow of the Liouvillian at energies differing by multiples of the voltage arises because the Matsubara frequencies of the different reservoirs are shifted by different electrochemical potentials: this is typical feature of renormalization in a non-equilibrium system²⁶. We discuss the effect of neglecting the QD energy E -dependence in the RG equations in detail when we analyze the numerical results in Sec. (IV B).

2. Explicit 1-loop RG-equations for the Liouvillian

Inserting the spectral decomposition for $\bar{L}(E)$, c.f. Eq. (162),

$$\frac{d\bar{L}^0(E)}{d\Lambda} = \frac{\Gamma}{\pi} \frac{1}{\Lambda - i\Theta_1^k} \bar{G}_1^0 P_1^k \bar{G}_1^0, \quad (229)$$

we obtain, abbreviating $\Theta_1^k = E_1 - \lambda^k(E_1)$,

$$\frac{d}{d\Lambda}(\kappa_3 |\bar{L}^0(E)| \kappa_0) = \frac{\Gamma}{\pi} (\kappa_3 | \mathcal{M} | \kappa_0), \quad (230)$$

where $|\kappa_i\rangle$ are elements of basis (91)-(96) and the super matrix elements are sums ($\kappa_{1,2}$ sums implicit) of factored contributions:

$$(\kappa_3 | \mathcal{M} | \kappa_0) = i \sum_i (\kappa_3 | \bar{G}_1^0 | \kappa_2) (\kappa_1 | \bar{G}_1^0 | \kappa_0) (\kappa_2 | \Pi_1^i | \kappa_1)$$

The product of \bar{G}^0 matrix elements gives a simple numerical factor 0 or ± 1 (see expansions (119)-(121)), whereas the super matrix elements

$$i(\kappa_2 | \Pi_1^i | \kappa_1) = \frac{1}{\Lambda - i\Theta_1^i} (\kappa_2 | P_1^i | \kappa_1)$$

arise from the spectral decomposition of the resolvent, $\Pi^0(E_1, \Lambda) = \sum_i \Pi_1^i$. To explicitly sum over η (contained in the multiindex $1 = \eta, \sigma, r$) which enters the resolvents only through $E_1 = E - \eta \mu_r := E_{\eta r}$ we abbreviate for now $\lambda^i(E_1) := \lambda_{\eta r}$, $P^i(E_1) := P_{\eta r}$ and

$$i\Pi_{\eta r}^i = \frac{P^i(E_1)}{\Lambda - iE_{\eta r} + i\lambda_{\eta r}^i} \quad (231)$$

Expanding Eq. (228) in basis Eq. (91), Eq. (96) we obtain:

$$\begin{aligned} \frac{d\bar{L}^0(E)}{d\Lambda} = \frac{i\Gamma}{\pi} & \left[- \left((\alpha_{-\sigma}^- | \Pi_{-r}^{\alpha_{-\sigma}^-} | \alpha_{-\sigma}^+) + (\alpha_{+\sigma}^- | \Pi_{+r}^{\alpha_{+\sigma}^-} | \alpha_{+\sigma}^+) \right) |Z_R\rangle \langle Z_L| + \left((\alpha_{-\sigma}^- | \Pi_{-r}^{\alpha_{-\sigma}^-} | \alpha_{-\sigma}^-) - (\alpha_{+\sigma}^- | \Pi_{+r}^{\alpha_{+\sigma}^-} | \alpha_{+\sigma}^-) \right) |Z_R\rangle \langle \chi_\sigma| \right. \\ & + \left((\alpha_{-\sigma}^+ | \Pi_{-r}^{\alpha_{-\sigma}^+} | \alpha_{-\sigma}^+) - (\alpha_{+\sigma}^+ | \Pi_{+r}^{\alpha_{+\sigma}^+} | \alpha_{+\sigma}^+) \right) | \chi_\sigma \rangle \langle Z_L| - \left((\alpha_{+\sigma}^+ | \Pi_{+r}^{\alpha_{+\sigma}^+} | \alpha_{+\sigma}^-) + (\alpha_{-\sigma}^+ | \Pi_{-r}^{\alpha_{-\sigma}^+} | \alpha_{-\sigma}^-) \right) | \chi_\sigma \rangle \langle \chi_\sigma| \\ & + \left((\alpha_{+\sigma}^+ | \Pi_{+r}^{\alpha_{+\sigma}^+} | \alpha_{+\sigma}^-) + (\alpha_{-\sigma}^+ | \Pi_{-r}^{\alpha_{-\sigma}^+} | \alpha_{-\sigma}^-) \right) |S_\sigma\rangle \langle S_\sigma| - (\alpha_{+\sigma}^+ | \Pi_{+r}^{\alpha_{+\sigma}^+} | \alpha_{+\sigma}^-) |T_+\rangle \langle T_+| - (\alpha_{-\sigma}^+ | \Pi_{-r}^{\alpha_{-\sigma}^+} | \alpha_{-\sigma}^-) |T_-\rangle \langle T_-| \\ & - \left((\chi_\sigma | \Pi_{-r}^\chi | \chi_\sigma) + (T_+ | \Pi_{+r}^{T_+} | T_+) - (S_\sigma | \Pi_{-r}^{S_\sigma} | S_\sigma) \right) | \alpha_{+\sigma}^- \rangle \langle \alpha_{+\sigma}^+ | \\ & \left. - \left((\chi_\sigma | \Pi_{+r}^\chi | \chi_\sigma) + (T_- | \Pi_{-r}^{T_-} | T_-) - (S_\sigma | \Pi_{+r}^{S_\sigma} | S_\sigma) \right) | \alpha_{-\sigma}^- \rangle \langle \alpha_{-\sigma}^+ | \right] \end{aligned} \quad (232)$$

Here we leave implicit the summation over σ and r , as well as the summation over the two eigenvalues in the χ

and $\alpha_{\eta\sigma}$ subspaces (cf. Eq. (162)). The first two terms in the equation do not contribute to the calculation the

remaining terms of the effective Liouvillian or the transport current but are written here for completeness. Due to $(Z_L|\bar{G} = 0$ (cf. discussion of Eq. (85)) the zero eigen projector P^{Z_L} does not appear in Eq. (232), ensuring that none of the resolvents can diverge during the RG-flow.

Using the relations $K(\Lambda - i(E - \bar{L}(E)))^{-1}K = (\Lambda - i(-E^* - \bar{L}(-E^*)))^{-1}$, cf. Eq. (70), (117) and (118), and

expanding resolvents into eigen-projectors Eq. (231) we obtain the explicit RG equations for the Liouvillian expansion coefficients. We first have a set of equations for 10 complex coefficients on an infinite, discrete grid of frequencies E

$$\frac{d\xi_{\sigma,\bar{\sigma}}(E)}{d\Lambda} = i\frac{\Gamma}{\pi} \left(\frac{(\alpha_{-\bar{\sigma}}^+|P_{-r}^{\alpha-\sigma}|\alpha_{-\bar{\sigma}}^-)}{\Lambda - i(E_{-r} - \lambda_{-r}^{\alpha-\sigma})} + \frac{(\alpha_{+\sigma}^+|P_{+r}^{\alpha+\sigma}|\alpha_{+\sigma}^-)}{\Lambda - i(E_{+r} - \lambda_{+r}^{\alpha+\sigma})} \right) \quad (233)$$

$$\frac{dE_\sigma(E)}{d\Lambda} = i\frac{\Gamma}{\pi} \left(\frac{(\alpha_{+\sigma}^+|P_{+r}^{\alpha+\sigma}|\alpha_{+\sigma}^-)}{\Lambda - i(E_{+r} - \lambda_{+r}^{\alpha+\sigma})} + \frac{(\alpha_{-\sigma}^+|P_{-r}^{\alpha-\sigma}|\alpha_{-\sigma}^-)}{\Lambda - i(E_{-r} - \lambda_{-r}^{\alpha-\sigma})} \right) = \frac{dE_\sigma^*(-E^*)}{d\Lambda} \quad (234)$$

$$\frac{dM_+(E)}{d\Lambda} = -i\frac{\Gamma}{\pi} \frac{(\alpha_{+\sigma}^+|P_{-r}^{\alpha+\sigma}|\alpha_{+\sigma}^-)}{\Lambda - i(E_{-r} - \lambda_{-r}^{\alpha+\sigma})} \quad (235)$$

$$\frac{dM_-(E)}{d\Lambda} = -i\frac{\Gamma}{\pi} \frac{(\alpha_{-\sigma}^+|P_{+r}^{\alpha-\sigma}|\alpha_{-\sigma}^-)}{\Lambda - i(E_{+r} - \lambda_{+r}^{\alpha-\sigma})} = \frac{dM_+^*(-E^*)}{d\Lambda} \quad (236)$$

$$\frac{dF_{+\sigma}^{+-}(E)}{d\Lambda} = -i\frac{\Gamma}{\pi} \left(\frac{(\chi_{\bar{\sigma}}|P_{-r}^{\chi}|\chi_{\sigma})}{\Lambda - i(E_{-r} - \lambda_{-r}^{\chi})} + \frac{(T_+|P_{+r}^{T_+}|T_+)}{\Lambda - i(E_{+r} - \lambda_{+r}^{T_+})} - \frac{(S_\sigma|P_{-r}^{S_\sigma}|S_\sigma)}{\Lambda - i(E_{-r} - \lambda_{-r}^{S_\sigma})} \right) \quad (237)$$

$$\frac{dF_{-\sigma}^{+-}(E)}{d\Lambda} = -i\frac{\Gamma}{\pi} \left(\frac{(\chi_\sigma|P_{+r}^{\chi}|\chi_{\bar{\sigma}})}{\Lambda - i(E_{+r} - \lambda_{+r}^{\chi})} + \frac{(T_-|P_{-r}^{T_-}|T_-)}{\Lambda - i(E_{-r} - \lambda_{-r}^{T_-})} - \frac{(S_\sigma|P_{+r}^{S_\sigma}|S_\sigma)}{\Lambda - i(E_{+r} - \lambda_{+r}^{S_\sigma})} \right) = -\frac{d(F_{+\bar{\sigma}}^{+-}(-E^*))^*}{d\Lambda} \quad (238)$$

Importantly, the eigen projectors of the Liouvillian \bar{L}^0 , $P_\eta^i = P^i(E - \eta\mu_r)$ with eigenvalues $\lambda_\eta^i = \lambda^i(E - \eta\mu_r)$ (cf. Eq. (149)) depend on the frequency $E - \eta\mu_r$. The explicit expressions for the projector matrix elements on the right hand side are given in Eq. (151),(153),(154)(156) and (160) and involve only the 10 coefficients appearing on the left hand side. Eq. (233)-(238) thus form a closed set of equations. This derives from the fact that the eigenprojectors of \bar{L}_Λ that involve the zero eigen supervectors Z_L and Z_R drop out on the right hand side by Eq. (162). Note that the fermionic matrix elements in the equations for the coefficients of bosonic terms that do not involve a Z_L or Z_R ($\xi_{\sigma\sigma'}$, E_σ and M_η) display the restriction (162).

right hand side of Eq. (233)-(238). Their RG-equations

$$\frac{d\psi_\sigma(E)}{d\Lambda} = \quad (239)$$

$$i\frac{\Gamma}{\pi} \left(\frac{(\alpha_{-\bar{\sigma}}^+|P_{-r}^{\alpha-\sigma}|\alpha_{-\bar{\sigma}}^+)}{\Lambda - i(E_{-r} - \lambda_{-r}^{\alpha-\sigma})} - \frac{(\alpha_{+\sigma}^+|P_{+r}^{\alpha+\sigma}|\alpha_{+\sigma}^+)}{\Lambda - i(E_{+r} - \lambda_{+r}^{\alpha+\sigma})} \right)$$

$$\frac{d\zeta(E)}{d\Lambda} = \quad (240)$$

$$-i\frac{\Gamma}{\pi} \left(\frac{(\alpha_{-\bar{\sigma}}^-|P_{-r}^{\alpha-\sigma}|\alpha_{-\bar{\sigma}}^+)}{\Lambda - i(E_{-r} - \lambda_{-r}^{\alpha-\sigma})} + \frac{(\alpha_{+\sigma}^-|P_{+r}^{\alpha+\sigma}|\alpha_{+\sigma}^+)}{\Lambda - i(E_{+r} - \lambda_{+r}^{\alpha+\sigma})} \right)$$

$$\frac{d\phi_\sigma(E)}{d\Lambda} = \quad (241)$$

$$i\frac{\Gamma}{\pi} \left(\frac{(\alpha_{-\sigma}^-|P_{-r}^{\alpha-\sigma}|\alpha_{-\sigma}^-)}{\Lambda - i(E_{-r} - \lambda_{-r}^{\alpha-\sigma})} - \frac{(\alpha_{+\bar{\sigma}}^-|P_{+r}^{\alpha+\sigma}|\alpha_{+\bar{\sigma}}^-)}{\Lambda - i(E_{+r} - \lambda_{+r}^{\alpha+\sigma})} \right)$$

are therefore not required for the solution of Eq. (233)-(238), but do depend on the solution of the latter. However, for the calculation of the current only ψ_σ is required. In contrast, the coefficients ζ and ϕ_σ are not required. However, these coefficients *do* renormalize and are required if one wishes to calculate, e.g., the stationary density matrix (152).

The following 5 complex coefficients do not appear in the eigenvalues and projector matrix elements on the

The remaining coefficients do not flow under the 1-loop RG, and remain at their initial values. For the two

diagonal matrix elements of the coefficient matrix ξ in the bosonic sector we have

$$\frac{d\xi_{\sigma\sigma}}{d\Lambda}(E) = 0, \quad (242)$$

which is valid only within the present 1-loop approximation. In contrast, for the remaining 16 fermionic coefficients we have in general (e.g., also in 2-loop order)

$$\frac{dF_{\eta\sigma}^{+\pm}}{d\Lambda}(E) = \frac{dF_{\eta\sigma}^{\pm-}}{d\Lambda}(E) = 0, \quad (243)$$

due to the causal structure (cf. Sec. (IID 3) and Sec. (IIIB 4)). We furthermore note that Eq. (233)-(241) explicitly satisfy the Hermiticity conditions Eq. (145) and (148). Moreover, the proper transformation under charge and spin-rotations is explicitly guaranteed by our use of irreducible tensor superoperators, cf. Sec. (IIC 5 b).

Finally, for calculation of the current at a specific electrode $r = \pm$ we need RG equations for the coefficients of its self-energy component \bar{L}^r , cf. Eq. (211). These are simply obtained from the above equations by (i) giving all coefficients a superscript r and (ii) suppressing the summation over r contained in the multiindex 1 on the right hand side, i.e. setting $1 = \eta, \sigma, +, \omega$.

Before we proceed to calculate the 2-loop corrections to Eq. (224) we first show that already in the above 1-loop approximation we obtain the exact solution for the current in the limit $U = 0$. This is important since it demonstrates that *for the current* both the 2-loop corrections to \bar{L} , the 1-loop corrections to the vertex \bar{G} , and the ω frequency dependence that we neglected here, are intimately connected with interaction effects. We note, however, that for $U = 0$ there are *non-zero* 2-loop corrections which do not affect the current⁵⁰.

3. Non-interacting case $U = 0$: exact solution

Without local interaction, $U = 0$, the Hamiltonian Eq. (11) is quadratic in the fermionic operators and the non-equilibrium Anderson model can be solved exactly in this limit. A solution using the real-time approach was reported in Ref. 51,52. We now show (i) how using superfermionic algebra one can obtain this solution within RT-RG framework and (ii) that within the 1-loop, frequency-independent approximation (224) this result is recovered upon careful inspection.

a. Exact current In general, to calculate the current according to Eq. (191), we need the elements ξ and ψ_σ of the bosonic part of the effective Liouvillian \bar{L}_Λ . From these we can then easily find the other required coefficients ξ^r and ψ_σ^r of \bar{L}_Λ^r which we do at the end. The coefficients ξ and ψ_σ in turn require the solution of Eq. (233)-(238) which we first discuss. We show then that higher order correction as well as frequency corrections which we neglected in deriving Eq. (233)-(238) have no influence on the stationary current. We start by noting that on the right hand side of RG Eq. (233)-(236) for

the bosonic sector only resolvent matrix elements appear with intermediate fermionic states. We therefore first calculate the eigenvalues of the fermionic projectors to which these coefficients couple. From Eq. (164) it follows that for $U = 0$

$$\lambda^{\alpha_{\eta\sigma}, \pm} = \eta\epsilon + \sigma\frac{B}{2} - 2i\Gamma \pm i\Gamma, \quad (244)$$

$$P^{\alpha_{\eta\sigma}, \pm} = \frac{1}{2} \left(\alpha_{\eta\sigma}^0 \pm \eta\alpha_{\eta\sigma}^3 \mp \eta\frac{\Delta F_{\eta\sigma}^{-+}}{\Gamma}\alpha_{\eta\sigma}^- \right) \quad (245)$$

Importantly: (i) Since $U = 0$ the eigenvalues are independent of $\Delta F_{\eta\sigma}^{-+}$, i.e. they are not renormalized (cf. Sec. (IID 3)) and therefore do not acquired a frequency dependence (ii) The right hand side of the RG equation of any bosonic superoperator that is relevant for the current (i.e., excluding ζ, ϕ), *with the exception* ψ_σ by the general property (222) contain the off-diagonal super matrix elements

$$(\alpha_{\eta\sigma}^+ | \Pi_1^{\alpha_{\eta\sigma}} | \alpha_{\eta\sigma}^-) = 0 \quad (246)$$

as a factor. It vanishes for $U = 0$ by Eq. (245). This implies in fact that that these coefficients do not renormalize *in any higher loop order* since such terms on the right hand side of Eq. (208) always contain this factor at least once by Eq. (223). (iii) The renormalization of the quantities ψ_σ at $E = 0$ involve fermionic virtual states with the simple factors

$$i(\alpha_{+\sigma}^+ | \Pi_{+r}^{\alpha_{+\sigma}} | \alpha_{+\sigma}^+) = \sum_r (\alpha_{+\sigma}^+ | \frac{1}{\Lambda - irV/2 + i\lambda_{+r}^{\alpha_{+\sigma}}(rV/2)} | \alpha_{+\sigma}^+) \quad (247)$$

$$= \sum_r \frac{1}{\Lambda + \Gamma + i(\epsilon_\sigma - rV/2)} \quad (248)$$

instead, where $\epsilon_\sigma := \epsilon + \sigma B/2$. Importantly, for $U = 0$ these matrix elements are independent of $\Delta F_{\eta\sigma}^{-+}$. Higher loop corrections for ψ_σ vanish since they contain the factor (246) at least once by Eq. (221). Therefore Eq. (239) is the exact RG equation for ψ_σ at $E =$ and for $U = 0$:

$$\frac{d\psi_\sigma(0)}{d\Lambda} = \sum_r \frac{2\Gamma}{\pi} \text{Im}(\alpha_{+\sigma}^+ | i\Pi_{+r}^{\alpha_{+\sigma}} | \alpha_{+\sigma}^+) \quad (249)$$

$$= \sum_r \frac{2\Gamma}{\pi} \frac{\epsilon_\sigma - rV/2}{(\Lambda + \Gamma)^2 + (\epsilon_\sigma - rV/2)^2} \quad (250)$$

where we again used the K -conjugation properties Eq. (70), (117) and (118). With the initial value $\psi_{\sigma, \Lambda=\infty} = 0$ (cf. Eq. (135).) we obtain

$$\psi_\sigma(0) = - \sum_r \frac{2\Gamma}{\pi} \arctan \left(\frac{\epsilon_\sigma - rV/2}{\Gamma} \right)$$

Leaving out the summation over the electrode r in the above calculation, we obtain the coefficients of the self-

energy component $\bar{L}_\Lambda^r|_{\Lambda=0} = \Sigma^r(0)$, required for the current (cf Eq. (191)),

$$\begin{aligned} \langle I^r \rangle &= \frac{1}{\sqrt{2}} \left[(T_0 | \vec{\psi}^r \rangle - (T_0 | \xi^r \xi^{-1} | \vec{\psi} \rangle) \right] \\ &= \frac{1}{4} \sum_{\sigma} (\psi_{\sigma}^r - \psi_{\sigma}^{\bar{r}}), \end{aligned} \quad (251)$$

using $\frac{1}{\sqrt{2}}(T_0 | = \frac{1}{2} \sum_{\sigma} (\chi_{\sigma} |$ and $\xi^r = \xi/2$ giving finally

$$\langle I \rangle = \sum_{r, \sigma=\pm} r \frac{\Gamma}{2\pi} \arctan \left(\frac{\epsilon_{\sigma} + rV/2}{\Gamma} \right) \quad (252)$$

and for the non-linear differential conductance:

$$\frac{dI}{dV} = \frac{1}{4\pi} \sum_{r, \sigma=\pm} \frac{\Gamma^2}{\Gamma^2 + (\epsilon_{\sigma} + rV/2)^2} \quad (253)$$

in our units $e = 1$, $\hbar = 1$ Restoring CGS units the current and conductance prefactors become $\frac{\Gamma}{2\pi} \rightarrow \Gamma \frac{e}{\hbar} \frac{\Gamma}{2\pi} \rightarrow \Gamma \frac{e^2}{2\hbar}$ giving in linear response a conductance of e^2/h per spin channel. The importance of recovering this exact result for $U = 0$ is that already at this level of approximation our the RT-RG approach captures correctly the weak interaction limit $U \ll \Gamma$, while treating the tunneling non-perturbatively in Γ . Moreover, it shows that the 2-loop corrections to the Liouvillian and 1-loop corrections to the vertices *which affect the stationary current* are generated by the Coulomb interaction. In general, however, the non-interacting limit requires a 2-loop treatment.

D. 2 loop RG equations

1. Vertex frequency dependence

As concluded in Sec. (III C 1) in the 2-loop approximation for the Liouvillian we should consider the vertex renormalization and ω -dependence of both \bar{G} and \bar{L} . Indeed, we find below that these effects are comparable and involve important cancellations. By systematically expanding about the frequency-independent bare vertex \bar{G}^0 , we can incorporate the vertex corrections into a single effective equation for the 2-loop Liouvillian, Eq. (272) below. We proceed in three steps:

Step 1 Starting point is the 1-loop approximation defined by Eq. (228) for any E . This we use to calculate a first approximation for the ω -dependence of both the Liouvillian and the propagator. We expand

$$\bar{L}(E, \omega) \approx \bar{L}^0(E) + \bar{L}^1(E, \omega) \quad (254)$$

$$\Pi(E, \omega) \approx \Pi^0(E, \omega) + \Pi^1(E, \omega) \quad (255)$$

The 1-loop equation accounting for the leading frequency dependence is obtained by setting $G \approx G^0$ and $\Pi(E, \omega) \approx \Pi^0(E, \omega)$ the 1-loop part of Eq. (208):

$$\frac{d\bar{L}(E, \omega)}{d\Lambda} = i \frac{\Gamma}{\pi} \bar{G}_1^0 \Pi^0(E_1, \Lambda + \omega) \bar{G}_1^0 \quad (256)$$

Subtracting Eq. (228), we obtain

$$\frac{d\bar{L}^1(E, \omega)}{d\Lambda} \approx i \frac{\Gamma}{\pi} \bar{G}_1^0 (\Pi^0(E_1, \omega + \Lambda) - \Pi^0(E_1, \Lambda)) \bar{G}_1^0.$$

Shifting the integration variable in the $\Pi(E_1, \Lambda)$ term we obtain (in wide band limit assumed throughout):

$$\bar{L}^1(E, \omega) \approx \int_{\Lambda-\omega}^{\Lambda} i \frac{\Gamma}{\pi} \bar{G}_1^0 \Pi^0(E_1, \omega + \Lambda) \bar{G}_1^0 \quad (257)$$

Eq. (257) does not need to be calculated further since it cancels out below. Note that the correction vanishes at zero frequency, $\bar{L}^1(E, 0) = 0$, for all E as required. Expanding the full resolvents Eq. (206) with the approximation Eq. (254) to the first order in $\bar{L}^1(E, \omega)$, we obtain:

$$\Pi^1(E, \omega) = \Pi^0(E, \omega) \bar{L}^1(E, \omega) \Pi^0(E, \omega) \quad (258)$$

Step 2 In a similar way, we now calculate the ω corrections in the leading 1-loop order for the vertices:

$$\bar{G}_1(E, \omega, \omega_1) \approx \bar{G}^0 + \bar{G}_1^1(E, \omega, \omega_1) : \quad (259)$$

Keeping on the right hand side of Eq. (209) only the leading term we obtain with the same approximations as above

$$\bar{G}_1^1(E, \omega, \omega_1) = -i \frac{\Gamma}{\pi} \int_D^{\Lambda} d\Lambda' \bar{G}_2^0 \Pi^0(E_2, \omega + \Lambda') \bar{G}_1^0 \Pi^0(E_{12}, \omega + \omega_1 + \Lambda') \bar{G}_2^0 \quad (260)$$

We stress that the argument under the integral depends on Λ' both through the explicit arguments as well as

through the cut-off dependence of $\bar{L}_{\Lambda'}$ (G^0 is the bare

vertex). Restoring the latter explicitly,

$$\Pi_{\Lambda'}^0(E, \omega + \Lambda') = \frac{1}{\omega + \Lambda' - i\bar{L}_{\Lambda'}^0(E)} \quad (261)$$

Since this is the only point where this is important we stick with the implicit notation.

Step 3 Using the expansions for the resolvents Eq. (258) and vertices Eq. (260) we can now calculate an approximation to the right hand side of Eq. (208), keeping the leading order frequency corrections:

$$\frac{d\bar{L}}{d\Lambda} = \frac{d\bar{L}^{(1\text{ loop})}}{d\Lambda} + \frac{d\bar{L}^{(2\text{ loop})}}{d\Lambda} + \frac{d\bar{L}^{(\text{vertex})}}{d\Lambda} \quad (262)$$

all written at frequencies E and ω , where

$$\frac{d\bar{L}^{(1\text{ loop})}}{d\Lambda} = i\frac{\Gamma}{\pi} \left[\bar{G}_1^0 \Pi^0(E_1, \Lambda) \bar{G}_1^0 + \bar{G}_1^0 \Pi^1(E_1, \Lambda) \bar{G}_1^0 \right] \quad (263)$$

are the terms appearing from expansion of 1-loop diagram in Π^1 ,

$$\begin{aligned} \frac{d\bar{L}^{(2\text{ loop})}}{d\Lambda} &= \frac{\Gamma^2}{\pi^2} \bar{G}_1^0 \Pi^0(E_1, \Lambda) \bar{G}_2^0 \\ &\times \Pi^0(E_{12}, \Lambda + \omega_2) \bar{G}_2^0 \Pi^0(E_1, \Lambda) \bar{G}_1^0 \end{aligned} \quad (264)$$

is 2-loop term with bare vertices, and

$$\frac{d\bar{L}^{(\text{vertex})}}{d\Lambda} = i\frac{\Gamma}{\pi} \bar{G}_1^1(E, 0, \Lambda) \Pi^0(E_1, \Lambda) \bar{G}_1^0 \quad (265)$$

$$+ i\frac{\Gamma}{\pi} \bar{G}_1^0 \Pi^0(E_1, \Lambda) \bar{G}_1^1(E_1, \Lambda, -\Lambda) \quad (266)$$

are the terms appearing from the expansion of \bar{G} in \bar{G}^1 in the 1-loop diagram. Inserting Eq. (257) into the 1-loop Liouvillian frequency correction (last term in Eq. (263)), we see that it exactly cancels the 2-loop term Eq. (264). Neither term therefore needs to be calculated, simplifying the approach to a great extent.

The above holds for any E and ω : integrating the Eq. (262) at $\omega = 0$ using the above calculated right hand side we obtain a new approximation for $\bar{L}^0(E)$, improving over our initial approximation based on the 1-loop equation Eq. (228). In principle, with this steps 1 and 2 should be repeated, resulting in corrections of higher orders which we neglect. We thus equate $d\bar{L}/d\Lambda \approx \bar{L}^0/d\Lambda$ on the left hand side of Eq. (262). We obtain a central result of the this section: an effective 2-loop RG equation for the Liouvillian at $\omega = 0$

$$\begin{aligned} \frac{d\bar{L}^0(E)}{d\Lambda} &= i\frac{\Gamma}{\pi} \bar{G}_1^0 \Pi^0(E_1, \Lambda) \bar{G}_1^0 \\ &+ i\frac{\Gamma}{\pi} \bar{G}_1^1(E, 0, \Lambda) \Pi^0(E_1, \Lambda) \bar{G}_1^0 \\ &+ i\frac{\Gamma}{\pi} \bar{G}_1^0 \Pi^0(E_1, \Lambda) \bar{G}_1^1(E_1, \Lambda, -\Lambda) \end{aligned} \quad (267)$$

Notably, due to the cancellation the entire leading reservoir (ω) frequency dependence comes from the vertex corrections Eq. (260). This single equation yields a significant simplification over the coupled equations Eq. (208)

and Eq. (209). As expected, the elimination of Eq. (209) makes Eq. (267) an integro-differential equation for \bar{L} . However, it can be converted into a differential RG equation by analytically performing the integral in Eq. (260), see Sec. (III D 2). Furthermore, since we can work with the bare vertex super operators and we can make use of their simple anti-commutation relations Eq. (53), that are *not* preserved under the RG (in contrast to other useful properties of the vertex, see App. G). The QD frequency (E) dependence in Eq. (267) is of the same type as for the 1-loop equations Eq. (232): the RG equation for $L^0(0)$ depends on $L^0(\bar{\mu}_1) = L^0(\eta_1 r_1 V/2)$, etc. It therefore has to be solved in the same way by including multiple Matsubara axes and converging the energy-hierarchy of equations, see Sec. (III C 1) and Sec. (IV). Finally, we also note that one can indeed neglect the frequency dependence generated by vertex renormalization since it is indeed small, as we assumed in our derivation of the 1-loop equations. This can be seen if one substitutes the calculated correction Eq. (260) into Eq. (209). Here we anticipate the projector expansion of \bar{G}^1 , Eq. (271): it is seen that \bar{G}^1 is a well behaved function of the cut-off and frequency, decaying at small Λ , and it generates only small corrections in agreement with our approximation Eq. (226).

2. Explicit 2-loop RG equations for the Liouvillian

To obtain a differential RG equation from Eq. (267), the integration Eq. (260) needs to be performed. This complicated by the implicit Λ' dependence in the propagators pointed out with Eq. (261). We now make an adiabatic approximation by expanding *only* this dependence about $\Lambda' = \Lambda$, i.e. we substitute

$$\bar{L}_{\Lambda'} \approx \bar{L}_{\Lambda} \quad (268)$$

in Eq. (261) and neglect corrections $\sim d\bar{L}_{\Lambda'}/d\Lambda$ which, by the RG equation Eq. (267), are of higher order and should therefore be neglected. To preserve the compact form of the equations we define

$$\Theta_{1\dots n}^i = E_{1\dots n} - \lambda^i(E_{1\dots n}) \quad (269)$$

$$P_{1\dots n}^i = P^i(E_{1\dots n}) \quad (270)$$

where $P^i(E)$ and $\lambda^i(E)$ are eigenprojectors and eigenvalues from Eq. (149) at cut-off Λ (not Λ') and we will implicitly sum over all appearing eigenvalue labels i, j, k below. To perform the integral we insert the projector expansion Eq. (149) of \bar{L} evaluated at Λ under the integral

and obtain the explicit ω -dependent vertex correction:

$$\begin{aligned} \bar{G}_1^1(E, \omega, \omega_1) = & \quad (271) \\ & -i \frac{\Gamma}{\pi} \int_D^\Lambda d\Lambda' \frac{\bar{G}_2^0 P^i(E_2) \bar{G}_1^0 P^j(E_{12}) \bar{G}_2^0}{(\Lambda' + \omega - i\Theta_2^i) (\Lambda' + \omega + \omega_1 - i\Theta_{12}^j)} \\ = & i \frac{\Gamma}{\pi} \frac{\bar{G}_2^0 P^i(E_2) \bar{G}_1^0 P^j(E_{12}) \bar{G}_2^0}{\omega_1 - i(\Theta_{12}^j - \Theta_2^i)} \ln \left(\frac{\Lambda + \omega - i\Theta_2^i}{\Lambda + \omega + \omega_1 - i\Theta_{12}^j} \right) \end{aligned}$$

Combining the rest of Eq. (263) with Eq. (265) we obtain:

$$\begin{aligned} \frac{d\bar{L}^0(E)}{d\Lambda} = & \frac{\Gamma}{\pi} \frac{1}{\Lambda - i\Theta_1^k} \bar{G}_1^0 P_1^k \bar{G}_1^0 \quad (272) \\ & - i \frac{\Gamma^2}{\pi^2} \frac{1}{\Lambda - i\Theta_1^k} \frac{1}{\Lambda - i(\Theta_{12}^j - \Theta_2^i)} \ln \left(\frac{2\Lambda - i\Theta_{12}^j}{\Lambda - i\Theta_2^i} \right) \\ & \times \left[\bar{G}_1^0 P_1^k \bar{G}_2^0 P_{12}^j \bar{G}_1^0 P_2^j \bar{G}_2^0 + \bar{G}_2^0 P_2^j \bar{G}_1^0 P_{12}^j \bar{G}_2^0 P_1^k \bar{G}_1^0 \right] \end{aligned}$$

This explicit result is a central result of this paper.

The explicit evaluation of Eq. (272) for the Anderson model is required for our numerical implementation, but also allows us to draw some general conclusions about the 2-loop (and higher) corrections. The 1-loop part is that given by Eq. (228) and we proceed analogously for the 2-loop part:

$$\left. \frac{d\bar{L}^0(E)}{d\Lambda} \right|_{2\text{ loop}} = -i \frac{\Gamma^2}{\pi^2} (\kappa_7 | \mathcal{M} | \kappa_0) | \kappa_7 \rangle \langle \kappa_0 | \quad (273)$$

where the super matrix elements are factored as follows:

$$\begin{aligned} (\kappa_7 | \mathcal{M} | \kappa_0) = & \quad (274) \\ & \sum_{\kappa_6 \dots \kappa_1} (\kappa_7 | \bar{G}_1^0 | \kappa_6) (\kappa_5 | \bar{G}_2^0 | \kappa_4) (\kappa_3 | \bar{G}_1^0 | \kappa_2) (\kappa_1 | \bar{G}_2^0 | \kappa_0) \\ & \times \mathcal{N} \left((\kappa_6 | P_1^k | \kappa_5), (\kappa_4 | P_{12}^j | \kappa_3), (\kappa_2 | P_2^i | \kappa_1) \right) \end{aligned}$$

The product of \bar{G}^0 matrix elements gives a simple numerical factor, whereas the remaining part,

$$\mathcal{N} \left((\kappa_6 | P_1^k | \kappa_5), (\kappa_4 | P_{12}^j | \kappa_3), (\kappa_2 | P_2^i | \kappa_1) \right) = \quad (275)$$

$$\mathcal{S}(\Theta_1^k, \Theta_2^i, \Theta_{12}^j) (\kappa_6 | P_1^k | \kappa_5) (\kappa_4 | P_{12}^j | \kappa_3) (\kappa_2 | P_2^i | \kappa_1)$$

contains the product of the non-trivial projector matrix elements and the propagator factors

$$\begin{aligned} \mathcal{S}(\Theta_1^k, \Theta_2^i, \Theta_{12}^j) = & \frac{\ln \left(\frac{2\Lambda - i\Theta_{12}^j}{\Lambda - i\Theta_2^i} \right)}{(\Lambda - i\Theta_1^k) (\Lambda - i(\Theta_{12}^j - \Theta_2^i))} \\ & + (\Theta_1^k \leftrightarrow \Theta_2^i) \quad (276) \end{aligned}$$

The argument of this function is constructed by formally putting the variables containing the eigenvalues of the

three projectors in the argument \mathcal{N} into the corresponding arguments of the scalar function Θ . With this we can give explicit expressions for Eq. (273). In App. G it is shown how the conservation of Hermiticity by the self-energy can be used to minimize the number of terms to be calculated.

For the right hand side of Eq. (273) we now give explicitly half of terms:

$$- |\chi_\sigma\rangle \langle \chi_\sigma| \quad (277)$$

$$\begin{aligned} & [\mathcal{N}((\alpha_{+\sigma}^+ | P_1^{\alpha+\sigma} | \alpha_{+\sigma}^-), (T_+ | P_{12}^T | T_+), (\alpha_{+\sigma}^+ | P_2^{\alpha+\sigma} | \alpha_{+\sigma}^-)) \\ & + \mathcal{N}((\alpha_{+\sigma}^+ | P_1^{\alpha+\sigma} | \alpha_{+\sigma}^-), (S_\sigma | P_{12}^S | S_\sigma), (\alpha_{-\sigma}^+ | P_2^{\alpha-\sigma} | \alpha_{-\sigma}^-))] \\ & + |\chi_\sigma\rangle \langle \chi_\sigma| \quad (278) \end{aligned}$$

$$\begin{aligned} & \mathcal{N}((\alpha_{+\sigma}^+ | P_1^{\alpha+\sigma} | \alpha_{+\sigma}^-), (\chi_{\bar{\sigma}} | P_{11}^X | \chi_\sigma), (\alpha_{-\sigma}^+ | P_1^{\alpha-\sigma} | \alpha_{-\sigma}^-)) \\ & - |\chi_\sigma\rangle \langle Z_L| \quad (279) \end{aligned}$$

$$\begin{aligned} & [\mathcal{N}((\alpha_{+\sigma}^+ | P_1^{\alpha+\sigma} | \alpha_{+\sigma}^-), (T_+ | P_{12}^T | T_+), (\alpha_{+\sigma}^+ | P_2^{\alpha+\sigma} | \alpha_{+\sigma}^-)) \\ & - \mathcal{N}((\alpha_{+\sigma}^+ | P_1^{\alpha+\sigma} | \alpha_{+\sigma}^-), (S_\sigma | P_{12}^S | S_\sigma), (\alpha_{-\sigma}^+ | P_2^{\alpha-\sigma} | \alpha_{-\sigma}^-)) \\ & + \mathcal{N}((\alpha_{+\sigma}^+ | P_1^{\alpha+\sigma} | \alpha_{+\sigma}^-), (\chi_{\bar{\sigma}} | P_{11}^X | \chi_\sigma), (\alpha_{-\sigma}^+ | P_1^{\alpha-\sigma} | \alpha_{-\sigma}^-))] \\ & - |S_\sigma\rangle \langle S_\sigma| \quad (280) \end{aligned}$$

$$\begin{aligned} & [\mathcal{N}((\alpha_{+\sigma}^+ | P_1^{\alpha+\sigma} | \alpha_{+\sigma}^-), (T_+ | P_{12}^T | T_+), (\alpha_{+\sigma}^+ | P_2^{\alpha+\sigma} | \alpha_{+\sigma}^-)) \\ & + \mathcal{N}((\alpha_{+\sigma}^+ | P_1^{\alpha+\sigma} | \alpha_{+\sigma}^-), (\chi_{\bar{\sigma}} | P_{12}^X | \chi_{\bar{\sigma}}), (\alpha_{-\sigma}^+ | P_2^{\alpha-\sigma} | \alpha_{-\sigma}^-))] \\ & - |T_- \rangle \langle T_-| \quad (281) \end{aligned}$$

$$\begin{aligned} & [\mathcal{N}((\alpha_{-\sigma}^+ | P_1^{\alpha-\sigma} | \alpha_{-\sigma}^-), (S_\sigma | P_{12}^S | S_\sigma), (\alpha_{-\sigma}^+ | P_2^{\alpha-\sigma} | \alpha_{-\sigma}^-)) \\ & + \mathcal{N}((\alpha_{-\sigma}^+ | P_1^{\alpha-\sigma} | \alpha_{-\sigma}^-), (\chi_{\bar{\sigma}} | P_{12}^X | \chi_{\bar{\sigma}}), (\alpha_{-\sigma}^+ | P_2^{\alpha-\sigma} | \alpha_{-\sigma}^-))] \quad (282) \end{aligned}$$

$$\begin{aligned} & + |\alpha_{+\sigma}^- \rangle \langle \alpha_{+\sigma}^+| \\ & [\mathcal{N}((T_+ | P_1^T | T_+), (\alpha_{+\sigma}^+ | P_{11}^{\alpha+\sigma} | \alpha_{+\sigma}^-), (S_\sigma | P_1^S | S_\sigma)) \\ & + \mathcal{N}((T_+ | P_1^T | T_+), (\alpha_{+\sigma}^+ | P_{12}^{\alpha+\sigma} | \alpha_{+\sigma}^-), (\chi_\sigma | P_2^X | \chi_\sigma))] \quad (283) \end{aligned}$$

$$\begin{aligned} & + |\alpha_{-\sigma}^- \rangle \langle \alpha_{-\sigma}^+| \\ & [\mathcal{N}((\chi_\sigma | P_1^X | \chi_\sigma), (\alpha_{+\sigma}^+ | P_{12}^{\alpha+\sigma} | \alpha_{+\sigma}^-), (S_\sigma | P_2^S | S_\sigma)) \\ & + \mathcal{N}((\chi_\sigma | P_1^X | \chi_\sigma), (\alpha_{-\sigma}^+ | P_{12}^{\alpha-\sigma} | \alpha_{-\sigma}^-), (T_- | P_2^T | T_-)) \\ & + \mathcal{N}((S_\sigma | P_1^S | S_\sigma), (\alpha_{-\sigma}^+ | P_{11}^{\alpha-\sigma} | \alpha_{-\sigma}^-), (T_- | P_1^T | T_-)) \\ & + \mathcal{N}((S_\sigma | P_1^S | S_\sigma), (\alpha_{+\sigma}^+ | P_{12}^{\alpha+\sigma} | \alpha_{+\sigma}^-), (\chi_{\bar{\sigma}} | P_2^X | \chi_{\bar{\sigma}})) \\ & - \mathcal{N}((\chi_\sigma | P_1^X | \chi_{\bar{\sigma}}), (\alpha_{+\sigma}^+ | P_{12}^{\alpha+\sigma} | \alpha_{+\sigma}^-), (\chi_\sigma | P_2^X | \chi_{\bar{\sigma}}))] \quad (284) \end{aligned}$$

Here we use the notation

$$P_i^k = P^k(-\eta_i \mu_i), \quad P_{ij}^k = P^k(-\eta_i \mu_i - \eta_j \mu_j) \quad (285)$$

We fixed the particle-hole index η in the multiindices 1 and 2 to be + (and therefore - for the $\bar{1}, \bar{2}$):

$$\eta_{i(j)} = \begin{cases} +, & i(j) = 1, 2 \\ -, & i(j) = \bar{1}, \bar{2} \end{cases} \quad (286)$$

All other indices in Eq. (277)-(284) are implicit summed over. The other half of the terms of Eq. (273) can be constructed in the same way by taking into account the opposite sign of η_1 using the recipe of Appendix G). For

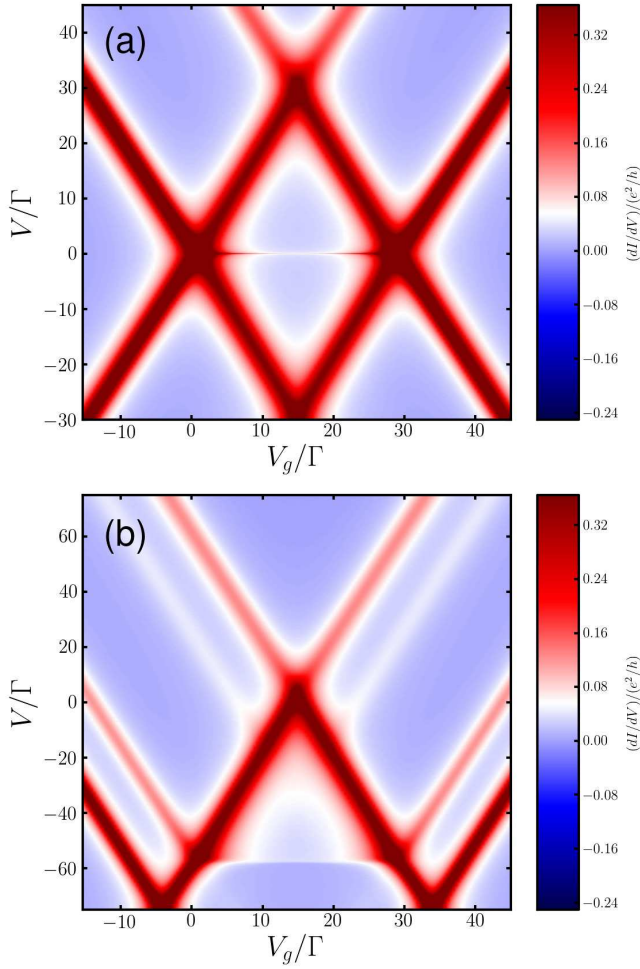


FIG. 6: Zero-temperature non-linear conductance dI/dV vs bias V and gate voltage $V_g = -\epsilon$ for strong interaction $U = 30\Gamma$ and (a) zero magnetic field $B = 0$ and (b) finite field $B = 9\Gamma$. Both figures are calculated in 2-loop RG (Eq. (228),(273)) and are converged with respect to the number of non-equilibrium Matsubara axes (cf. Sect.III B 1) using a sufficiently large bandwidth $D = 10^3\Gamma$. The linear conductance in (b) shows good agreement with the Friedel sum rule, cf. Fig. 7.

the calculation of the current only the leftmost reservoir index r_1 should not be summed over.

We presented Eq. (277)-(284) in order to show a number of important general properties. First, in the fermionic sector (281)-(284), the structure is the same as for the 1-loop equation, i.e., only terms $|\alpha_{\eta\sigma}^- \rangle \langle \alpha_{\eta\sigma}^+|$ appear as discussed Sec. (III B 3). This property holds in any order of RG and is manifestation of the general properties Eq. (133)-(134).

Secondly, Eq. (277)-(284) only lists the terms of the 2-loop RG equations which are relevant for the current. The right hand side of all these equations are proportional to the matrix elements $\langle \alpha_{\eta\sigma}^+ | P^{\alpha_{\eta\sigma}} | \alpha_{\eta\sigma}^- \rangle$ as was anticipated in Sec. (III C 3). This is also a general property which holds in any loop order of the RG. In the

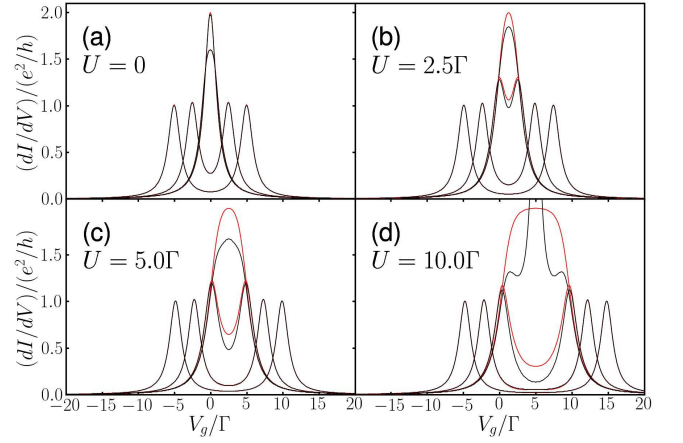


FIG. 7: Linear conductance $dI/dV|_{V=0}$ as function of the gate voltage V_g , obtained numerically for bias $V = 0.001\Gamma$ for which the response was checked to be linear for all V_g . Our 2-loop RT-RG results (black curves) are compared with Friedel sum rule conductance $\sum_{\sigma} g_{\sigma}$ (red curves) which are obtained from Eq. (287) using the occupations $\langle n_{\sigma} \rangle$ calculated within our RG. Across panels (a)-(d) the interaction increases, $U/\Gamma = 0.0, 2.5, 5.0, 10.0$. Within each panel the magnetic field is increased, $B/\Gamma = 0.0, 1.0, 5.0, 10.0$. Panel (a) for $U = 0.0$ serves as a reference, numerically confirming the analytic result Eq. (253) that already in 1-loop we include the exact non-interacting solution.

non-interacting limit, $U = 0$, this implies that all 2-loop (and higher loops) corrections *relevant to the current* vanish exactly c.f. Eq. (245). We emphasize there are additional terms not listed in Eq. (277)-(284) which are irrelevant for the current. These describe the 2-loop renormalization of the ζ coefficient: these involve factors $\langle \alpha_{\eta\sigma}^- | P^{\alpha_{\eta\sigma}} | \alpha_{\eta\sigma}^+ \rangle$ and therefore do *not vanish*, even for $U = 0$. However corrections to this coefficient beyond 2-loops order do contain the factors (246) and vanish for $U = 0$. See for more details Ref. 50.

IV. RESULTS

In this section we perform a detailed numerical investigation of the zero-temperature 2-loop RT-RG equations $\frac{d\tilde{L}^0(E)}{d\Lambda} = \frac{d\tilde{L}^0(E)}{d\Lambda} \Big|_{1\text{loop}} + \frac{d\tilde{L}^0(E)}{d\Lambda} \Big|_{2\text{loop}}$ where the right hand sides are given by Eq. (228) and (273), obtaining the current as indicated below Eq. (211). We focus on the dependence on the interaction U and the magnetic field B as function of both the bias and gate voltage. To clearly structure the discussion we first summarize the central features of the calculated conductance as exemplified in Fig. 6(a) and (b) for zero and finite magnetic field B , respectively, and assess the limits of applicability.

A. Overview and limits of applicability

At zero magnetic field the dominant features in Fig. 6(a) are the Coulomb blockade diamonds defined by lines along which a SET resonance appears. In our calculated results, these dI/dV peaks are broadened on the scale Γ due to non-perturbative tunneling processes and have a peak height e^2/h , i.e., the quantum conductance. Going into either of the Coulomb blockade regimes where the charge is quantized to $N = 0, 1$ and 2 , the current decays non-exponentially due to higher order tunneling (cotunneling and higher order processes). At very small bias, however, the conductance shows a pronounced anomaly, but only in the $N = 1$ regime where the dot has an unpaired spin. We stress from the start that this should not be naively identified with the Kondo anomaly of the Anderson model: the correct description of the Kondo peak requires 3-loop RT-RG corrections which are beyond the scope of this work^{27,53}. To clarify in which regimes of voltages our results apply we first discuss the linear conductance through the spin-channel σ : $g_\sigma = (dI_\sigma/dV)_{V=0}$, in particular the consistency with the Friedel sum rule

$$g_\sigma = \frac{e^2}{h} \sin^2(\pi \langle n_\sigma \rangle) \quad (287)$$

In Fig. 7 it is clearly seen that at zero field $B = 0$ the conductance increasingly violates the Friedel sum rule between the two SET peaks for larger U , the violation becoming maximal at the particle hole symmetry point: our result reaches $4e^2/h$ instead of $2e^2/h$. At best, in this regime our 2-loop approach can be a starting point for further 3-loop corrections containing the log-divergent Kondo corrections: However, it should be noted that the violation is *finite*, even at zero T : The key observation in Fig. 7 is that beyond a magnetic field $B \sim \Gamma$ only a *renormalized* elastic cotunneling background remains and our results rapidly becomes consistent with the Friedel sum rule. Clearly, at voltages above $B \sim \Gamma$ the 3-loop Kondo renormalization is expected to be negligible compared to the 1- and 2-loop corrections that we accounted for here. In all further analyses, the low bias regime $V < \Gamma$ will thus be ignored for magnetic fields $B \lesssim \Gamma$. We do, however, show our results in this bias regime for two reasons: (i) knowing the behavior of the 2-loop scheme is of interest as it presents a starting point for future 3-loop calculations and (ii) the behavior of the 2-loop approach can be compared with that for other methods in this regime. We note, e.g., that for $U = 2.5\Gamma$ the violation of the Friedel sum rule is still rather modest, even at zero field. Our 2-loop RG thus accounts non-perturbatively for the strong tunneling effects at zero temperature, covering the complete *finite bias* stability diagram, where previous perturbative generalized master / kinetic equation approaches^{29,30} break down.

Based on the above, we expect that for a finite magnetic field $B \gtrsim \Gamma$ the 2-loop RT-RG calculations reliably address transport features, illustrated in Fig. 6(b), at

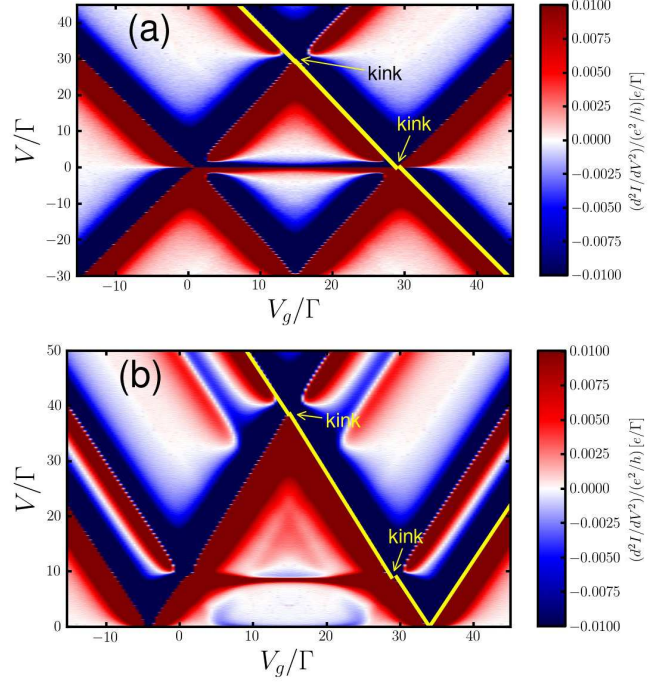


FIG. 8: Peak positions of dI/dV : shown is dI^2/dV^2 in a zoom of Fig. 6, making the zeros of dI/dV stand out as curves separating red (positive) and blue (negative) regions. The yellow lines are guides to the eye obtained by accurate extrapolation of the linear parts of the resonance lines (including data points outside the figure). These emphasize the change of the slope of the linear parts of the resonance positions, in addition to the non-linear renormalizations close to the kinks. In (a) kinks occur at $V \approx 0$ and $V \approx \pm U$, whereas in (b) they occur at $V \approx \pm B$ and $V \approx \pm U + B$. Note that in (b) there is no discernible kink at $V = \pm(U - B)$: at this energy there is a SET resonance “hitting” the Coulomb blockade diamond edge but there is *no onset of inelastic cotunneling*, in contrast to $V = \pm B$ where there is such an excitation. This signals the importance of inelastic cotunneling for the appearance of such kinks.

all applied voltages. Clearly, the SET resonance peaks have been split due the Zeeman effect. The zero-bias anomaly splits into two inelastic cotunneling resonances at finite bias $V \approx B$ (Zeeman excitations). A much smaller zero-bias anomaly remains which should be ignored, as mentioned above. The above mentioned features are of course known from previous studies and have been observed in many experiments. Our new approach, however, includes renormalization effects of these basic transport signatures, which are non-perturbative in Γ far from equilibrium. The following more detailed analysis, bearing the above restrictions in mind, indeed reveals several low-temperature renormalization effects that may be of experimental relevance.

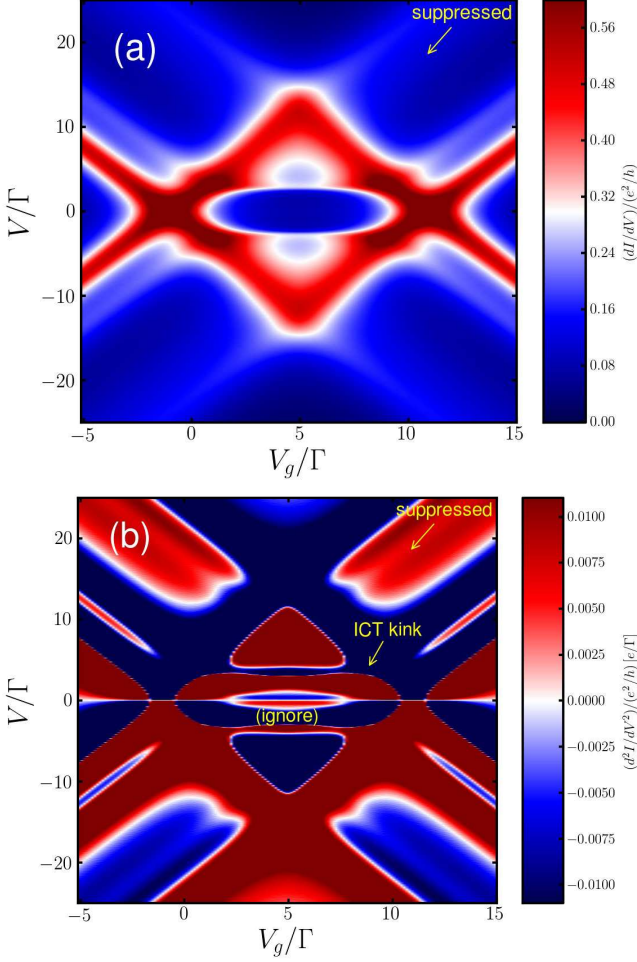


FIG. 9: (a) Non-linear conductance dI/dV as in Fig. 6(b) but for reduced interaction $U = 10\Gamma$ and magnetic field $B = 3\Gamma$. (b) Derivative of (a), d^2I/dV^2 , highlighting the renormalization of SET peak position (see caption Fig. 8(b)), in particular at the onset of ICT.

B. Single electron resonance: level renormalization and broadening

1. Kinks

Careful inspection reveals that the SET resonance lines in fact change their slope when crossing $V = 0$ and $V = U$. This can already be seen for small Γ in Fig. 6(a) where we plot the V -derivative of Fig. 6(a) to follow the peak positions, adding a linear extrapolation. The SET resonance lines of the inner diamond change in such a way that the charge gap hardly renormalizes for $U \gg \Gamma$, although diamond distortions are visible by kinks in the linear extrapolations. The charge gap can both be determined from the height of the diamond (non-linear response) or from the width of the diamond (linear response) and no significant deviation is found in this limit.

A related effect arises in a magnetic field: the SET slope below (above) the ICT threshold is smaller (larger)

than the slope of the bare resonance line. As a result the SET lines now show a kink at finite $V = \pm B$. We note that no such kink is seen at $V = U - B$: this indicates that indeed the ICT is responsible for this effect since at $V = U - B$, in contrast to $V = B$ there is *no* ICT excitation. In (a) at $V = 0$ there is some non-linearity around $V = \Gamma$ (small V should be ignored, see above) which persists in (b) around $V = B$ in a magnetic field.

Upon increasing Γ relative to U these effects are enhanced as shown in Fig. 9(a). The edges of the $N = 1$ Coulomb-blockade regime tend to bend inwards, towards the diamond center. Notably, above the onset of COT the slope is slightly larger than that of the bare resonance line. We furthermore observe that this also leads to the suppression of the excitation $|\downarrow\rangle \rightarrow |2\rangle$ at $\mu_L - \mu_R = \epsilon_\uparrow + U$ in Fig. 9 (see arrow), which is still clearly visible in Fig. 6, see arrows in Fig. 9(a) and (b).

2. Analysis

It seems not possible to analytically extract a simple physical picture explaining the above non-linearities. The following analysis aims to indicate why this is the case: we trace back at which stage of the 2-loop RG scheme the various effects are generated taking the parameter set of Fig. 9(b) as a starting point. In Fig. 10 we show the conductance calculated both in 1- and 2-loop RG and both with and without converging the calculations with respect to the non-equilibrium Matsubara axes.

Clearly, the different slopes and non-linearities already arise in the 1-loop RG: it is visible from Fig. 10(b). Their strength correlates with that of the signatures of ICT appearing in the stability map in the various approximations. However, for this it is crucial that the Matsubara axes are accounted for: this is seen by directly comparing Fig. 10(a), Fig. 10(b) and is confirmed by Fig. 11 where we explicitly plot the difference of former two figures.

Overall, the 2-loop corrections are most pronounced along the SET-regime boundaries and the ICT threshold as comparison of Fig. 10(b) and Fig. 10(d) and the plot of their difference in Fig. 12 shows. Also in 2-loop order, the kinks are most pronounced in the Matsubara-converged result. We conclude that the 2-loop fluctuation effects result in a non-trivial energy dependence of the vertices and Liouvillian which shows up in anomalous features of the measurable stability diagram, even for such a simple Anderson model of a quantum dot. We emphasize that these features are not related to renormalization processes that generate the Kondo effect (3-loop, not included here) and have an effect at $V \sim B \gtrsim \Gamma$.

3. Experimental implications

Having traced the origin of the change of the slopes and the non-linearities of the SET resonances we discuss

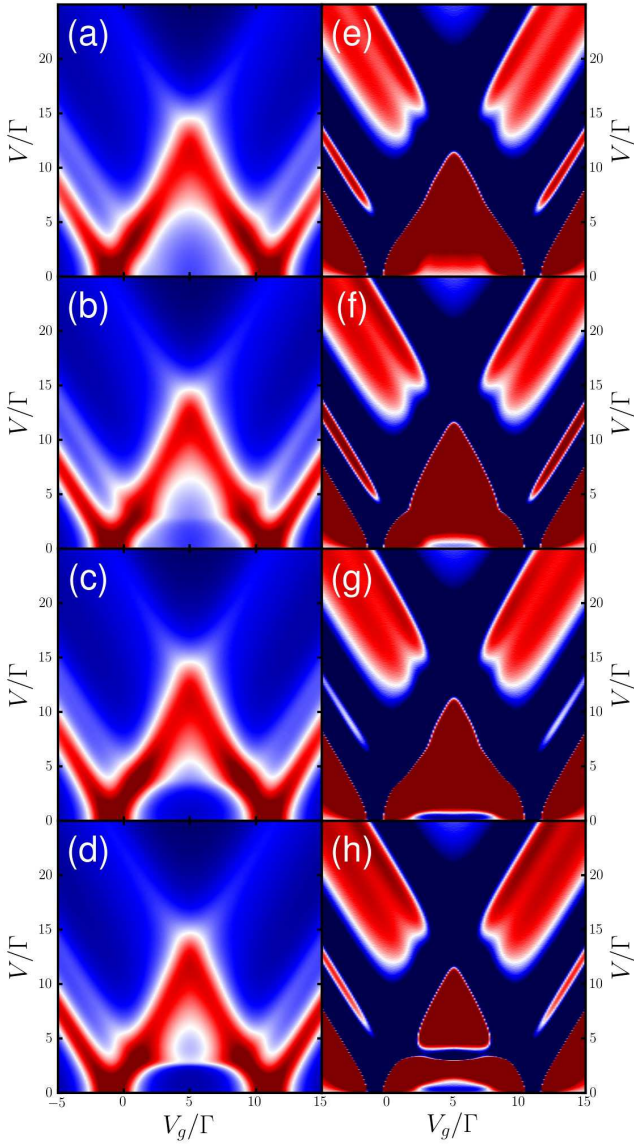


FIG. 10: Comparison of dI/dV calculated (same color scale as Fig. 9) in the 1-loop (a-b) and 2-loop (c-d) approximation neglecting all Matsubara axes altogether (a,c) and fully converging using 15 frequency axes (b,d). The 2nd column shows the corresponding d^2I/dV^2 maps, allowing the dI/dV peak positions to be followed (see caption Fig. 8(b)) In particular, the inelastic cotunneling excitation at $V = B$ evolves from a step in (a)-(c) into a peak in (d). Clearly, the non-equilibrium Matsubara frequency dependence is responsible for the “kinks” in the SET resonance (they already appear in 1-loop with quantitative modifications in 2-loop).

their relevance to experiments. In fact, kinks in SET resonances are often observed in various type of quantum dot systems^{54–57}. Our calculations indicate that tunnel-induced renormalization is a possible mechanism for their occurrence, but other (e.g. electrostatic mechanisms^{58,59}) should not be ruled out in an experimental situation. However, for strong coupling it is physically

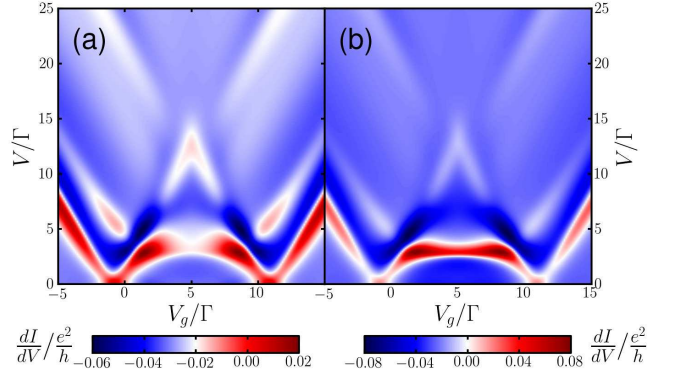


FIG. 11: Effect of Matsubara axes convergence: plotted is the converged result minus the result neglecting all Matsubara axes for (a) 1-loop RG (Fig. 10(b)–(a)) and for (b) 2-loop RG Fig. 10(d)–(c)). Adjacent red and dark blue regions indicate that the correction is an S-shaped curve which, when added to a peaked curve, results in a shift the peak position. Clearly, the Matsubara frequency dependence has an impact on the positions of all resonances and should be accounted for fully.

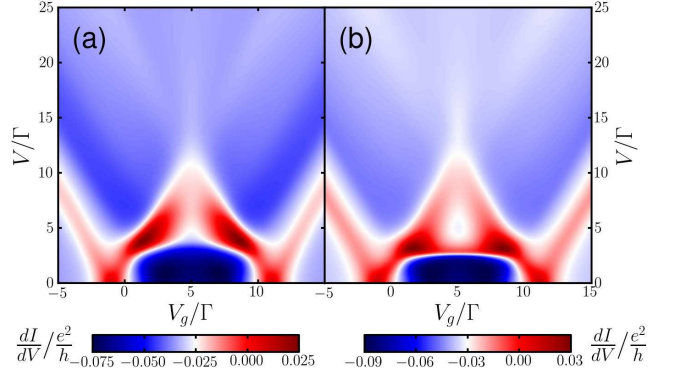


FIG. 12: Effect of 2-loop corrections: shown is the 2-loop result minus the 1-loop result in (a) without Matsubara frequency dependence (Fig. 10(c)–(Fig. 10(a)) and in (b) for converged Matsubara frequency dependence (Fig. 10(d)–(Fig. 10(b))) Note the positive corrections to magnitude of the inelastic cotunneling in (b).

not unexpected that when ICT sets on the level renormalization significantly changes, resulting in such a kink.

A direct test of this assumption would be to track the Coulomb diamond as function of the coupling strength Γ . In Fig. 13(a) and (b) we show predictions for the evolution of the SET resonance point for two fixed gate voltages, one below and one above the ICT threshold, respectively. The main observation from such a plot is that the peaks evolve along curves that are *not* simply offset by a constant bias. This indicates that the renormalization of SET resonance becomes increasingly nonlinear and a kink must develop. (Note that experimentally Γ may change non-linearly with control voltages but this does not spoil the argument.) It is important to properly choose the point above the ICT threshold: depending

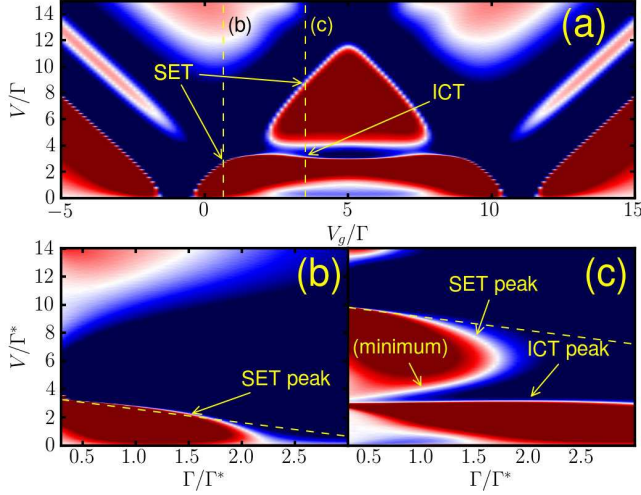


FIG. 13: Distortion of the stability diagram with increasing tunnel coupling Γ . (a) Zoom in of Fig. 9 of dI^2/dV^2 (same scales and units) highlighting the gate voltage dependence of the SET and ICT bias thresholds generated by tunnel renormalization. Here $U = 10.0\Gamma^*$, $B = 3.0\Gamma^*$ and Γ^* is the reference value of Γ . In panel (b) and (c) we show the evolution of the zeros of dI^2/dV^2 as the tunnel coupling is increased from $\Gamma = 0.3\Gamma^*$ to $3.0\Gamma^*$ along a fixed gate-voltage cut in (a), marked the vertical dashed line $V_g = -\epsilon = 0.65\Gamma^*$ for (b) and $V_g = -\epsilon = 3.50\Gamma^*$ for (c). Also U and B are kept fixed. The dashed linear approximation to the renormalized SET positions in (c) is copied with a vertical offset to (b), showing that the renormalization is *non-uniform* in the gate-voltage. This signals a distorted stability diagram. The ICT peak has a weaker Γ dependence that is non-monotonic (not visible).

on the gate voltage position the peak may renormalize stronger or weaker than the peak below the threshold. We are aware that experimentally such tuning of Γ with gate voltages may lead to other side effects which may be hard to distinguish from the effect. Here the different renormalization of the ICT resonance can be of use, which is discussed next.

C. Cotunneling resonance: gap renormalization and reduced broadening

Having discussed the effect of the ICT on the SET resonances, we now study the ICT features themselves in more detail. Fig. 14 shows how the inelastic cotunneling resonance exhibits a Zeeman splitting with increasing magnetic field. Despite the zero temperature, the width of the inelastic cotunneling feature is finite and clearly seen to depend on the magnetic field, and thereby on the voltage at which this resonance occurs. This is in contrast to high-temperature 2-loop perturbation theory^{29,30} where this resonance appears as a thermally broadened feature at the unrenormalized excitation energy. At larger voltage $V = B$, the resonance width increases, reflecting a decreasing life-time. This

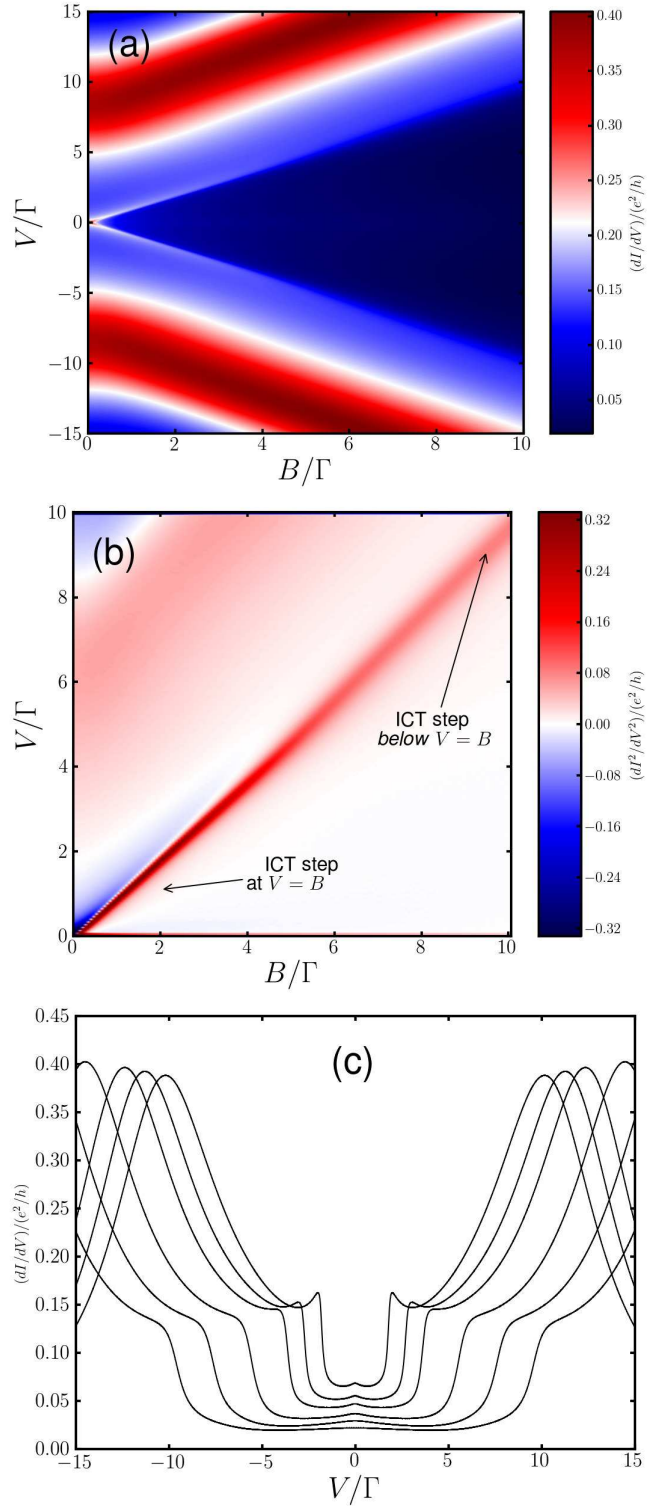


FIG. 14: (a) Zeeman splitting of the cotunneling resonance (change in blue color) and shift of the SET peaks (red peak). $U = 30\Gamma$, $V_g = (U/2 - U/3)\Gamma = U/6 = 5\Gamma = -\epsilon$ (b) dI/dV traces of (a) for $B/\Gamma = 2.0, 3.0, 4.0, 6.0, 8.0, 10.0$ (c) Zoom in of the bias-derivative of (a), i.e., dI^2/dV^2 showing the resonance position. The peak in dI/dV in (a) follows the line $V = B$ (marked dotted line starting at (0,0)) The step in dI/dV in (a) instead follows a parallel line that is offset by a constant magnetic field (in this case $\approx 0.45\Gamma$, marked by the dotted line starting at (10,10)). For lower field, this step position starts to deviate from the linear behavior when the peak starts to develop and the transition sharpens.

energy-dependence of the width is generated by our 2-loop renormalization since the initial Liouvillian of the RG flow, Eq. (136), has imaginary parts that are all $\sim \Gamma$.

Next, as the magnetic field is reduced, but still on the order of several times Γ the differential conductance develops a pronounced peak on top of the inelastic tunneling step: in Fig. 14(b) this is signaled by the onset of a negative second-derivative of the current (blue) and clear from the conductance traces in Fig. 14(c). It is known that part of such a peak on top of the well-known inelastic tunneling step⁶⁰ is due to non-equilibrium occupations^{30,61–63} that we also fully take into account. The enhanced conductance at the cotunneling resonance is due to the 2-loop renormalization, including the frequency dependence. Only after including both 2-loop corrections *and* converging with respect to the Matsubara frequency axes the ICT resonance evolves from a dI/dV step into a peak. This was illustrated (for smaller U) in Fig. 10: (a)-(c) show no ICT peak (since their derivatives (e)-(g) have no zero at the ICT threshold $V \approx B$) in contrast to Fig. 10(d), see also Fig. 13. These effects thus cannot be explained by a simpler, yet still accurate effective picture, underlining the importance of the general approach developed here.

This enhancement is not related to Kondo-exchange tunneling, which is known to lead to additional logarithmic enhancements^{27,62}: their renormalization is not included in our 2-loop calculations and is expected to be of limited importance at this large magnetic fields (several times Γ). The qualitative change of the inelastic conductance feature from a step to a peak in Fig. 14(b) implies some ambiguity in the extraction of the excitation energy as either the inflection point of the step (upper right corner) or the peak position (lower left corner).

Finally, close inspection Fig. 13(a) shows that the ICT bias peak position has a weak gate voltage dependence. In contrast, in the high-temperature limit this resonance lies at the unrenormalized cotunneling excitation $V = B$. Strong tunneling thus leads to an apparent renormalization in the cotunneling peak position, even for this simple model, c.f.⁶⁴. Although our effective Liouvillian contains parameters E_σ and $F_{\eta\sigma}$ that relate to the magnetic field (compare Eq. (136) and Eq. (137)), these parameters depend on energy and their values at several different energy scales go into our full result since many non-equilibrium Matsubara frequency axes must be accounted for.

V. OVERVIEW AND OUTLOOK

We have studied the standard model of an interacting quantum dot, modeled as an Anderson impurity, in the low-temperature, non-equilibrium limit. We have calculated the effective time-evolution kernel $L(z) = L + \Sigma(z)$ for the kinetic equation of the reduced density operator, where Σ is the non-trivial self-energy superoperator. In contrast to many previous studies using such a gen-

eralized / quantum master equation approach, we have calculated this time-evolution kernel using the real-time renormalization group (RG). The equations for the effective kernel are integrated as function of a cut-off parameter Λ : as Λ is reduced, the renormalized Liouvillian \bar{L}_Λ in principle flows to the exact result, $\bar{L}_\Lambda|_{\Lambda=0} = L(z)$. This RG calculation of the effective kernel involves a number of key elements:

- Transitions between *all Liouville space supervectors* need to be accounted for. This includes those elements of \bar{L}_Λ and $L(z)$ which in a perturbative calculation of the kernel drop out of the calculation due to conservation laws (charge, spin, and possibly particle-hole symmetry). The reason for this is that as one integrates out energy scales, effectively higher-order diagrams are included into a renormalization of the kernel which describe *virtual* intermediate states which are less restricted by conservation laws.
- The dependence of the kernel on the *real QD frequency* (E) (Laplace variable conjugate to time) is important *even in the stationary state*. During the RG flow the renormalized Liouvillian at frequency E self-consistently couples to its action on virtual intermediate states at frequencies differing from E by multiples of the bias voltage $\mu_L - \mu_R$. We have shown that this non-equilibrium effect leads to significant quantitative corrections and may require tens of bias-multiples to achieve convergence.
- The *reservoir-frequency* ($i\omega$) dependence of both the kernel and the vertices becomes important when going beyond the leading, 1-loop approximation, in addition to the QD frequency E . This dependence is generated on the imaginary frequency axis when the reservoirs are integrated out and it may *cancel* 2-loop corrections calculated without frequency dependence.

We have systematically accounted for the leading frequency correction within a 1 plus 2-loop approximation to the exact RT-RG equations and derived an effective RG equation for the time-evolution kernel *only*. This includes the relevant vertex renormalization corrections. Importantly, the leading frequency correction of the 1-loop renormalization of the Liouvillian \bar{L}_Λ was found to exactly cancel the 2-loop zero frequency term.

For the non-interacting Anderson problem ($U = 0$) we found that the current is exactly captured already in the 1-loop approximation without any frequency dependence even though the complete solution (i.e., including the density operator) is contained only within the 1 plus 2-loop approximation. For the strongly interacting case of interest the non-linear transport spectrum (dI/dV stability diagrams) was calculated for a wide range of parameters. The different, intrinsic broadening of the single-electron tunneling and cotunneling resonances was captured, as well as the zero-temperature renormalization of

their positions. As emphasized throughout, due to the restriction to 1- and 2-loop diagrams, the limited Kondo regime cannot be addressed. This regime has been recently studied in detail using RT-RG approach based on the mapping to a Kondo model. This allowed the entire crossover from weak to strong coupling to be described⁵³. Our study thus provides a starting point for a 3-loop analysis of the non-equilibrium Anderson model in which the interplay of Kondo spin-fluctuations and charge-fluctuations can be described.

The RT-RG study benefited a lot from an extensive reformulation of the underlying real-time perturbation theory in terms of vertex superoperators \bar{G} and \tilde{G} . Although originally introduced in the RT-RG²⁷ we have revealed their full significance as fermionic field superoperators that directly generate the Liouville Fock space in complete analogy to *closed* quantum many-body systems:

- Field super operators obey definite anticommutation relations, and a simple fluctuation-dissipation relation similar to the underlying field operators. The Wick theorem in Liouville space at finite temperature can be obtained *algebraically* using relation (59) as usual⁶⁵. In contrast to the path-integral formulation³⁴ this was previously not obvious⁴¹ and complicated by fermionic parity signs²⁷.
- The causal structure of the theory is reflected by the vanishing of 2 out of 4 reservoir correlation functions (rather than 1 out of 4 as in the Keldysh Green function technique). This results in an exponential reduction of the terms contributing to the time-evolution kernel (additional to the reduction in the wide-band limit). The remaining contributing diagrams are easily identified by their topology.

We have extended the use of these fermionic field superoperators to the perturbation theory underlying the RT-RG. This resulting *causal representation* of the perturbation theory has many advantages:

- Probability conservation of the kernel is manifest term-by-term, allowing non-conserving approximations to be easily spotted. In addition, other *exact* eigenvectors and eigenvalues of the kernel were found, that limit the form of the exact effective Liouvillian $L(z)$ as expressed in our central result Eq. (137).
- Term-by-term *diagrammatic* evaluation of the wide-band limit. Diagrams that vanish in this limit can be identified by their topology and the cut-off independence of the remaining diagrams can be shown from the fundamental fermionic algebra of the fields superoperators. This results in a further strong reduction in the number of contributing terms as function of the perturbation order. Moreover, the advantage of working with the complete space of the QD states becomes explicit.

- Finally, the fundamental importance of the infinite temperature limit becomes explicit. It defines the Liouville Fock-space vacuum and the perturbation theory can be explicitly decomposed into infinite temperature renormalization effects and the non-trivial finite-temperature contributions. This provides a natural starting point for the RT-RG, which readily suggests itself.

Besides their application to the RT-RG, we have already found useful application of some of these points in perturbative studies as discussed here in connection to Ref. 38 and elsewhere⁵⁰ for adiabatic driving³⁷.

Acknowledgments

This work was initiated by intense discussions with H. Schoeller which are gratefully acknowledged. We thank D. DiVincenzo, T. Costi and J. Splettstoesser for valuable comments and A. Flesch, E. Gorelov and F. Reckermann for suggestions regarding the numerical calculations. We are grateful to D. Kosov for pointing out Prosen's work and his kind help in establishing the relations between our and other existing superfermion approaches. This work has also benefited from a preliminary study undertaken together with M. Kurz.

Appendix A: Wick theorem for causal field superoperators of the reservoirs J^q

Here we show how the algebraic proof of the Wick theorem⁶⁵ for standard field operators directly applies to the field superoperators J in the causal representation. In this proof one considers the average of n reservoir field superoperators $J_i^{q_i}$ defined Eq. (52),

$$X = \text{Tr}_R (J_1^{q_1} \dots J_n^{q_n} \rho^R), \quad (\text{A1})$$

(which is nonzero only for even n) and commutes $J_n^{q_n}$ to the left side, using that the fields obey the usual anticommutation relations (54). We first consider the case $q_n = -$ and make use of zero trace property of the causal representation (62). This reduces the average to expressions of the same form

$$X = \sum_{k \neq n} (-1)^{N_{k,n}} \tilde{\gamma}_{k,n} X_{k,n} \quad (\text{A2})$$

but with averages over $n - 2$ operators

$$X_{n,k} = \text{Tr}_R (J_1^{q_1} \dots J_{k-1}^{q_{k-1}} J_{k+1}^{q_{k+1}} \dots J_{n-1}^{q_{n-1}} \rho_{res}) \quad (\text{A3})$$

weighted with a contraction function

$$\tilde{\gamma}_{k,n} = \frac{\Gamma_0}{2\pi} \delta_{k,\bar{n}} \delta_{+,q_k} \quad (\text{A4})$$

Here $N_{k,n} = n - k - 1$ is the number of permutations to bring $J_k^{q_k}$ and $J_n^{q_n}$ together.

For $q_n = +$ we proceed in the same way, except that when $J_n^{q_n}$ has been permuted to the far left we apply the fluctuation-dissipation superoperator identity (59). This transforms the expression into that for the $q_n = -$ case multiplied with the Keldysh distribution function: Eq. (A2) applies again but with $\tilde{\gamma}_{k,n}$ replaced by

$$\tilde{\gamma}_{k,n} = \tanh(\eta_n \omega_n / 2T_{r_n}) \tilde{\gamma}_{k,n} \quad (\text{A5})$$

when the multi-index n of $J_n^{q_n}$ reads $n = \eta_n \sigma_n r_n \omega_n$.

We thus find the standard Wick recursion relation

$$X = \sum_{k \neq n} (-1)^{N_{k,n}} \gamma_{k,n} X_{k,n} \quad (\text{A6})$$

with $\gamma_{k,n} = \tilde{\gamma}_{k,n} \delta_{+,q_n} + \tilde{\gamma}_{k,n} \delta_{-,q_n}$ which by iteration gives the Wick theorem Eq. (60) with contractions (64)-(63).

Appendix B: The main properties of the causal vertex superoperators G^q : proof

a. "Bare" vertices In the (IIB2) the main properties (53) and (57) the causal superoperators \bar{G} and \tilde{G} were introduced, namely, their anticommutation relations (53) and their relation by Hermitian conjugation in Liouville space (57). We now give the proof of the latter relation. We note that both relations are fundamental as they imply a formal correspondence of causal $G^\pm = \bar{G}, \tilde{G}$ operators with the usual fermionic field operators and allow us to develop the "2nd quantization" technique for fermionic Liouville Fock-space.

Super Hermitian conjugation is defined relative to the scalar product in Liouville space $(A|B) = \text{Tr} A^\dagger B$ where A and B are dot operators. To prove Eq. (57) we first notice that the "naive" field superoperators (40) obey

$$(\mathcal{G}_1^p)^\dagger = \mathcal{G}_1^p \quad (\text{B1})$$

where $1 = \eta\sigma$ and $\bar{1} = \bar{\eta}\bar{\sigma}$. Superoperators with the same Keldysh index p are thus conjugated to each other in the usual way: Hermitian conjugation is equivalent to inverting the particle-hole index η . This follows by using the cyclic property of the trace:

$$\begin{aligned} (A|\mathcal{G}_1^+|B) &= \text{Tr} A^\dagger d_\sigma^\eta B = (\text{Tr} B^\dagger d_\sigma^{\bar{\eta}} A)^* \\ &= (B|\mathcal{G}_1^+|A)^* = (B|(\mathcal{G}_1^+)^\dagger|A)^*, \end{aligned} \quad (\text{B2})$$

$$\begin{aligned} (A|\mathcal{G}_1^-|B) &= \text{Tr} A^\dagger B d_\sigma^\eta = (\text{Tr} d_\sigma^{\bar{\eta}} B^\dagger A)^* = (\text{Tr} B^\dagger A d_\sigma^{\bar{\eta}})^* \\ &= (B|\mathcal{G}_1^-|A)^* = (B|(\mathcal{G}_1^-)^\dagger|A)^*, \end{aligned} \quad (\text{B3})$$

where $*$ denotes complex-conjugation and \dagger denotes either usual hermitian-conjugation or super-hermitian-conjugation depending on whether it acts on operators or superoperators respectively. These superoperators, however, have the disadvantage that they satisfy no definite fermionic or bosonic commutation relations, cf. (45).

The transformed field superoperators (47) that include the fermion-parity sign do anticommute (cf. Eq. (49)). However, they are not related by super-Hermitian conjugation in the usual way:

$$(\mathcal{G}_1^p)^\dagger = p \mathcal{G}_1^p \quad (\text{B4})$$

which follows from Eq. (B1) and the properties $(L^n)^\dagger = L^n$ and $[L^n, G_1^q] = \eta G_1^q$ of $L^n = [n, \bullet]_-$

$$(\mathcal{G}_1^p)^\dagger = (p^{L^n} \mathcal{G}_1^p)^\dagger = (\mathcal{G}_1^p)^\dagger p^{L^n} = p^{L^n+1} \mathcal{G}_1^p = p \mathcal{G}_1^p. \quad (\text{B5})$$

Finally, the causal field superoperators (51) obtained from \mathcal{G}^p by a Keldysh-rotation obey both definite commutation relations (53) and standard Hermitian-superconjugation relations (57): using $p^2 = 1$

$$(G_1^q)^\dagger = \frac{1}{\sqrt{2}} \sum_p p^{(1+q)/2} (\mathcal{G}_1^p)^\dagger \quad (\text{B6})$$

$$= \frac{1}{\sqrt{2}} \sum_p p^{(1-q)/2} \mathcal{G}_1^p = G_1^{\bar{q}} \quad (\text{B7})$$

key This clearly demonstrates the fundamental advantage of the causal representation over the other ones.

Note that due to the p -dependent superoperators entering in the definition Eq. (51) of our superoperator $\bar{G}_{\eta\sigma}$ the latter is either a commutator or anticommutator with the fermionic operator d_σ^η depending on the argument on which it acts. For example $\bar{G}_{\eta,\sigma} A = [d_\sigma^\eta, A]$ if A is a fermionic dot operator (odd in charge, see Eq. (96)) and $\bar{G}_{\eta,\sigma} A = [d_\sigma^\eta, A]_+$ if A is bosonic (even in charge, see Eq. (91)). For the $\tilde{G}_{\eta,\sigma}$ the opposite holds. The crucial relation Eq. (55) nevertheless holds always for the superoperators \bar{G} : one obtains zero in the first case as a trace of a commutator and in the second as a trace of an operator which is off-diagonal in charge.

The analogy to usual field operators extends also to the transformation behavior under spin-rotations. For usual field operators in Fock space $d_\sigma^\dagger, \sigma d_\sigma$ transform as irreducible tensor operators (ITOs) of rank 1/2 and index $\sigma/2$. Particle ($\eta = +$) $G_{+\sigma}^q$ and hole ($\eta = -$) field superoperators with the appropriate prefactors, $\sigma G_{-\sigma}^q$, are similarly irreducible tensor superoperators (ITSOs) of rank 1/2 with index $\sigma/2$. This applies to all the representations of the field superoperators that we used: the same holds for $\mathcal{G}_{+\sigma}^p, \sigma \mathcal{G}_{-\sigma}^p$ and $\mathcal{G}_{+\sigma}^p, \sigma \mathcal{G}_{-\sigma}^p$.

To prove this we note that for any two superoperators A^p and $B^{p'}$ generated by two operators A and B , in the same way as G_1^p (cf. Eq. (40)),

$$A^p \bullet = \begin{cases} A^\bullet, & p = + \\ \bullet A, & p = - \end{cases} \quad (\text{B8})$$

the commutator of superoperators can be expressed in the superoperator corresponding to the commutator: $[A^p, B^{p'}]_- = p \delta_{p,p'} ([A, B]_-)^p$. This directly shows that the field super operators \mathcal{G}_1^p (40) transform in the

same way as the field operators d_1 under spin-rotations: $[L^{S_i}, \mathcal{G}_1^p]_- = ([S_i, d_1]_-)^p$. The superoperators (47) and (51) simply inherit this property since spin and charge superoperators commute, $[L^{S_i}, L^n] = 0$.

Appendix C: Relation of the causal fermionic superoperators G^q and Prosen's superoperators

We note that fermionic superoperators (i.e. possessing anticommutation Eq. (53) and Hermitian conjugation Eq. (57) relations) and a Liouville Fock-space similar to ours (Eq. (51) and Eq. (91)-(96)) were also constructed in Ref. 31 for the problem of steady state of an open system described by Lindblad equation quadratic in fermion operators. It can be checked that superoperators c_j^\dagger from that work also satisfy Eq. (55) and thus possess causal structure.

In the work³¹ the opposite order of construction was used: i.e. first a Fock-space was constructed as an ordered product of the Majorana operators (which are linear combinations of usual fermion creation and annihilation operators) and then fermionic superoperators were defined on it. The fermionic parity superselection rule we use was implicitly taken into account by ordering of the Majorana operators and by a specific definition of the creation and annihilation superoperators. Careful comparison of the Fock spaces shows that superoperators c_j^\dagger from the work³¹ are related to our $\bar{G}_{\eta,\sigma}$ by the following unitary transformation:

$$\begin{aligned} c_j^\dagger &= \frac{1}{\sqrt{2}} (\bar{G}'_{+,m} + \bar{G}'_{-,m}), \quad j = 2m - 1 \\ c_j^\dagger &= \frac{i}{\sqrt{2}} (\bar{G}'_{-,m} - \bar{G}'_{+,m}), \quad j = 2m \end{aligned} \quad (C1)$$

(relations for the superoperators c_j can be obtained from Eq. (C1) by superHermitian conjugation). Here $m = 1, 2, 3, \dots$ are the indices numerating fermionic channels and $\bar{G}'_{\eta,m}$ are the \bar{G}_1 superoperators renumbered by the channel index. For the single level model we have only spin channels and:

$$\bar{G}'_{\eta,m} \equiv \begin{cases} \bar{G}_{\eta,\downarrow}, & m = 1 \\ \bar{G}_{\eta,\uparrow}, & m = 2 \end{cases} \quad (C2)$$

For the multilevel model with discrete channels $k = 1, 2, 3, \dots$:

$$\bar{G}'_{\eta,m} \equiv \bar{G}_{\eta,\sigma}^k, \quad m = 2k + (\sigma - 1)/2 \quad (C3)$$

For the case of infinite and especially continuous number of channels it is not directly seen from the definition of the work³¹ how one should construct superoperators c_j^\dagger . Then relation (C1) can be used as a definition of the c_j, c_j^\dagger superoperators, since the superoperators \bar{G}_1, \bar{G}'_1 have a proper definition also in this limit, see Eq. (54). In contrast to our case the superoperators c_j^\dagger are neither ITOs

in spin nor in particle-hole space. This fact complicates the group-classification we performed in Sec. II C 3. The causal structure of the kernel in the representation³¹ also remains implicit which in general plays a crucial role as our analysis shows. Finally, we emphasize the different scope of application of field superoperators in our work: whereas Prosen's approach was formulated to calculate steady states of quadratic effective Liouvillians, we here extend it to the reservoirs with continuous fields as well and to simplify the microscopic *derivation* of the effective Liouvillians for *non-quadratic* problems.

Appendix D: Schmutz's fermionic superoperators

We note that in the Ref. 32–34 alternative field superoperators $a_\sigma, a_\sigma^\dagger$ and $\tilde{a}_\sigma, \tilde{a}_\sigma^\dagger$ were introduced. In our notation (15)-(17) and (39),(40) they read:

$$a_1^p = a_{\eta,\sigma}^p = \begin{cases} a_\sigma^\eta, & p = +1 \\ \tilde{a}_\sigma^\eta, & p = -1 \end{cases} \quad (D1)$$

They are related to our “intermediate” superoperators Eq. (47) as follows:

$$a_{\eta,\sigma}^p = p^{\frac{1-\eta}{2}} \mathcal{G}_{\eta,\sigma}^p \quad (D2)$$

(the definition of the work³⁴ contains an additional inessential p signs). The use of the additional η -dependent superoperator $p^{\frac{1-\eta}{2}}$ allows one to compensate the inconvenient signs p in the anticommutation relations Eq. (49) and in the Hermitian-conjugation relation Eq. (B4), thus restoring the usual fermionic algebra without the use of the Keldysh-rotation:

$$[a_1^{p_1}, a_2^{p_2}]_+ = \delta_{1,2} \delta_{p_1,p_2}, \quad (a_1^p)^\dagger = a_1^p \quad (D3)$$

The spin and particle-hole group transformations of these superoperators coincide with those introduced by us. However they do not reveal the important property Eq. (55) which is crucial in our formulation. Also the explicit η -dependence of the sign-prefactor does not allow one to perform a simple Keldysh rotation of the a_1^p superoperators to recover this property.

Appendix E: Fermion-parity operator and superoperator

In Sec. (II C 2) the operator Z_R , the right eigen superoperator $|Z_R\rangle$ of causal field superoperator \bar{G}_1 (cf. Eq. (86)), turned out to play an important role. Here we discuss its additional properties to further clarify its physical meaning.

b. Fermion parity The causal field superoperators (51), written out in terms of field operators, read

$$G_1^q \bullet = \frac{1}{\sqrt{2}} \{d_1 \bullet + q(-1)^n \bullet d_1(-1)^n\}, \quad (E1)$$

where we used $(-1)^{L^n} \bullet = (-1)^n \bullet (-1)^n$. Note that $n = \sum_{\sigma} n_{\sigma}$ is the occupation *operator* with $n_{\sigma} = d_{\sigma}^{\dagger} d_{\sigma}$. The definition of this representation is based on the fermion-parity superselection rule, cf. Sec. (IIB 2). The explicit form (E1) makes clear that $G_1^- = \bar{G}_1$ has

$$Z_R = \frac{1}{2}(-1)^n \quad (\text{E2})$$

as right zero eigen supervector: upon substitution the two terms in Eq. (E1) simply cancel since $(-1)^{2n} = 1$. Noting that $(-1)^n = \prod_{\sigma} e^{i\pi n_{\sigma}} = \prod_{\sigma} (1 - 2n_{\sigma})$ we recover

$$Z_R = \frac{1}{2}(2n_{\uparrow} - 1)(2n_{\downarrow} - 1) = 2\hat{n}_{\uparrow}\hat{n}_{\downarrow} - \hat{n} + \frac{1}{2}, \quad (\text{E3})$$

the result (90) in the main text. Clearly, from Eq. (E2)

$$Z_R^2 = \frac{1}{4}\mathbb{1} \quad (\text{E4})$$

which implies the normalization of the supervector $|Z_R\rangle$. The eigenvalue equation (86), $\bar{G}_1|Z_R\rangle = [d_1, Z_R]_+ = 0$ requires Z_R to *anticommute* with all the fermionic fields: Z_R is therefore the unique operator (up to normalization and a phase) that (anti)commutes with all QD bosonic (fermionic) operators in the QD Liouville space, in close analogy to Grassmann numbers used in functional integral approaches⁴³. Eq. (E2) most clearly illustrates the physical meaning of the operator Z_R : we identify Z_R as the *fermion-parity operator* (up to a constant),

$$\begin{cases} 2Z_R|n\rangle = |n\rangle, & n = \text{even} \\ 2Z_R|n\rangle = -|n\rangle, & n = \text{odd} \end{cases} \quad (\text{E5})$$

Finally, that $|Z_L\rangle = \frac{1}{2}\mathbb{1}$ is a zero eigenvector of G_1^- follows from $(-1)^n d_1 (-1)^n = -d_1$. The eigenvalue equation (85), $\bar{G}_1|Z_L\rangle = [d_1, Z_L]_- = 0$, requires Z_L , considered as an operator, to commute with the QD field operators and therefore with all QD operators, implying that indeed Z_L is proportional to the unit operator.

c. Spin and charge rotations By construction the two independent operators Z_L and Z_R transform as scalars under both spin- and charge-rotations (cf. Table I). They must therefore be related the two scalars of these groups (Casimir operators of their Lie-algebras), $S^2 = \sum_i S_i^2$ and $T^2 = \sum_i T_i^2$:

$$Z_L = \frac{1}{2}\mathbb{1} = \frac{2}{3}(T^2 + S^2), \quad Z_R = \frac{2}{3}(T^2 - S^2) \quad (\text{E6})$$

This relation follows from the fact that these act as unit operators in their respective 2-dimensional subspaces: $S^2 = 3/4 \sum |\sigma\rangle\langle\sigma|$ and $T^2 = 3/4(|0\rangle\langle 0| + |2\rangle\langle 2|)$.

d. Fermion-parity superoperator We next consider the *fermion-parity superoperator*, defined naturally by the right action of the fermion-parity operator on an operator (identical results follow for the left action):

$$U \bullet = \bullet 2Z_R = \bullet (-1)^n \quad (\text{E7})$$

This unitary and Hermitian superoperator ($U^{\dagger} = U, U^2 = \mathbb{1}$) transforms the two types of field superoperators into each other,

$$UG_1^q U = G_1^{\bar{q}}. \quad (\text{E8})$$

We can thus interchange the role of creation and annihilation superoperators in Liouville Fock-space by a linear transformation U . This is similar to the field operators d_{σ} and d_{σ}^{\dagger} that generate the standard Fock-space: the η index distinguishing can be inverted by a unitary transformation

$$\begin{aligned} e^{i\pi(T_y - S_y)} d_{\eta\sigma} e^{-i\pi(T_y - S_y)} &= d_{\bar{\eta}\sigma} \\ &= e^{i\pi(L_{T_y} - L_{S_y})} d_{\eta\sigma}. \end{aligned} \quad (\text{E9})$$

c.f. Eq. (106) and Eq. (109). Note that $Kd_{\eta\sigma} = d_{\bar{\eta}\sigma}$ as well, but this is an anti-unitary transformation.

This result follows by considering an arbitrary fermionic operator F for which $(-1)^{L^n} F = (-1)^n F (-1)^n = -F$. The superoperator U transforms a commutator of F with *any* operator to an anticommutator and *vice versa*: defining $L_F^{\pm} \bullet = [F, \bullet]_{\pm} = F \bullet \pm \bullet F$:

$$UL_F^{\pm} U \bullet = F \bullet (-1)^{2n} \pm \bullet (-1)^n F (-1)^n \quad (\text{E10})$$

$$= F \bullet \mp \bullet F = L_F^{\mp} \bullet \quad (\text{E11})$$

Commutators with any bosonic operator B remain unaffected. Since the superoperator \bar{G}_{σ} is a (anti)commutator when acting on a fermionic (bosonic) operator and *vice versa* for \tilde{G} , the superoperator U interchanges these two: $U\bar{G}_1 U = \tilde{G}_1$ and- $U\tilde{G}_1 U = \bar{G}_1$.

e. Multi-orbital Anderson models Finally, we indicate how the operators $|Z_L\rangle$ and $|Z_R\rangle$ can be constructed for more general multi-orbital Anderson-type models. The super vacuum state is

$$|Z_L\rangle = \frac{1}{2^N} \mathbb{1},$$

where N is the number of orbitals and the prefactor takes into account normalization ($\langle Z_L | Z_L \rangle = 1$). Eq. (87) is then simply extended to the maximally occupied state with respect to this vacuum

$$|Z_R\rangle = \prod_{k=1}^N \prod_{\sigma} \left(\prod_{\eta} \bar{G}_{\eta\sigma}^k \right) |Z_L\rangle \quad (\text{E12})$$

Using Eq. (E12) and Eq. (89) Eq. (90) generalizes to

$$|Z_R\rangle = \frac{1}{2^N} \prod_k \prod_{\sigma} (2n_{\sigma}^k - \mathbb{1}) = \frac{1}{2^N} e^{i\pi n} \quad (\text{E13})$$

implying $Z_R^2 = \frac{1}{4^N} \mathbb{1}$. Here $n = \sum_{k,\sigma} n_{\sigma}^k$ is the total dot particle-number operator. All properties of single-orbital Z_R operator ((anti)commutation relations with fermionic (bosonic) operators, transformation properties under charge and spin rotation, etc.) hold for the multi-orbital case as well.

Appendix F: Symmetry of the self-energy

In this Appendix we derive the symmetry for QD Eq. (101) in contact with the reservoirs from the global

symmetries Eq. (25) and (26). Quite generally, a quantity with QD and reservoir contributions, $A^{\text{tot}} = A + A^R$, is globally conserved when $[A^{\text{tot}}, H^{\text{tot}}] = 0$. The corresponding Liouville super operators $L^{A^{\text{tot}}} = [A^{\text{tot}}, \bullet]$ and $L^{\text{tot}} = [H^{\text{tot}}, \bullet]$, then also commute:

$$[L^{A^R}, L^R] = 0, \quad (\text{F1})$$

$$[L^{A^{\text{tot}}}, L^{\text{tot}}] = 0. \quad (\text{F2})$$

The commutator of the local part $L^A = [A, \bullet]$ with the Laplace transformed evolution super operator $\Pi(z) = \text{Tr}_R i(z - L^{\text{tot}})^{-1} \rho^R$ of the reduced density operator (cf. Eq. (31)) must then vanish:

$$\begin{aligned} L^A \Pi(z) &= L^A \text{Tr}_R \frac{i}{z - L^{\text{tot}}} \rho^R = \text{Tr}_R L^{A^{\text{tot}}} \frac{i}{z - L^{\text{tot}}} \rho^R \\ &= \text{Tr}_R \frac{i}{z - L^{\text{tot}}} L^A \rho^R = \Pi L^A \end{aligned} \quad (\text{F3})$$

using subsequently $\text{Tr}_R L^{A^R} \bullet = \text{Tr}_R [H^R, \bullet] = 0$, Eq. (F2), and finally $L^{A^R} \rho^R = 0$ which follows from Eq. (21) and Eq. (F1). Clearly, this proof applies also for the time-evolution superoperator Π_0 without any QD-reservoir interaction, i.e., for $L^V = 0$. Then, using $[L^A, \Pi(z)] = [L^A, \Pi_0(z)] = 0$ and taking the commutator of L^A with the Dyson equation that defines the self-energy $\Sigma(z)$, $\Pi(z) = \Pi_0(z) - i\Pi_0(z)\Sigma(z)\Pi(z)$, we find that $[L^A, \Sigma(z)] = 0$.

Appendix G: Hermiticity

f. Hermitian conjugation superoperator The density operator is restricted to be invariant under Hermitian conjugation in Hilbert space. When considering density operators as supervectors in Liouville space this Hermitian conjugation of an *operator* then corresponds to a superoperator that we denote by K ,

$$K|A\rangle \equiv |A^\dagger\rangle. \quad (\text{G1})$$

It is to be distinguished from the Hermitian conjugation of a superoperator. K is antilinear and satisfies

$$K^2 = \mathcal{I} \quad (\text{G2})$$

where \mathcal{I} is the unit superoperator. Changing the basis in Liouville space by the superoperator K we effect an antilinear transformation of a superoperator (denoted as c -transform in Ref. 26): $S \rightarrow KSK$. In the time representation the density operator is invariant under this transformation: $K\rho(t) = \rho(t)$, implying for the Laplace-transformed density matrix Eq. (32) $K\rho(z) = \rho(-z^*)$. Applying K to the kinetic equation (35) we obtain a conjugation relation restricting the kernel $\Sigma(z)$:

$$K\Sigma(z)K = -\Sigma(-z^*) \quad (\text{G3})$$

This property holds of course also for initial Liouvillian: $KLK\bullet = [H, \bullet^\dagger]^\dagger = -[H^\dagger, \bullet] = -[H, \bullet] = -L\bullet$.

The transformation of the fields \mathcal{G}^p follows by applying K to Eq. (40) using $(d^\dagger \bullet)^\dagger = \bullet^\dagger d = (K\bullet)d$:

$$K\mathcal{G}_1^p K = \mathcal{G}_1^{\bar{p}} \quad (\text{G4})$$

giving with Eq. (47), (G2) and $KL^n K = -L^n$

$$K\mathcal{G}_1^p K = p^{-L^n} \mathcal{G}_1^{\bar{p}} = (-1)^{L^n} \mathcal{G}_1^{\bar{p}}. \quad (\text{G5})$$

The transformation of the causal field superoperators G^q , giving Eq. (120) in the main text, follows from Eq. (51):

$$KG_1^q K = q(-1)^{L^n} G_1^q. \quad (\text{G6})$$

g. Simplifications using conjugation The transformation behavior of the kernel $\Sigma(z)$ under conjugation K of the basis vectors, $K\bar{\Sigma}(z)K = -\bar{\Sigma}(-z^*)$ restricts the structure of the contributions to $\bar{\Sigma}(z)$ in the renormalized perturbation theory Eq. (79). The RG-equation for the Liouvillian Eq. (208), (224), (267) have a similar structure (since we can eliminate the renormalized vertices, even in the 2-loop RG approximation, we can restrict our considerations to only the bare vertices \bar{G} as in Eq. (79)). To make use of this, we decompose it into conjugate pairs. To illustrate the idea, consider first the 1-loop approximation to $\bar{\Sigma}(z)$ in perturbation theory:

$$\bar{\Sigma}(z) = \sum_1 \bar{\Sigma}_{1\bar{1}}(z) \quad (\text{G7})$$

where we now write the sum over 1 explicitly and $\bar{\Sigma}_{1\bar{1}}(z) = \bar{\gamma}(x_1)\bar{G}_1\Pi_1\bar{G}_{\bar{1}} = -K\bar{\Sigma}_{1\bar{1}}(-z^*)K$ denotes a term in which the multiindex 1 has a *fixed* value and $\Pi_1 = (z - \bar{L} - x_1)^{-1}$. Using this and that 1 is dummy summation variable, we can restrict the summation one *fixed* η configuration, e.g., $\eta_1 = +$, while manifestly preserving the structure $K\bar{\Sigma}(z)K = -\bar{\Sigma}(-z^*)$:

$$\bar{\Sigma}(z) = \sum_1 \delta_{\eta_1+} (\bar{\Sigma}_{1\bar{1}}(z) - K\bar{\Sigma}_{1\bar{1}}(-z^*)K) \quad (\text{G8})$$

The calculation of the supermatrix elements is now simplified: using the notation of Sec. (III) and the antilinearity of K , $(A|KSK|B) = (KA|S|KB)^*$ we obtain:

$$(\kappa_3|\bar{\Sigma}(z)|\kappa_0) = \quad (\text{G9})$$

$$\begin{aligned} &\sum_1 \delta_{\eta_1+} ((\kappa_3|\bar{G}_1|\kappa_2)(\kappa_1|\bar{G}_{\bar{1}}|\kappa_0)(\kappa_1|\Pi_1(z)|\kappa_0) \\ &((K\kappa_3|\bar{G}_1|\kappa_2)^*(\kappa_1|\bar{G}_{\bar{1}}|K\kappa_0)^*(\kappa_1|\Pi_1(-z^*)|\kappa_0)^*)) \end{aligned}$$

In our Liouville-Fock basis the matrices representing G^q are of course real since these are the field operators. When the basis supervectors $|\kappa_3\rangle, |\kappa_0\rangle$ correspond to diagonal operators $(Z_i, \chi_\sigma, S_0, T_0)$, the second term in Eq. (G9) simply relates to the first one since these supervectors are mapped onto themselves by K , cf. Eq. (115). Eq. (G9) simplifies to

$$\begin{aligned} (\kappa_3|\bar{\Sigma}(z)|\kappa_0) &= \sum_1 \delta_{\eta_1+} (\kappa_3|\bar{G}_1|\kappa_2)(\kappa_1|\bar{G}_{\bar{1}}|\kappa_0) \\ &((\kappa_1|\Pi_1(z)|\kappa_0) - (\kappa_1|\Pi_1(-z^*)|\kappa_0)^*) \end{aligned} \quad (\text{G10})$$

which is explicitly imaginary at $z = i0$ as it should be. Supervectors corresponding to non-diagonal operators $(S_\sigma, T_\eta, \alpha_{\eta\sigma}^\nu)$ come in pairs related by inversion of both indices η and σ . The superoperator K maps these pairs onto each other (with a sign change for $\nu = -\sigma\eta$, cf. Eq. (117). Noting also that \bar{G} only has non-zero matrix elements for one superkets of each pair, cf. Eq. (119)-(121), we see that in (G8) either only the first or second term contributes (or neither) when κ_3 and/or κ_0 is a non-diagonal operator. In this way we have effectively eliminated the need to evaluate the terms for the $\eta_1 = -$ using the conjugation relations. This consideration is generalized to 2-loop expressions by adding to Eq. (G8)

$$\sum_{12} \delta_{\eta_1} + \delta_{\eta_2} + (\bar{\Sigma}_{1\bar{1}2\bar{2}}(z) - K\bar{\Sigma}_{1\bar{1}2\bar{2}}(-z^*)K) \quad (\text{G11})$$

where $\bar{\Sigma}_{1\bar{1}2\bar{2}}(z)$ collects all 2-loop terms with a fixed multiindices 1 and 2. The same analysis applies to terms in the RG equations Eq. (208),(224),(267).

h. Conjugation properties under RG flow In contrast to the charge and spin transformation properties, the conjugation property (G6) – associated with the fundamental Hermiticity of the density operator – is exactly preserved under the RG flow. We first note that the vertices $\tilde{G} = G^+$ only determine the initial value of the Liouvillian \bar{L} and therefore are not affected by the ensuing RG flow: they therefore simply obey Eq. (G6). However, the vertices $\bar{G} = G^-$ flow together with the Liouvillian \bar{L} and thereby acquire a dependence on the dot frequency z . These vertices obey the following generalization of Eq. (G6) to non-zero z :

$$K\bar{G}_1^q(z)K = q(-1)^{L^n} \bar{G}_1^q(-z^*) \quad (\text{G12})$$

To prove Eq. (G12) we use that the bare vertices, providing the initial values of the RG flow, possess the property (G12). It remains to show that for each scale Λ the infinitesimal correction to the \bar{G} generated by the RG flow also possesses this property. We therefore apply $K \bullet K$ to the RG Eq. (209) for vertex \bar{G}_α , insert Eq. (G2), using Eq. (G3) and assume that the property Eq. (G12) holds:

$$K \frac{d\bar{G}_\alpha}{d\Lambda} K = (-1)^{(k+1)L^n + k(k+1)/2} \left(\frac{d\bar{\gamma}}{d\Lambda} \prod_i \bar{\gamma}_i(\bar{\omega}_i) \right)_{\text{irr}} \bar{G}_1 \frac{1}{z_1^* + \bar{L}(-z_1^*)} \bar{G}_2 \dots \bar{G}_{\alpha-1} \bar{G}_{\alpha+1} \dots \bar{G}_{k-1} \frac{1}{z_l^* + \bar{L}(-z_l^*)} \bar{G}_k \quad (\text{G13})$$

$$= (-1)^{L^n} \left(\frac{d\bar{\gamma}}{d\Lambda} \prod_i \bar{\gamma}_i(\bar{\omega}_i) \right)_{\text{ir}} \quad (\text{G14})$$

$$\bar{G}_1 \frac{\bar{\gamma}(\bar{\omega}_1)}{-z_1^* - \bar{L}(-z_1^*)} \bar{G}_2 \dots \bar{G}_\alpha \dots \bar{G}_{k-1} \frac{\bar{\gamma}(\bar{\omega}_l)}{-z_l^* - \bar{L}(-z_l^*)} \bar{G}_k = -(-1)^{L^n} \frac{d\bar{G}_\alpha}{d\Lambda}(-z^*) \quad (\text{G15})$$

At the first equality a sign factor arises when commuting of all $(-1)^{L^n}$ factors to the left, using the fermion-parity property $(-1)^{L^n} G = G(-1)^{L^n+1}$ which is preserved under the RG as well (since both sides of Eq. (209) have an odd number of \bar{G} 's). At the second equality we inverted all dummy multiindices $i \rightarrow \bar{i}$ and inverted the integration variable $\bar{\omega}_i \rightarrow -\bar{\omega}_i$, giving a sign $(-1)^{k/2}$ due to the $k/2$ antisymmetric contraction functions (counting $\bar{\gamma}$'s and $d\bar{\gamma}/d\Lambda$), where k is the even number of vertices other than \bar{G}_α . Since $k/2$ and $k(k+1)/2$ have opposite parity for even k the result follows.

-
- ¹ L. I. Glazman and M. E. Raikh, JETP Lett. **47**, 452 (1988).
 - ² T. K. Ng and P. A. Lee, Phys. Rev. Lett. **61**, 1768 (1988).
 - ³ R. Bulla, T. Costi, and T. Pruschke, Rev. Mod. Phys. **80**, 395 (2008).
 - ⁴ J. Eckel, F. Heidrich-Meisner, S. Jakobs, M. Thorwart, M. Pletyukhov, and R. Egger, New J. Phys. **12**, 043042 (2010).
 - ⁵ F. B. Anders, Phys. Rev. Lett. **101**, 066804 (2008).
 - ⁶ A. Rosch, Euro. Phys. Journ. **85**, 6 (2012).
 - ⁷ S. R. White and A. E. Feiguin, Phys. Rev. Lett. **93**, 076401 (2004).
 - ⁸ A. Daley, C. Kollath, U. Schollwöck, and G. Vidal, J. Stat. Mech.: Theor. Exp. p. P04005 (2004).
 - ⁹ P. Schmitteckert, Phys. Rev. B **70**, 121302 (2004).
 - ¹⁰ S. Weiss, J. Eckel, M. Thorwart, and R. Egger, Phys. Rev. B **77**, 195316 (2008).
 - ¹¹ D. Segal, A. J. Millis, and D. R. Reichman, Phys. Rev. B **82**, 205323 (2010).
 - ¹² D. Segal, A. J. Millis, and D. R. Reichman (2011), arXiv:1103.1867v1.
 - ¹³ G. Cohen and E. Rabani, Phys. Rev. B **84**, 075150 (2011).
 - ¹⁴ J. E. Han, Phys. Rev. B **81**, 245107 (2010).

- ¹⁵ L. Mühlbacher, D. F. Urban, and A. Komnik, Phys. Rev. B **83**, 075107 (2011).
- ¹⁶ N. S. Wingreen and Y. Meir, Phys. Rev. B **49**, 11040 (1994).
- ¹⁷ K. Haule, S. Kirchner, J. Kroha, and P. Wölfle, Phys. Rev. B **64**, 155111 (2001).
- ¹⁸ R. VanRoermund, S. Y. Shiao, and M. Lavagna, Phys. Rev. B **81**, 165115 (2010).
- ¹⁹ P. Mehta and N. Andrei, Phys. Rev. Lett. **96**, 216802 (2006).
- ²⁰ R. M. Konik, H. Saleur, and A. W. Ludwig, Phys. Rev. B **66**, 125304 (2002).
- ²¹ P. Wang and S. Kehrein, Phys. Rev. B **82**, 125124 (2010).
- ²² A. Oguri, Phys. Rev. B **64**, 153305 (2001).
- ²³ A. A. Aligia, Phys. Rev. B **74**, 155125 (2006).
- ²⁴ E. Munoz, C. Bolech, and S. Kirchner (2011), arXiv:1111.4076v1.
- ²⁵ J. Paaske, A. Rosch, and P. Wölfle, Phys. Rev. B **69**, 155330 (2004).
- ²⁶ H. Schoeller, Eur. Phys. Journ. B **168**, 179 (2009).
- ²⁷ H. Schoeller and F. Reininghaus, Phys. Rev. B **80**, 045117 (2009).

- ²⁸ H. Schoeller and G. Schön, Phys. Rev. B **50**, 18436 (1994).
- ²⁹ S. Koller, M. Grifoni, M. Leijnse, and M. R. Wegewijs, Phys. Rev. B **82**, 235307 (2010).
- ³⁰ M. Leijnse and M. R. Wegewijs, Phys. Rev. B **78**, 235424 (2008).
- ³¹ T. Prosen, New J. Phys. **10**, 043026 (2008).
- ³² M. Schmutz, Z. Phys. B **30**, 97 (1978).
- ³³ A. Dzhioev and D. Kosov, J. Chem. Phys. **134**, 044121 (2011).
- ³⁴ U. Harbola and S. Mukamel, Phys. Rep. **465**, 191 (2008).
- ³⁵ S. Andergassen, M. Pletyukhov, D. Schuricht, H. Schoeller, and L. Borda, Phys. Rev. B **83**, 205103 (2011).
- ³⁶ J. König, H. Schoeller, and G. Schön, Phys. Rev. Lett. **76**, 1715 (1996).
- ³⁷ F. Reckerman, M. Wegewijs, J. Splettstoesser, and R. Saptsov, in preparation (2012).
- ³⁸ L. D. Contreras-Pulido, J. Splettstoesser, M. Governale, J. König, and M. Büttiker, Phys. Rev. B **85**, 075301 (2012).
- ³⁹ G. C. Wick, A. S. Wightman, and E. P. Wigner, Phys. Rev. **88**, 101 (1952).
- ⁴⁰ Y. Aharonov and L. Susskind, Phys. Rev. **155**, 1428 (1967).
- ⁴¹ S. Mukamel, Phys. Rev. E **68**, 021111 (2003).
- ⁴² A. I. Larkin and Y. Ovchinnikov, Zh. Eksp. Teor. Fiz. **68**, 1915 (1975), [Sov. Phys. JETP **41**, 960 (1975)].
- ⁴³ A. Kamenev and A. Levchenko, Adv. Phys. **58**, 197 (2009).
- ⁴⁴ M. Esposito, U. Harbola, and S. Mukamel, Rev. Mod. Phys. **81**, 1665 (2009).
- ⁴⁵ E. Lifshitz and L. Pitaevskii, *Physical kinetics*, Course of theoretical physics (Butterworth-Heinemann, 1981).
- ⁴⁶ J. König, J. Schmid, H. Schoeller, and G. Schön, Phys. Rev. B **54**, 16820 (1996).
- ⁴⁷ J. Rammer and H. Smith, Rev. Mod. Phys. **58**, 323 (1986).
- ⁴⁸ T. Korb, F. Reininghaus, H. Schoeller, and J. König, Phys. Rev. B **76**, 165316 (2007).
- ⁴⁹ S. Mukamel, Phys. Rep. **93**, 1 (1982).
- ⁵⁰ R. Saptsov and M. R. Wegewijs, in preparation (2012).
- ⁵¹ H. Schoeller, *Mesoscopic Electron Transport* (Kluwer, 1997), chap. Transport through interacting quantum dots, p. 291.
- ⁵² H. Schoeller, *Interactions and transport properties* (Springer, 1999), chap. An Introduction to Real-Time Renormalization Group, p. 137, Low-Dimensional Systems.
- ⁵³ M. Pletyukhov and H. Schoeller, Phys. Rev. Lett. **108**, 260601 (2012), arXiv:1201.6295.
- ⁵⁴ K. Goß, S. Smerat, M. Leijnse, M. R. Wegewijs, C. M. Schneider, and C. Meyer, Phys. Rev. B **83**, 201403(R) (2011).
- ⁵⁵ A. Eliassen, J. Paaske, K. Flensberg, S. Smerat, M. Leijnse, M. R. Wegewijs, H. I. Jørgensen, M. Monthieux, and J. Nygård, Phys. Rev. B **81**, 155431 (2010).
- ⁵⁶ S. J. Tans, M. H. Devoret, R. J. A. Groeneveld, and C. Dekker, Nature **394**, 761 (1998).
- ⁵⁷ T. H. Oosterkamp, J. W. Janssen, L. P. Kouwenhoven, D. G. Austing, T. Honda, and S. Tarucha, Phys. Rev. Lett. **82**, 2931 (1999).
- ⁵⁸ S. M. Reimann, M. Koskinen, M. Manninen, and B. R. Mottelson, Phys. Rev. Lett. **83**, 3270 (1999).
- ⁵⁹ S. M. Reimann and M. Manninen, Rev. Mod. Phys. **74**, 1283 (2002).
- ⁶⁰ J. Lambe and R. C. Jaklevic, Phys. Rev. **165**, 821 (1968).
- ⁶¹ M. Eto, Jpn. J. Appl. Phys. **40**, 1929 (2001).
- ⁶² J. Paaske, A. Rosch, P. Wölfle, N. Mason, C. M. Marcus, and J. Nygård, Nature Physics **2**, 460 (2006).
- ⁶³ A. S. Zyazzin, J. W. van den Berg, E. A. Osorio, H. S. van der Zant, N. P. Konstantinidis, F. May, M. Leijnse, W. Hofstetter, M. R. Wegewijs, C. Danieli, et al., Nano Lett. **10**, 3307 (2010).
- ⁶⁴ J. V. Holm, H. I. Jørgensen, K. Grove-Rasmussen, J. Paaske, K. Flensberg, and P. E. Lindelof, Phys. Rev. B **77**, 161406 (2008).
- ⁶⁵ M. Gaudin, Nucl. Phys. **15**, 89 (1960).
- ⁶⁶ Our η sign convention is opposite to that in Ref. 26 to treat the reservoir and dot field operators in the same way.
- ⁶⁷ This gives the correct grand-canonical average over the reservoirs, see Appendix A in Ref. 26 for a proof.
- ⁶⁸ Formulating the theory in real-time³⁷ one can directly identify the retarded and Keldysh Green functions with their usual definitions⁴⁷, $\langle \mathcal{T} \bar{J}_1(t) \bar{J}_2 \rangle = -i\theta(t) \langle [b_1(t), b_2]_+ \rangle$ and $\langle \mathcal{T} \bar{J}_1(t) \bar{J}_2 \rangle = -i \langle [b_1(t), b_2]_- \rangle$ with the time-ordering superoperator \mathcal{T} . In Laplace space, their time-evolution frequencies X are convoluted together with the dot Liouvillian into $1/(z - X - L)$ in the diagram rules (68). The retarded function $\langle \mathcal{T} \bar{J}_1(t) \bar{J}_2 \rangle$ thus contributes only spectral information through X since Eq. (63) contains only $\langle \bar{J}_1 \bar{J}_2 \rangle_R = \frac{1}{2} \langle [b_1, b_2]_+ \rangle_R = \frac{1}{2}$, whereas the Keldysh function $\langle \mathcal{T} \bar{J}_1(t) \bar{J}_2 \rangle$ additionally includes statistical information through Eq. (64) containing $\langle \bar{J}_1 \bar{J}_2 \rangle_R = \frac{1}{2} \langle [b_1, b_2]_- \rangle_R$.
- ⁶⁹ This is referred to as c -conjugation in²⁶.
- ⁷⁰ In the wide-band limit the energy independent contractions $\tilde{\gamma}$ correspond to the δ -functions in time, leaving no phase space for the ω -integrals when enclosing vertices.
- ⁷¹ For models not of the Anderson-type (bilinear coupling), higher skeleton diagrams and vertex renormalizations arise, requiring a more general discrete renormalization²⁶.
- ⁷² This relies on the anticommutation relations (53) of the bare vertices, which break down under renormalization.
- ⁷³ Since \bar{G} is a defect superoperator, $[\bar{G}] = 0$, eigenvectors $|Z_R\rangle$ and $|Z_L\rangle$ for the same eigenvalue can be orthogonal.
- ⁷⁴ We emphasize that charge off-diagonal dot operators *must* be taken into account since in a virtual intermediate state of an open system where, e.g., G has acted on a even fermion parity QD density operator, there is a corresponding fermion operator J acting on the reservoir. Although the latter is no longer explicitly present in the reduced density operator description (reservoirs are integrated out), there is no change of the fermion parity of the total system described by an elementary process in Σ in full agreement with the discussion of Eq. (38).
- ⁷⁵ Our definition of the contraction $\bar{\gamma}_\Lambda$ differs from that in Ref. 26 by factor -2Γ due to our (-1) sign convention for the η index⁶⁶, cf. Eq. (15), normalization of the *field* superoperators⁷⁷ such that $[\bar{G}_1, \bar{G}_1]_+ = 1$, and (Γ) inclusion of the coupling into the reservoir fields.
- ⁷⁶ The positive imaginary part (integration contour in the lower half-plane) contrasts with Ref. 26, but the final notation Eq. (204) agrees again with Ref. 26.
- ⁷⁷ Eq. (208) and (209) differ from those in Ref. 26 by a factor 2 for each loop due to our different normalization⁷⁵ of \bar{G} (reduced by factor $\sqrt{2}$) Sign difference in definition of the cut-off functions⁶⁶ is compensated by closing contour integration⁷⁶ in lower (instead of the upper) half-plane.
- ⁷⁸ We need the Liouvillian L for the density operator time-evolution through $L + \Sigma(z) = \bar{L} + \bar{\Sigma}(z) = \bar{L}_\Lambda + \bar{\Sigma}_\Lambda(z)$ but not for the current: $\Sigma^r(z) = \bar{\Sigma}^r + \bar{\Sigma}^r(z) = \bar{L}_\Lambda^r + \bar{\Sigma}_\Lambda^r(z)$